New applications of carbon stable isotope geochemistry to coprolites and plant fossils

by

Stephanie Marie Plaza-Torres

B.Sc., University of Puerto Rico at Mayagüez, 2019

A thesis submitted to the

Faculty of the Graduate School of the

University of Colorado in partial fulfillment

of the requirements for the degree of

Master of Science

Department of Geological Sciences

2023

Committee Members:

Dr. Boswell Wing

Dr. Karen Chin

Dr. Carl Simpson

Abstract

Plaza-Torres, Stephanie Marie (M.Sc., Department of Geological Sciences)

New applications of carbon stable isotope geochemistry to coprolites and plant fossils

Thesis advised by Associate Professor Boswell Wing

Coprolites and plant fossils can provide valuable information about the diets of ancient organisms and Earth's past terrestrial surface environment. In this thesis two research projects were undertaken: carbonate $\delta^{13}C$ analysis was used to estimate the microbial respiration rates recorded in herbivorous dinosaur coprolites, and a method for sampling and preparation was developed to analyze the organic matter $\delta^{13}C$ of fossil plants with minimal disturbance. Coprolites from the Two Medicine Fm. and Kaiparowits Fm. were used for the respiration rate project and plant fossils from the Creede Fm. and the Green River Fm. were used for the methodology project. Coprolite microbial respiration rates resulted to be higher than soil respiration rates modeled for paleosols from the same formations, suggesting that microbial activity influenced the mineralization of these coprolites. For the plant fossil sampling methodology, $\delta^{13}C$ data was obtained by only destroying sub-centimeter areas of a specimen, which opens the doors to sampling museum specimens for geochemical analysis with minimal damage that would not impact future research.

Acknowledgements

Thanks to the many people that helped me with this thesis: Dr. Boswell Wing, Dr. Karen Chin, Nicole Neu-Yagle, Dr. Ashley Maloney, Dr. Brett Davidheiser-Kroll, Jim Barkley, Dr. Ian Miller, Kristen MacKenzie, Dr. Carl Simpson, the CU Boulder SMART Program, Eduardo Cruz, Jonathan Rosario-De Jesús, Dr. Jennifer Reeve, Desireé Bayouth-García, Javier Martínez, Lizbeth Plaza-Torres, Alexandra Grajales, and Dr. Gussie Maccracken. Thanks to the Denver Museum of Nature & Science, the Museum of the Rockies, and Dr. Karen Chin for letting me conduct geochemical analyses on their specimens.

As well, thanks to the multiple grants and funding sources that supported this thesis and its fieldwork: the Tobacco Root Geological Society Field Scholarship, the CU Boulder Museum of Natural History Research Award, and the National Science Foundation Graduate Research Fellowship.

Kaiparowits Fm. coprolites are Courtesy of the Denver Museum of Nature & Science and the Bureau of Land Management. Two Medicine Fm. coprolites are courtesy of The Museum of the Rockies. Creede Fm. plant specimens and their photographs are courtesy of the Denver Museum of Nature & Science and the USDA Forest Service.

Table of Contents

List of Tables

List of Figures

List of Equations

Overview

This thesis tackles two individual projects related to carbon stable isotope analyses of fossil material. The goal of these projects was to explore novel ways of investigating paleontological specimens under the lens of geochemistry. The chapters focus broadly on different types of preservation and meaning of carbon stable isotope ratios of the carbonate (inorganic) fraction and the organic carbon fraction in fossil feces and plants.

In *Chapter 1: Microbial respiration rates estimated from carbonate carbon stable isotopes of coprolites,* carbonate carbon stable isotopes are explored to gain insight into what influenced their values and the role of microbial activity in the mineralization of carbonaceous coprolites.

In *Chapter 2: Minimally destructive sampling and preparation methodology for plant fossil stable isotope analysis,* organic carbon stable isotopes are explored in plant fossils, to assess the potential contamination of the rock matrix in the data obtained from sampled plant material. As well, methods of minimal destructive sampling are investigated to find ways of preserving palaeobotanical specimens for future research and engaging in collaboration with museums.

Chapter 1: Microbial respiration rates estimated from carbonate carbon stable isotopes of coprolites

Introduction

Motivation to study coprolites

Coprolites are fossilized feces that can be used to observe the diet of extinct organisms such as dinosaurs (Chin, 2007) and, more indirectly, to reconstruct ancient ecosystems (Chin and Gill, 1996). As well as constraining the environment and diet of the organism that produced the feces, coprolites can be a source of geochemical data that provides insight on the fossilization process of the specimen (Bajdek et al., 2014; Chin et al., 2003; Ghosh et al., 2003; Hollocher et al., 2001). In this chapter, the stable carbon isotopes of carbonate minerals in herbivorous dinosaur coprolites are studied to understand the mineralization process of these specimens. Stable carbon isotopes can offer insights into the respiration rates of the abundant microbial fecal and soil communities that produce CO_2 (Cerling, 1984; Sender et al., 2016; Stephen and Cummings, 1980). This CO_2 can be used to induce carbonate mineralization, which allows the carbon isotope composition of coprolite carbonates to be used to elucidate the role of microbial communities in feces in the fossilization of coprolites.

Out of the different diets of fecal-matter-producing organisms (herbivorous, carnivorous, or omnivorous), herbivorous feces pose a greater challenge to preservation due to the lesser amounts of phosphorus (a component of calcium phosphate which can mineralize soft tissues) in comparison to carnivorous coprolites (Hollocher et al., 2001). The herbivorous coprolites in this chapter are dominantly made of calcium carbonate minerals and, given the role that microbes have in biomineralization of calcium carbonate in other settings, it is of interest to investigate the role microbes have in the fossilization of herbivorous coprolites. These carbonates could be recording microbes that represent the dinosaur gut microbiome, as feces are the result of

digestive activity (Stephen and Cummings, 1980), or they could be influenced by the microbes present in the soil environment (Cerling, 1984). With this in mind, in this chapter herbivorous dinosaur coprolites are studied through carbon stable isotopes ($\delta^{13}C$) to reconstruct the microbial respiration rates represented by the carbonate stable isotope composition of the mineralized calcium carbonate in the coprolite samples.

Geological setting and sample description

The herbivorous dinosaur coprolite specimens in this study are from two formations, the Two Medicine Formation and the Kaiparowits Formation (see Table 1 and see Figure 1). The coprolites from the Two Medicine Fm. were first described in Chin and Gill (1996). All of the specimens except BSS-2 were found at the nonmarine Willow Creek Anticline locality, which is

Table 1. Coprolite sample names for the Two Medicine Fm. and Kaiparowits Fm. fossil assemblages. Museum catalog numbers are included in italic below the sample names.

Two Medicine Formation		Kaiparowits Formation	
Specimen ID	**Generalized coprofabric**	**Specimen ID**	**Generalized coprofabric**
BU-89-2 *(MOR 771)*	Woody	BP-12-13 *(DMNH EPV.62494)*	Woody
BSS-2	Woody	WC-13a-4 *(DMNH EPV.98868)*	Woody
HN-94-6 *(MOR 1618)*	Grey	GB-13-103 *(DMNH EPV.67228)*	Grey
TE-2015-19 *(MOR 1624)*	Brown	BR-13-9 *(DMNH EPV.72136)*	Woody
TE-2015-20 *(MOR 1624)*	Amorphous black	GC-13-2 *(DMNH EPV.98867)*	Woody
FN-94-1 *(MOR 1615)*	Grey	BP-12-1 *(DMNH EPV.62494)*	Woody

located at Choteau, Montana. These specimens are catalogued into the Museum of the Rockies (MOR) paleontological collections. The Two Medicine Fm. is formed by the volcaniclastic sediments of the Cordillera Highlands and the Elkhorn Mountain Volcanics, and it is

Figure 1. Locality map showing the approximate location of Two Medicine Fm. and Kaiparowits Fm.

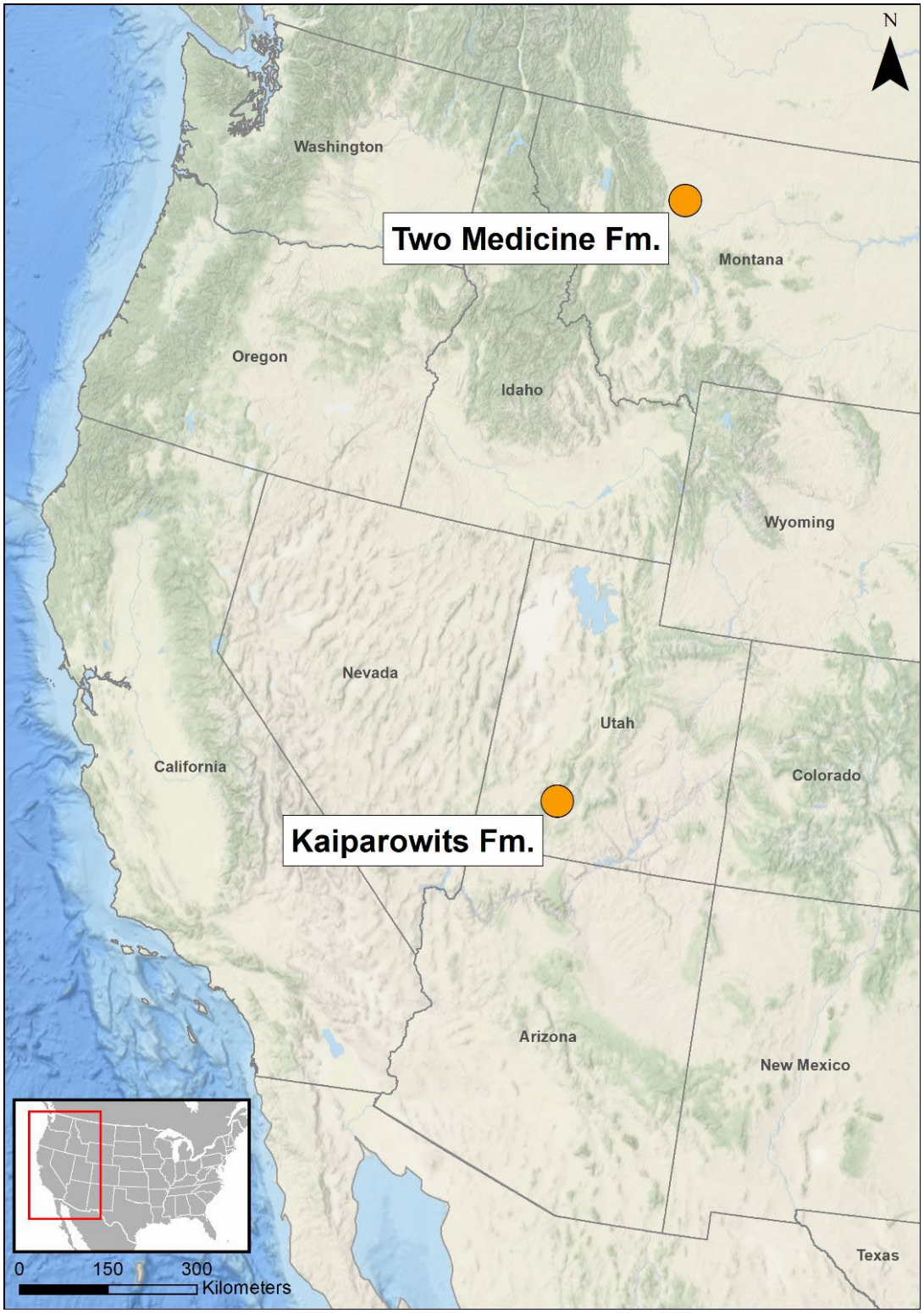

characterized by having fine-grained sand lenses intercalated with mudstones (Rogers et al., 1993). Its environment has been described as warm and semiarid, due to the presence of carbonate nodules, oxidized sediments, and the sparseness of carbonaceous plant remains (Chin, 2007). These Late Campanian feces were most likely deposited around 76.7 Ma (Chin, 2007) by large herbivores, due to the large size of the coprolites and the plant material identified in them. *Maiasaura*, a hadrosaurid dinosaur, is suspected to be the organism that deposited these feces as it is a fairly common fossil organism whose bones and nesting materials are found in the areas near where these samples were collected, which aligns with the herbivorous diet and large size observed in the coprolites (Chin, 2007; Chin and Gill, 1996). Some of the unique features of this Two Medicine Fm. coprolite assemblage are the presence of burrows in the dung associated to invertebrate/insect activity (which could potentially represent a rainy season), the wood fragments inside the specimens, and the carbonaceous preservation of the coprolite material (Chin, 2007; Chin and Gill, 1996).

The second assemblage of coprolites in this study comes from the Kaiparowits Formation of Grand Staircase-Escalante National Monument in southern Utah and are catalogued into the collections of the Denver Museum of Nature & Science. This formation is characterized by fossil-rich mudstones and blue-gray sandstones that were deposited in a low-relief alluvial plain environment, except for a discrete section of the formation that represents a tidally-influenced interval of deposition (Chin et al., 2017; Roberts, 2007; Roberts et al., 2005). Compared to the temperate Two Medicine Fm., the climate at Kaiparowits Fm. is interpreted as more subhumid/subtropical and wet (Chin et al., 2017; Roberts, 2007). The age of this formation is Late Campanian (approximately 76.0-74.1 Ma) (Roberts et al., 2005) and the coprolites found in this location are described by Chin et al. (2017) as rich in plant material and large in size, which

would suggest that these were produced by large herbivorous dinosaurs. Other peculiarities of these coprolites include a calcareous composition, conifer wood fragments preserved in the feces, burrows, and shell-like inclusion in the coprolite deposits (Chin et al., 2017).

Common coprofabrics between Two Medicine Fm. and Kaiparowits Fm. coprolites

The Two Medicine Fm. and Kaiparowits Fm. coprolites are related to each other due to their calcareous composition and the content of the feces. Both coprolite assemblages show wood-eating behavior of the herbivorous feces producers, which could have been assisted by white rot fungi that broke down the wood before ingestion (Chin, 2007; Chin et al., 2017). This is supported by the histological features of the wood fragments, where tracheids were dissociated from each other, a process that requires the breakdown of the lignin that binds the tracheids together in aerobic conditions (Chin, 2007; Chin et al., 2017).

A generalized coprofabric (main petrographic fabric) indicates the predominant composition and preservation shown by a coprolite specimen. Both of these assemblages show two main petrographic coprofabrics: woody and grey (see Table 1). The woody coprofabric usually has preserved fragments of wood that are either more predominant or surrounded by preserved dissociated tracheids that occur in the ground mass around the fragments of wood. On the other hand, grey coprofabrics show a more mottled appearance, with rare presence of small, preserved wood fragments. Grey coprolites are predominantly composed of a more micritic ground mass with indistinct cells, organic matter and sparse tracheids (Chin, 2007). There are other coprofabrics present, like black amorphous and brown, which are less frequent and less described, and represent specimens with very few recognizable plant cells. It is important to note that there can be great heterogeneity within a coprolite specimen and that there are many details and specific fabric variations within a single specimen. Due to the similarities of these two

coprolite assemblages, this study uses specimens from both locations to analyze and compare the carbon stable isotopes ($\delta^{13}C$) signatures preserved in the carbonates of these fossils.

Carbon stable isotopes ($\delta^{13}C$) background and Cerling (1984) soil carbonate model

Isotopes of an element contain the same number of protons (this specifies the element's identity) but a different number of neutrons in the nucleus that alters the mass number of each isotope. Here I focus on "stable" isotopes, in which the nuclei do not decay (Sharp, 2007). Given their stability, compounds that contain these isotopes are processed through physical, chemical, and biological processes at slightly different rates, thus enabling isotope "fractionation" – the separation or sorting of isotopes – to occur. This thesis focuses on carbon isotopes, of which there are two stable varieties: carbon-12 (^{12}C) and carbon-13 (^{13}C). The changes in the ratios of ^{13}C-^{12}C reflect carbon isotope fractionation in nature and these are usually reported with the "delta" notation or δ, in order to quantify the miniscule changes in $^{13}C/^{12}C$ ratios relative to a standard (Sharp, 2007). "Delta" notation is defined in Equation 1.

Equation 1. Delta notation for carbon stable isotopes.

$$\left[\frac{\left(\frac{^{13}C}{^{12}C}\right)_{sample} - \left(\frac{^{13}C}{^{12}C}\right)_{standard}}{\left(\frac{^{13}C}{^{12}C}\right)_{standard}}\right] \times 1000 = \delta^{13}C \; in \; ‰$$

Carbon stable isotope signatures preserved in the geologic record can be influenced by a myriad of biological, chemical, and physical processes. For this study the most important pools of carbon stable isotope delta (δ) values to consider are atmospheric CO_2 and soil-respired CO_2 (or fecal-respired in the case of coprolites) , as these are the primary sources of carbon in soil

carbonate (which are somewhat similar in formation to the coprolites studied here). Atmospheric CO_2 in the Cretaceous period and today is affected by factors such as outgassing from Earth's mantle, plant photosynthesis, the decomposition of biological material and the carbon dioxide-bicarbonate reaction in Earth's oceans (Battin et al., 2009; Falkowski et al., 2000; Sharp, 2007). On the other hand, soil-respired CO_2 is affected by microbial activity and the carbon isotope composition of plant litter in soil, which will be determined by the fraction of plants that perform C_3 or C_4 photosynthesis in an ecosystem (Cerling, 1984; Cerling and Quade, 1993). Microbes in soil will consume the available plant litter and will produce CO_2 through heterotrophic respiration pathways that lead to little carbon isotope fractionation (Blair et al., 1985; Cerling, 1984; Cerling and Quade, 1993; Ryan and Law, 2005).

Both atmospheric CO_2 and soil-respired CO_2 are the main contributors to the $\delta^{13}C$ of preserved soil carbonates in the geologic record since these two end-members will combine in the pore spaces of the soil and enable the precipitation of soil carbonates (Cerling, 1984; Cerling and Quade, 1993). Paleosol carbonates are relevant to this study because of their parallel formation process with the fossilization of calcareous coprolites, since both soil and feces share the common trait of high microbial abundance (Ryan and Law, 2005; Sender et al., 2016; Stephen and Cummings, 1980), and in turn microbially produced CO_2 that can be recorded in the geologic record through carbonate mineralization. Given the calcareous quality of the coprolite assemblages of this study and the potential high microbial content of these coprolites (Hollocher et al., 2001), I adapted the Cerling (1984) model for paleosol carbonate formation to estimate microbial respiration rates in the original feces as it was being mineralized. This procedure has not yet been applied to coprolites.

Previous carbon isotope work in coprolites has focused on reconstructing food webs and identifying organism diet (the C_3 vs. C_4 plant consumption or consumption of other non-plant food sources) through the $\delta^{13}C$ analysis of the organic contents of coprolites (Bajdek et al., 2014; Barrios-de Pedro et al., 2020; Ghosh et al., 2003; Iacumin et al., 1998; Witt et al., 2021). While $\delta^{13}C$ analysis of coprolites has been performed previously, carbonate $\delta^{13}C$ values have rarely been measured in comparison to the organic fraction of carbon in these types of fossils. Kocsis et al. (2014) looked into the $\delta^{13}C$ of phosphatic coprolites and analyzed the trace carbonates present in the samples, and the results pointed to their $\delta^{13}C$ values reflecting the burial conditions and organic matter recycling. Even so, these coprolites were not mineralogically similar to the calcareous assemblages of this study and came from a marine geological setting, which served as further motivation to investigate carbonate $\delta^{13}C$ values and the underlying controls on their variation.

Methods

Sample preparation

To analyze the $\delta^{13}C$ of the organic and carbonates, samples needed to be collected and prepared for the isotopic analysis. Kerogen coprolite powders were used for organic matter analysis. The kerogens represented hydrocarbons that were not soluble in organic solvents (Selley, 2005). These powders were produced by grinding up a small piece of each of the 12 coprolite specimens (see Table 1) from the inner parts of the fossil (this procedure was done by other researchers prior to this study) and extracting the kerogen. The carbonates in the powders were dissolved using 6 M HCl, which was added to the coprolite powder in a 50 mL combusted glass centrifuge tube. The acid was allowed to react with the coprolite powder at room temperature inside a fume hood overnight. Afterwards, the pellets were separated from the solution through centrifugation, and the supernatant solution was removed by decantation. Additional acid was added to check if there were any unreacted carbonates. After the sample was decalcified (as indicated by a lack of reaction when adding more acid), the centrifuge tubes were filled with MilliQ water up to half their volume to rinse the remaining sample three times. The process consisted of centrifuging the samples, decanting the supernatant liquid, and adding MilliQ again until the three rinses were completed. After rinsing the organic matter was isolated from the solution through centrifugation, the supernatant liquid was removed, and the samples were left to dry in a 60° C oven overnight.

For the carbonate $\delta^{13}C$ analysis coprolite specimens were drilled to obtain carbonate powders for two kinds of measurements: bulk composition and targeted sampling. The bulk composition sampling location in each of the 12 coprolites was selected based on three considerations: (1) it was accessible by being easy to drill; (2) drilling it would not compromise the structural integrity of the coprolite; and (3) it represented the most abundant intra-specimen

coprofabric of the coprolite. For the targeted sampling, three coprolite specimens were selected due to the coprofabric variation within each specimen: BP-12-13, BU-89-2, and HN-94-6. The purpose of this sampling was to assess the carbonate $\delta^{13}C$ differences among different textures within each specimen.

Pictures of the coprolites were taken before and after drilling to record the drilling location. The drilling workspace was cleaned before the drilling of each sample with 70% ethanol, to avoid cross contamination between coprolites. The drill bits were also cleaned with ethanol and dried with a Kimwipe prior to drilling each sample. To prepare specimens for drilling, the coprolite surfaces were wiped with ethanol to remove any particulates that could contaminate the powder or interfere with the drilling. The superficial layer of the coprolite was drilled away to access fresh coprolite for collection. Once the superficial layer was removed, the coprolite was drilled and using weighing paper, the powder was collected and then stored in 2 mL plastic centrifuge tubes labeled with the sample's name and drilling location. These carbonate powders were not processed further unlike the organic matter that needed to be extracted before doing the isotope analysis.

A total of 63 samples were collected, of which 51 were carbonate samples and 12 were kerogen organic matter samples. Each carbon isotope sample ID was based on the specimen ID assigned, a letter corresponding to the piece of the coprolite sampled, and a number that specified the drilling location within each specimen (Table 2). Each sample had an assigned intra-specimen coprofabric that described the fabric characteristics specific to the sampling location. In some cases, these were distinct from the generalized coprofabric of each specimen. Also, the distance from the sampling location to the surface of the coprolite specimen was measured for each sample. For samples for which the distance could not be measured, this

distance was estimated as the average of all the measured distances from all the coprolite samples. The organic matter samples were identified only by their specimen ID, given the nature of those samples. Additionally, mineralized sediments, a piece of calcified preserved wood, and carbonate nodules associated with some specimens were analyzed for carbonate carbon stable isotopes.

Table 2. List of carbonates sampled in the coprolite specimens from Two Medicine Fm. and Kaiparowits Fm. Asterisk (*) symbol indicates that measured distance was estimated.

Specimen ID	**Sample ID**	**Formation**	**Intra-specimen coprofabric**	**Measured distance to surface**
BP-12-13	BP-12-13 (R) #1	Kaiparowits Fm.	woody coprofabric	0.72 cm*
BP-12-13	BP-12-13 (R) #2	Kaiparowits Fm.	woody coprofabric	0.72 cm*
BP-12-13	BP-12-13 (R) #3	Kaiparowits Fm.	soft carbonate	0.72 cm*
BP-12-13	BP-12-13 (R) #4	Kaiparowits Fm.	suspected crustacean shell	0.72 cm*
BP-12-13	BP-12-13 (U) #2	Kaiparowits Fm.	woody coprofabric	1.3 cm
BP-12-13	BP-12-13 (U) #3	Kaiparowits Fm.	suspected crustacean shell	1.1 cm
BP-12-13	BP-12-13 (U) #4	Kaiparowits Fm.	soft carbonate	1 cm
BP-12-13	BP-12-13 (U) #5	Kaiparowits Fm.	woody coprofabric	0.6 cm
BP-12-13	BP-12-13 (U) #6	Kaiparowits Fm.	woody coprofabric	1.6 cm
BP-12-13	BP-12-13 (Q) #1	Kaiparowits Fm.	woody coprofabric	0.4 cm
BP-12-13	BP-12-13 (R) #5	Kaiparowits Fm.	suspected crustacean shell	0.72 cm*
BP-12-13	BP-12-13 (R) #6	Kaiparowits Fm.	woody coprofabric	0.72 cm*
BU-89-2	BU-89-2 (E2) #1	Two Medicine Fm.	brown carbonate	2 cm
BU-89-2	BU-89-2 (E2) #2	Two Medicine Fm.	white carbonate	0.5 cm
BU-89-2	BU-89-2 (E2) #3	Two Medicine Fm.	brown carbonate	0.55 cm
BU-89-2	BU-89-2 (E2) #4	Two Medicine Fm.	recrystallized carbonate	0.4 cm
BU-89-2	BU-89-2 (E2) #5	Two Medicine Fm.	woody coprofabric	0.5 cm
BU-89-2	BU-89-2 (E2) #6	Two Medicine Fm.	woody coprofabric	0.5 cm
BU-89-2	BU-89-2 (E2) #7	Two Medicine Fm.	woody coprofabric	1.4 cm

BU-89-2	BU-89-2 (E2) #8	Two Medicine Fm.	recrystallized carbonate	1.9 cm
BU-89-2	BU-89-2 (E1) #1	Two Medicine Fm.	white carbonate	0.4 cm
BU-89-2	BU-89-2 (E1) #2	Two Medicine Fm.	woody coprofabric	0.3 cm
BU-89-2	BU-89-2 (E1) #3	Two Medicine Fm.	cream carbonate	0.35 cm
HN-94-6	HN-94-6 (D) #1	Two Medicine Fm.	backfilled burrow	0.3 cm
HN-94-6	HN-94-6 (D) #2	Two Medicine Fm.	backfilled burrow	0.8 cm
HN-94-6	HN-94-6 (D) #3	Two Medicine Fm.	cream carbonate	0.75 cm
HN-94-6	HN-94-6 (C) #1	Two Medicine Fm.	backfilled burrow	0.2 cm
HN-94-6	HN-94-6 (C) #2	Two Medicine Fm.	grey coprofabric	0.4 cm
HN-94-6	HN-94-6 (C) #3	Two Medicine Fm.	cream carbonate	0.4 cm
HN-94-6	HN-94-6 (C) #4	Two Medicine Fm.	backfilled burrow	0.35 cm
HN-94-6	HN-94-6 (C) #5	Two Medicine Fm.	cream carbonate	0.5 cm
HN-94-6	HN-94-6 (C) #6	Two Medicine Fm.	backfilled burrow	0.8 cm
HN-94-6	HN-94-6 (C) #7	Two Medicine Fm.	backfilled burrow	0.4 cm
HN-94-6	HN-94-6 (E) #1	Two Medicine Fm.	grey coprofabric	0.4 cm
HN-94-6	HN-94-6 (E) #2	Two Medicine Fm.	backfilled burrow	0.3 cm
HN-94-6	HN-94-6 (E) #3	Two Medicine Fm.	backfilled burrow	0.45 cm
HN-94-6	HN-94-6 (G) #2	Two Medicine Fm.	grey coprofabric	0.4 cm
HN-94-6	HN-94-6 (G) #3	Two Medicine Fm.	cream carbonate	0.2 cm
HN-94-6	HN-94-6 (F) #1	Two Medicine Fm.	cream carbonate	0.1 cm
BU-89-2	BU-89-2 (E2) #9	Two Medicine Fm.	predominant coprofabric	2 cm
BSS-2	BSS-2 (D) #1	Two Medicine Fm.	predominant coprofabric	0.6 cm
HN-94-6	HN-94-6 (G) #1	Two Medicine Fm.	predominant coprofabric	0.8 cm

TE-2015-19	TE-2015-19 (A) #1	Two Medicine Fm.	predominant coprofabric	0.6 cm
TE-2015-20	TE-2015-20 (A) #1	Two Medicine Fm.	predominant coprofabric	0.8 cm
FN-94-1	FN-94-1 (B) #1	Two Medicine Fm.	predominant coprofabric	0.3 cm
BP-12-13	BP-12-13 (U) #1	Kaiparowits Fm.	predominant coprofabric	1.5 cm
WC-13a-4	WC-13a-4 (F) #1	Kaiparowits Fm.	predominant coprofabric	0.7 cm
GB-13-103	GB-13-103 (A) #1	Kaiparowits Fm.	predominant coprofabric	0.7 cm
BR-13-9	BR-13-9 (A) #1	Kaiparowits Fm.	predominant coprofabric	1.3 cm
GC-13-2	GC-13-2 (G) #1	Kaiparowits Fm.	predominant coprofabric	0.7 cm
BP-12-1	BP-12-1 (R) #1	Kaiparowits Fm.	predominant coprofabric	0.72 cm*

Isotope Ratio Mass Spectrometry

A ThermoScientific Delta V continuous flow isotope ratio mass spectrometer (CF-IRMS) was used to obtain the $\delta^{13}C$ values for all the samples in this study. Analyses were performed in the University at Colorado Boulder (CU Boulder) Earth Systems Stable Isotope Lab (CUBES-SIL) Core Facility (RRID:SCR_019300). The organic matter samples were combusted in a ThermoScientific Flash 2000 Organic Elemental Analyzer to produce CO_2. A ThermoScientifc GasBench II peripheral was used for the carbonate isotope analysis. To obtain the CO_2 for this peripheral, the sample vials with carbonate were flushed with helium to remove all unwanted atmospheric gases, then heated to 70°C, and finally 5 drops of 105% phosphoric acid were added using a flushed (with helium) syringe to react with the carbonate and release CO_2. Carbon isotope values were corrected using standards NBS-18, Yule marble (CU YULE) and Harding Icelandic Spar (HIS) for the carbonates, and with standards Acetanilide #1, Acetanilide #2, and Pugel for the organics. These corrections assist with potential size dependent effects on the

carbon isotope values and the normalization of the values to the Vienna Pee Dee Belemnite (VPDB) scale.

Respiration rates model

The Cerling (1984) model was adapted to calculate microbial respiration rates of the coprolite samples in this study. In Cerling (1984), the $\delta^{13}C$ of soil air is (δ_s) calculated as the result of the mixture of atmospheric CO_2 and the respired CO_2 by microbes. Microbes will consume the organic matter available in the soil, which is mostly comprised of plant material, and produce CO_2 that will mix with the diffused atmospheric CO_2 in the soil. The plant material in Cerling (1984) can comprise of a mixture of biomass from C_3 and C_4 plants. Equation 2 shows the Cerling (1984) model equation to calculate the $\delta^{13}C$ of soil air is (δ_s).

Equation 2. Cerling (1984) model for calculating $\delta^{13}C$ of soil air.

$$\delta_s = \left(\frac{1}{R_{\mathrm{PDB}}} \left[\frac{\left[\frac{\phi^*}{D_s^*}\left(Lz - \frac{z^2}{2}\right)\right]\left[\frac{D_s^*}{D_s^\beta}\right]\left[\widehat{\delta_\phi}\right] + C_0^* \widehat{\delta_a}}{\frac{\phi^*}{D_s^*}\left(Lz - \frac{z^2}{2}\right)\left[1 - \frac{D_s^*}{D_s^\beta}\widehat{\delta_\phi}\right] + C_0^*\left[1 - \widehat{\delta_a}\right]} \right] - 1 \right) \times 1000$$

Where:

$$\widehat{\delta_\iota} = \left[\frac{\left(\frac{\delta_i}{1000} + 1\right) R_{\mathrm{PDB}}}{1 + R_{\mathrm{PDB}}\left(\frac{\delta_i}{1000} + 1\right)} \right]$$

$\delta_s = \delta^{13}C$ of soil air
$\phi^* =$ Volumetric rate of CO_2 production (in units 10^{-3}moles per m^{-3} per hr^{-1})
$R_{\mathrm{PDB}} =$ Carbon Isotope Ratio ($^{13}C/^{12}C$) of Pee Dee Belemnite
$D_s^* =$ Bulk CO_2 (without isotopic distinction) diffusion coefficient in air (in units cm^2 per s^{-1})
$L =$ Maximum depth of soil profile / No-flux lower boundary (in units cm)
$z =$ Position within depth of soil profile (in units cm)
$D_s^\beta =$ Heavy carbon (^{13}C) CO_2 diffusion coefficient in air
$C_0^* =$ Atmospheric concentration of bulk CO_2 (without isotopic distinction) (in units ppm)
$\delta_a = \delta^{13}C$ of atmospheric CO_2

$\delta_\phi = \delta^{13}C$ of respired CO_2 (will be represented by $\delta^{13}C$ of the plant biomass)

If Equation 2 is rearranged the volumetric rate of CO_2 production (ϕ^*) can be calculated to then obtain the net soil respiration rate. Equation 3 shows the algebraic rearrangement to achieve this.

Equation 3. Rearranged Cerling (1984) model for calculating rate of CO_2 production.

$$\phi^* = \left[\frac{D_s^*}{\left(Lz - \frac{z^2}{2}\right)}\right] * \left[\frac{C_0^*\hat{\delta}_a - \left[\left(\frac{\delta_s R_{PDB}}{1000}\right) + R_{PDB}\right] * \left[C_0^*(1-\hat{\delta}_a)\right]}{\left[\left(\frac{\delta_s R_{PDB}}{1000}\right) + R_{PDB}\right] * \left[1 - \frac{D_s^*\hat{\delta}_\phi}{D_s^\beta}\right] - \frac{D_s^*\hat{\delta}_\phi}{D_s^\beta}}\right]$$

Where:

$$\hat{\delta}_\iota = \left[\frac{\left(\frac{\delta_i}{1000} + 1\right) R_{\mathrm{PDB}}}{1 + R_{\mathrm{PDB}}\left(\frac{\delta_i}{1000} + 1\right)}\right]$$

$\delta_s = \delta^{13}C$ of soil air
ϕ^* = Volumetric rate of CO_2 production (in units 10^{-3}moles per m^{-3} per hr^{-1})
R_{PDB} = Carbon Isotope Ratio ($^{13}C/^{12}C$) of Pee Dee Belemnite
D_s^* = Bulk CO_2 (without isotopic distinction) diffusion coefficient in air (in units cm^2 per s^{-1})
L = Maximum depth of soil profile / No-flux lower boundary (in units cm)
z = Position within depth of soil profile (in units cm)
D_s^β = Heavy carbon (^{13}C) CO_2 diffusion coefficient in air
C_0^* = Atmospheric concentration of bulk CO_2 (without isotopic distinction) (in units ppm)
$\delta_a = \delta^{13}C$ of atmospheric CO_2
$\delta_\phi = \delta^{13}C$ of respired CO_2 (will be represented by $\delta^{13}C$ of the plant biomass)

Once the volumetric rate of CO_2 production (ϕ^*) is calculated, the net soil respiration rate (Q) can be estimated by assuming CO_2 production is equally distributed over a specified distance ($L =$ maximum depth of soil profile), as shown by Equation 4.

Equation 4. Cerling (1984) relationship of rate of CO_2 production and net soil respiration rate.

$$\phi^* = \frac{Q}{L}$$

If rearranged,

$$Q = \phi^* * L$$

$\phi^* =$ Volumetric rate of CO_2 production (in units $10^{-3} moles\ per\ m^{-3}\ per\ hr^{-1}$)
$L =$ Maximum depth of soil profile (in m)
$Q =$ Net soil respiration rate (in units $10^{-3} moles\ per\ m^{-2}\ per\ hr^{-1}$)

With Equations 3 and 4 microbial respiration rates can be calculated from the $\delta^{13}C$ of soil air (δ_s), which can be obtained by incorporating the carbon isotope fractionation between CO_2 and calcite ($CaCO_3$), given that the $\delta^{13}C$ of the coprolite is measured from carbonate minerals, not the soil air directly. To convert the $\delta^{13}C$ of the coprolite carbonate to $\delta^{13}C$ of soil air (δ_s) the fractionation factor between CO_2 and calcite (Sade et al., 2022) was rearranged to obtain Equations 5, 6 and 7.

Equation 5. Calculation of the carbon isotope ratio ($^{13}C/^{12}C$) of coprolite carbonate (calcite).

$$R^{13}_{calcite} = \left[\frac{\delta^{13}C_{calcite}}{1000} + 1\right] * R_{\text{PDB}}$$

$\delta^{13}C_{calcite} = \delta^{13}C$ of coprolite carbonate (calcite)
$R_{\text{PDB}} =$ Carbon Isotope Ratio ($^{13}C/^{12}C$) of Pee Dee Belemnite
$R^{13}_{calcite} =$ Carbon Isotope Ratio ($^{13}C/^{12}C$) of coprolite carbonate (calcite)

Equation 6. Calculation of the carbon isotope ratio ($^{13}C/^{12}C$) of soil air (CO_2) while incorporating temperature dependance.

$$R^{13}_{CO_2} = \left[e^{\frac{\left(-2.4612+7.6663\cdot 10^3/\mathrm{T}-2.9880\cdot 10^6/\mathrm{T}^2\right)}{1000}} \right] * R^{13}_{calcite}$$

T = Temperature during coprolite carbonate (calcite) formation (in Kelvin)
$R^{13}_{CO_2}$ = Carbon Isotope Ratio ($^{13}C/^{12}C$) of soil air (CO_2)
$R^{13}_{calcite}$ = Carbon Isotope Ratio ($^{13}C/^{12}C$) of coprolite carbonate (calcite)

Equation 7. Calculation of the $\delta^{13}C$ of soil air (δ_s) using carbon isotope ratio ($^{13}C/^{12}C$) of soil air (CO_2).

$$\delta_s = \left[\frac{R^{13}_{CO_2} - R_{PDB}}{R_{PDB}} \right] \times 1000$$

$\delta_s = \delta^{13}C$ of soil air
R_{PDB} = Carbon Isotope Ratio ($^{13}C/^{12}C$) of Pee Dee Belemnite
$R^{13}_{CO_2}$ = Carbon Isotope Ratio ($^{13}C/^{12}C$) of soil air (CO_2)

Sensitivity analysis

With the model for the calculation of respiration rates developed, a sensitivity analysis was performed to reconstruct the ancient microbial respiration rates for the coprolite carbonate samples in Table 2 as well as for penecontemporaneous paleosol carbonate nodules studied in Burgener et al. (2019). Suspected crustacean shell coprofabric samples were not included in the sensitivity analysis. These likely represent material that was already crystallized as carbonate prior to consumption and defecation (Chin et al., 2017). The paleosol carbonate nodules from Burgener et al. (2019) were included in this study to assess the differences in the respiration rates of Cretaceous soils versus the coprolites from this study. RStudio and the R Programming

language were utilized to set up the sensitivity analysis using Equations 3, 4, 5, 6, and 7 (the sensitivity analysis code is available in the Supplemental Materials section). For the paleosols, the z and L parameters (the position within depth of soil profile and the maximum depth / no-flux lower boundary, respectively) were estimated based on the model parameters of Licht et al. (2020). All the parameters for the paleosol data were considered as set up in Equations 3-7. For the coprolite carbonate samples some parameters were redefined to fit the coprolite framework. In Equations 3-7 the $\delta^{13}C$ of soil air (δ_s) was redefined to represent the CO_2 reconstructed from the $\delta^{13}C$ of the coprolite carbonate samples (calcite, Table 2), and the net fecal respiration rate (Q) represented the net coprolite respiration rate. The z and L parameters (the position within depth of soil profile and the maximum depth / no-flux lower boundary, respectively) were reinterpreted as the position within the coprolite volume (z) (with volume estimated as a sphere with $V = \frac{4}{3}\pi r^3$) and the maximum distance of the feces material to the surface of the coprolite, where it is in contact with the atmosphere (L). These two parameters are shown in Figure 2. For this sensitivity analysis it was assumed that the coprolite was in contact with the atmosphere and not buried in the soil.

To solve for the fractionation of CO_2 to calcite shown in Equation 6, temperature values from Burgener et al. (2019) for the Two Medicine Fm. and Kaiparowits Fm. were utilized to estimate the temperature present when the coprolites were deposited as fresh feces. It was assumed that that the feces were not buried, so the values for air temperature found in Table 5 in Burgener et al. (2019) were used for the coprolite carbonate-CO_2 fractionation calculation. For calculation of rates associated with the Burgener et al. (2019) paleosol $\delta^{13}C$ data, the clumped isotope temperature reconstructions associated with each paleosol sample were utilized for the

Figure 2. Position within the coprolite volume (z) and the maximum distance of the feces to the surface of the coprolite (L). Surface of the coprolite is represented by the black outline surrounding the schematic feces, the white line represents the maximum distance from the coprolite surface to the deepest feces material (L), and the black bracket shows the possible positions within the coprolite volume (z) along the total L. White bubbles represent potential coprolite pore space.

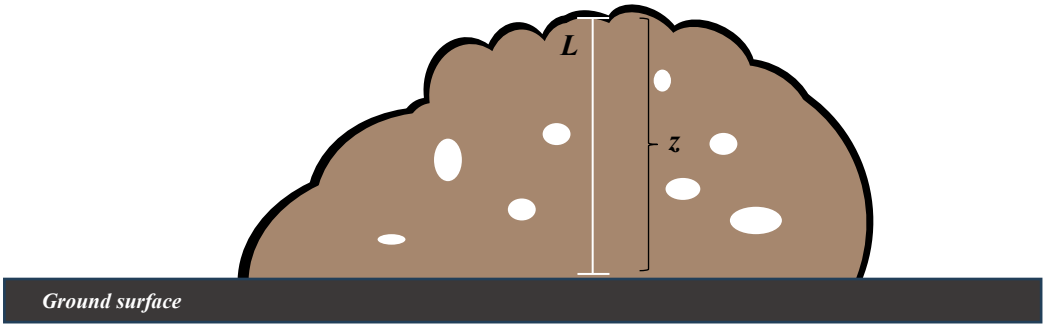

fractionation estimates since the clumped isotope temperature reconstructions reflect the carbonate formation temperature (Burgener et al., 2019).

For the atmospheric concentration of bulk CO_2 (C_0^*), the $\delta^{13}C$ of atmospheric CO_2 (δ_a), and the $\delta^{13}C$ of respired CO_2 (δ_ϕ) values in the sensitivity analysis, estimates were obtained from the literature. Sources were Foster et al. (2017), Barral et al. (2017), and Cornwell (2017) respectively. The data used from Foster et al. (2017) and Barral et al. (2017) was constrained based on the estimated age of all the coprolites in the study, 74.1-76.7 Ma (personal communication with Dr. Karen Chin). For these datasets the minimum and maximum values during the time period of the coprolites' fecal deposition were used. The Cornwell (2017) database was filtered to only include C_3 plant carbon isotope data, given that there were no C_4 plants in the Cretaceous (Edwards, 2014). All the other parameters not described in this Sensitivity Analysis section were obtained from Cerling (1984). Table 3 shows the parameter setup for the coprolite carbonate samples sensitivity analysis and Table 4 shows the parameter setup for the Burgener et al. (2019) paleosol $\delta^{13}C$ data sensitivity analysis. For the values set up as a distribution, the sensitivity analysis sampled from the set-up distribution

minimum/maximum or mean/standard deviation, depending on the distribution type. For each trial in the analysis, all parameters (represented by a distribution) were sampled so each trial contained a unique value for the calculation of the respiration rate. This resampling process was followed for both the coprolite carbonates and paleosols in order to obtain all the rates possible for each sample based on the uncertainties for each parameter.

Table 3. Parameter setup for calculation of coprolite respiration rates.

Model Parameter	**Parameter Value**	**Units**	**Distribution Type or Constant**	**Source**
Bulk CO_2 diffusion coefficient in air (D_s^*)	0.02	cm^2 per s^{-1}	Constant	Cerling (1984)
Heavy carbon (^{13}C) CO_2 diffusion coefficient in air (D_s^β)	1.004	cm^2 per s^{-1}	Constant	Cerling (1984)
Maximum distance of the feces material to the surface of the coprolite / No-flux lower boundary (L)	10	cm	Constant	Estimated based on sphere approximation applied to feces estimated volumes in Chin (2007)
Position within the coprolite volume (z)	Minimum z was estimated based on the measured distance to the surface of the coprolite obtained for each sample (see Table 2). Maximum z was constrained by L.	cm	Uniform distribution	This study and Chin (2007)
Atmospheric concentration of bulk CO_2 (without	Minimum = 212.3 Maximum = 1079.3	ppm	Uniform distribution	Foster et al. (2017)

isotopic distinction) (C_0^*)				
$\delta^{13}C$ of atmospheric CO_2 (δ_a)	Minimum = -7.3 Maximum = -5.0	‰	Uniform distribution	Barral et al. (2017)
$\delta^{13}C$ of coprolite carbonate ($\delta^{13}C_{calcite}$)	Mean = Measured $\delta^{13}C$ of coprolite carbonate samples (see Table 2 for sample names) Standard deviation = 0.1 (due to mass spectrometer analytical precision)	‰	Normal distribution	This study
$\delta^{13}C$ of coprolite air (δ_s)	Once $\delta^{13}C_{calcite}$ is resampled value is calculated with Equations 5-7	‰	Constant	This study and Sade et al. (2022)
Carbon Isotope Ratio ($^{13}C/^{12}C$) of Pee Dee Belemnite (R_{PDB})	0.011	none	Constant	Cerling (1984)
$\delta^{13}C$ of respired CO_2 (represented by $\delta^{13}C$ of the plant biomass in coprolite) (δ_ϕ)	Mean = -28.7 Standard Deviation = 2.68	‰	Normal distribution	Cornwell (2017)
Temperature during carbonate formation (T) for Two Medicine Fm. samples	Minimum = 11 Maximum = 21	°C	Uniform distribution	Burgener et al. (2019)
Temperature during carbonate formation (T) for Two Medicine Fm. samples	Minimum = 18 Maximum = 22	°C	Uniform distribution	Burgener et al. (2019)
Number of trials	10,000	-	-	-

Table 4. Parameter setup for calculation of paleosol respiration rates.

Model Parameter	**Parameter Value**	**Units**	**Distribution Type or Constant**	**Source**
Bulk CO_2 diffusion coefficient in air (D_s^*)	0.02	cm^2 per s^{-1}	Constant	Cerling (1984)
Heavy carbon (^{13}C) CO_2 diffusion coefficient in air (D_s^β)	1.004	cm^2 per s^{-1}	Constant	Cerling (1984)
Maximum depth of soil profile / No-flux lower boundary (L)	Minimum = 80 Maximum = 120	cm	Uniform distribution	Licht et al. (2020)
Position within depth of soil profile (z)	Minimum = 40 Maximum = 60	cm	Uniform distribution	Licht et al. (2020)
Atmospheric concentration of bulk CO_2 (without isotopic distinction) (C_0^*)	Minimum = 212.3 Maximum = 1079.3	ppm	Uniform distribution	Foster et al. (2017)
$\delta^{13}C$ of atmospheric CO_2 (δ_a)	Minimum = -7.3 Maximum = -5.0	‰	Uniform distribution	Barral et al. (2017)
$\delta^{13}C$ of paleosol carbonate ($\delta^{13}C_{calcite}$)	Mean = Measured $\delta^{13}C$ of paleosol carbonate Standard deviation = Reported standard deviation for each paleosol carbonate sample	‰	Normal distribution	Burgener et al. (2019)
$\delta^{13}C$ of soil air (δ_s)	Once $\delta^{13}C_{calcite}$ is resampled value is calculated with Equations 5-7	‰	Constant	Burgener et al. (2019) and Sade et al. (2022)

Carbon Isotope Ratio ($^{13}C/^{12}C$) of Pee Dee Belemnite (R_{PDB})	0.011	none	Constant	Cerling (1984)
$\delta^{13}C$ of respired CO_2 (represented by $\delta^{13}C$ of the plant biomass in coprolite) (δ_ϕ)	Mean = -28.7 Standard Deviation = 2.68	‰	Normal distribution	Cornwell (2017)
Temperature during carbonate formation (T)	Mean = Clumped isotope temperature data for each measured paleosol carbonate Maximum = Reported standard deviation for each paleosol carbonate sample clumped isotope temperature	°C	Normal distribution	Burgener et al. (2019)
Number of trials	10,000	-	-	-

L and z sensitivity analysis

To test the effects of coprolite size on the coprolite samples' respiration rates an additional sensitivity analysis was performed by varying the *z* and *L* parameters in the model. All other parameters were kept the same as Table 3. The purpose of this was to test if the respiration rates obtained were affected by changes in *z* and *L* or if they were mostly controlled by the $\delta^{13}C$ of coprolite carbonate ($\delta^{13}C_{calcite}$). By varying these parameters, it could also be assumed that each $\delta^{13}C_{calcite}$ value represents a carbonate nodule in the soil at varying depths, assuming the coprolite was buried instead of direct contact with the atmosphere like in the main sensitivity analysis. The maximum distance of the coprolite to the surface (*L*) parameter (where there is direct contact with the atmosphere) was tested with *L* = 100 cm, 200 cm, 300 cm, 400 cm, 500 cm, 5000 cm, where *z* would be randomly sampled from a uniform distribution between *z* = 0.1

cm and $z = L$ cm. L would be the maximum depth and a $z = 0.1$ cm would be near the surface that is in contact with the atmosphere. An additional test was performed (only for predominant coprofabrics) where $z = L$ and both parameters were fixed at the measured distance of the sampling location to the surface of the coprolite obtained for each sample (see Table 2). The aim for this was to model more extreme respiration rates, given that the small z would imply close proximity to atmospheric CO_2 and would require respiration rates to be higher to maintain a lower value for the δ_s.

Modern soil and manure respiration rates

Modern soil respiration rates were obtained from Jian et al. (2021) and modern manure rates were obtained for cattle, hens, pigs, and humans (Castro-Herrera et al., 2023; Chowdhury et al., 2014; Cronjé et al., 2004). These values were collected from the literature to compare with the calculated respiration rates for the coprolites and the paleosols. For the modern soil respiration rates the annual carbon flux from soil respiration (in g C m^{-2}, *Rs_annual*) was converted into units 10^{-3}moles per m^{-2} per hr^{-1} in order to be able to compare it to the calculated rates. As well, the data was filtered to only include Temperate (excluding Desert ecosystem types), Mediterranean, and Subtropical biomes given that the Two Medicine Fm. and Kaiparowits Fm. are suggested to represent temperate and subtropical climates, respectively (Chin et al., 2017; Roberts, 2007). Modern manure rates were usually reported in units of $g\ CO_2 - C\ per\ kg^{-1}\ of\ Total\ Solids\ per$ hr^{-1} , $g\ CO_2\ per\ kg^{-1}\ of\ Total\ Solids\ per$ hr^{-1} or $g\ CO_2 - C\ per\ m^{-2}\ per$ day^{-1} and were collected from tables and figures. The units of the collected data were converted into 10^{-3}moles per m^{-2} per hr^{-1} using their corresponding studies and Wang et al. (2019) to be able to compare with the calculated respiration rates. Conversion details can be found in the Supplemental Materials section.

Results

Coprolite kerogen organic carbon stable isotopes

Kerogen powders were acidified to remove any carbonates from the sample successfully. Although an exact percentage of kerogen versus carbonates was not obtained for each specimen, overall, it was observed that the samples were mostly composed of carbonate with minimal organic carbon present. This is congruent with Hollocher et al. (2001) where it was shown that the yield of the acidification preparation was around 0.2% for a Two Medicine Fm. coprolite. Once prepared, the IRMS analyzed organic carbon from kerogens had variable carbon percentages (from 0.15% to 43%), with the grey coprolites showing the lowest carbon percentages relative to the other coprofabrics present. Nevertheless, the carbon stable isotopes of kerogen ($\delta^{13}C_{OM}$) were fairly consistent, with most samples showing values between -20‰ and -24‰ (see Table 5). The results are consistent with the range of values of C_3 photosynthesis, which is presumed to be the only type of photosynthesis present in the Cretaceous (Tipple and Pagani, 2007).

Table 5. Carbon stable isotope results for organic carbon from coprolite kerogens.

Specimen ID	**$\delta^{13}C_{OM}$ (‰)**	**Formation**
BU-89-2	-20.6	Two Medicine Fm.
BSS-2	-21.0	Two Medicine Fm.
HN-94-6	-23.5	Two Medicine Fm.
TE-2015-19	-21.5	Two Medicine Fm.
TE-2015-20	-21.1	Two Medicine Fm.
FN-94-1	-20.5	Two Medicine Fm.
BP-12-13	-21.8	Kaiparowits Fm.
WC-13a-4	-21.5	Kaiparowits Fm.
GB-13-103	-23.5	Kaiparowits Fm.
BR-13-9	-21.4	Kaiparowits Fm.
GC-13-2	-21.8	Kaiparowits Fm.
BP-12-1	-21.8	Kaiparowits Fm.

Predominant coprofabric coprolite carbonate carbon stable isotopes

The predominant coprofabric in each coprolite was sampled to obtain carbonates for carbon and oxygen isotopic analyses. These analyses showed great variability in the $\delta^{13}C$ and oxygen stable isotope ($\delta^{18}O$) values between samples (see Figure 3). This variability was broader for $\delta^{13}C$ than $\delta^{18}O$. Samples from the Kaiparowits Fm. were more clustered together, probably due to most of them sharing a similar woody coprofabric, compared to the Two Medicine Fm. coprolites. The Kaiparowits' coprolites show an approximately 10‰ variation in $\delta^{13}C$ and an approximately 3‰ variation in $\delta^{18}O$. Comparably, the Two Medicine Fm. coprolites range from approximately -15‰ to 10‰ VPDB in $\delta^{13}C$ and from approximately -16‰ to -10‰ VPDB in $\delta^{18}O$.

Figure 3. Carbonate carbon and oxygen stable isotopes for predominant coprofabrics sampled in each coprolite specimen.

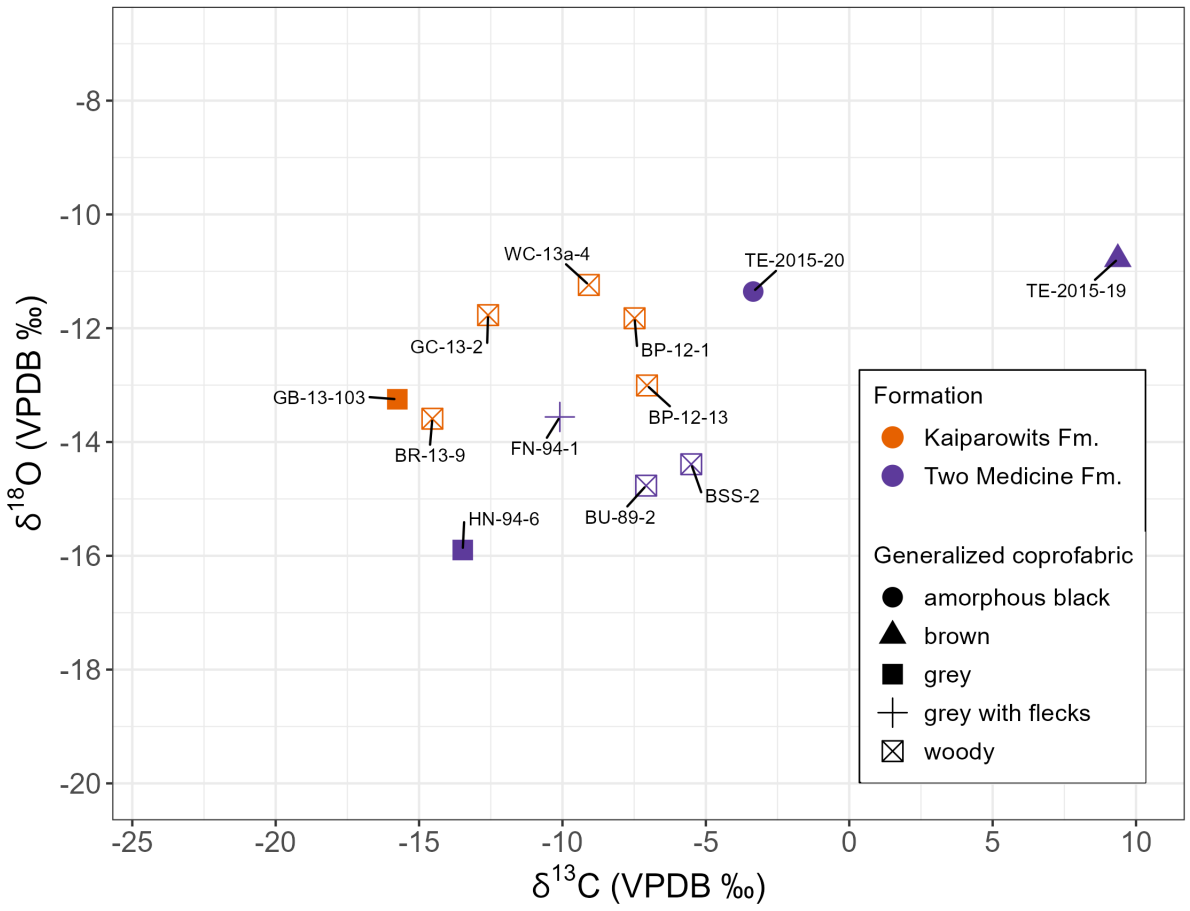

Sediment, wood, and carbonate nodule carbonate carbon stable isotopes

Coeval, non-coprolite supporting samples were only obtained for specimens with field numbers TE, BP, BU, WC, and GB (see Table 6). It is important to note that most of these samples were not attached to the coprolite surface but were instead found in a similar horizon to or near the coprolite specimens. Although some $\delta^{13}C$ values were somewhat close to the predominant coprofabric $\delta^{13}C$ values, no sediment, wood, or carbonate nodule samples directly overlap with their respective coprolite specimens.

Table 6. Carbonate carbon stable isotopes for sediment, wood, and carbonate nodules.

Sample	**Formation**	**Associated specimen**	**Type**	**Replicates**	$\boldsymbol{\delta^{13}C}$ **(‰)**	$\boldsymbol{\delta^{18}O}$ **(‰)**	**Notes**
TM-SED-TE-2015	Two Medicine Fm.	TE	sediment	n = 2	-2.7	-8.9	Obtained from surface of TE coprolite
					-1.6	-6.4	
K-SED-BP	Kaiparowits Fm.	BP	sediment	n = 2	-0.8	-7.5	Sampled from same level as BP coprolite
					1.2	-5.4	
BU-W-2 (B) #1	Two Medicine Fm.	BU	non-ingested calcareously preserved wood	n = 1	-4.8	-13.8	Sampled from intact wood unaffected by white-rot fungi
K-CAL-WC	Kaiparowits Fm.	WC	carbonate nodule	n = 1	-11	-8.3	Sampled near WC coprolite
TM-SED-GB-13	Two Medicine Fm.	GB	sediment	n = 1	-0.3	-8.7	Obtained from container storing GB coprolite

Targeted sampling of carbonates within specimens BU-89-2, HN-94-6, and BP-12-13

Specimens BU-89-2, HN-94-6, and BP-12-13 were sampled multiple times within each specimen to assess the variability of $\delta^{13}C$ and $\delta^{18}O$ in the carbonates of each specimen. Each sample within a specimen was assigned an intra-specimen coprofabric (see Table 7) that described the characteristics and details of each sample obtained (within the context of the generalized coprofabric). It is important to note that these intra-specimen coprofabrics could not always be supported by thin section to confirm the microscopic components present in the sample and that most of these were based on the macroscopic appearance of the coprolite sample. An example of where the intra-specimen coprofabrics were sampled and how a same coprofabric can vary is shown in Figure 4. The results for the $\delta^{13}C$ and $\delta^{18}O$ of the carbonates sampled in specimens BU-89-2, HN-94-6, and BP-12-13 can be found in Figures 5, 6 and 7.

Table 7. Description of intra-specimen coprofabrics observed in the targeted-sampled coprolites.

Intra-specimen coprofabric	**Description**
Woody coprofabric	Similar to the generalized woody coprofabric, this describes areas of the coprolite that are likely dominated by preserved disassembled tracheids and preserved wood fragments as described in Chin (2007). There is a spectrum of the level of "woodiness" of each sample, some may contain more wood fragments, meanwhile others might have a higher abundance of a matrix of disassembled tracheids.
Grey coprofabric	Like the generalized grey coprofabric, this describes areas of the coprolite that are likely dominated by preserved indistinct plant cells, very small wood fragments, isolated tracheids, and amorphous organic matter as described in Chin (2007).
Soft carbonate	Represents an intra-specimen coprofabric that could not be related to either grey or woody generalized coprofabrics. It is characterized by its white color and crumbly texture in comparison to the rest of a coprolite. It is usually found in association with the suspected crustacean shell. It could have preserved plant material, but it has not been confirmed by thin section.
Suspected crustacean shell	Although not directly confirmed by thin section for the samples in this study, this coprofabric is supported by the

	confirmed presence of crustacean cuticle fragments in other parts of BP specimens (shown in Chin et al. (2017).
Cream carbonate	Although not directly confirmed by thin section for the samples in this study, it has been observed that these cream carbonates could represent preserved colorless indistinguishable plant cells. Alternatively, though less likely, some cream carbonates could represent sediments preserved in the coprolite.
Backfilled burrows	These are described in detail by Chin and Gill (1996). They can be viewed macroscopically and show the activity of dung beetles that make burrows that are then infilled with sediment and feces material from the coprolite (prior to fossilization) and their surroundings.
White carbonate	This is present in a similar color as the soft carbonate, but it does not share its texture (it is hard. The details of this coprofabric are unknown.
Brown carbonate	Only identified as an intra-specimen coprofabric in in the BU-89-2 specimen, this is seen as an oval patch in the middle of the specimen when cross-sectioned. Its composition and details are unknown.
Recrystallized carbonate	Represents patches and veins that contained carbonate crystals that were not as micritic (as the rest of the preserved coprolite), larger, and a white translucent color.

Figure 4. Example of targeted sampling locations in a piece of specimen BP-12-13.

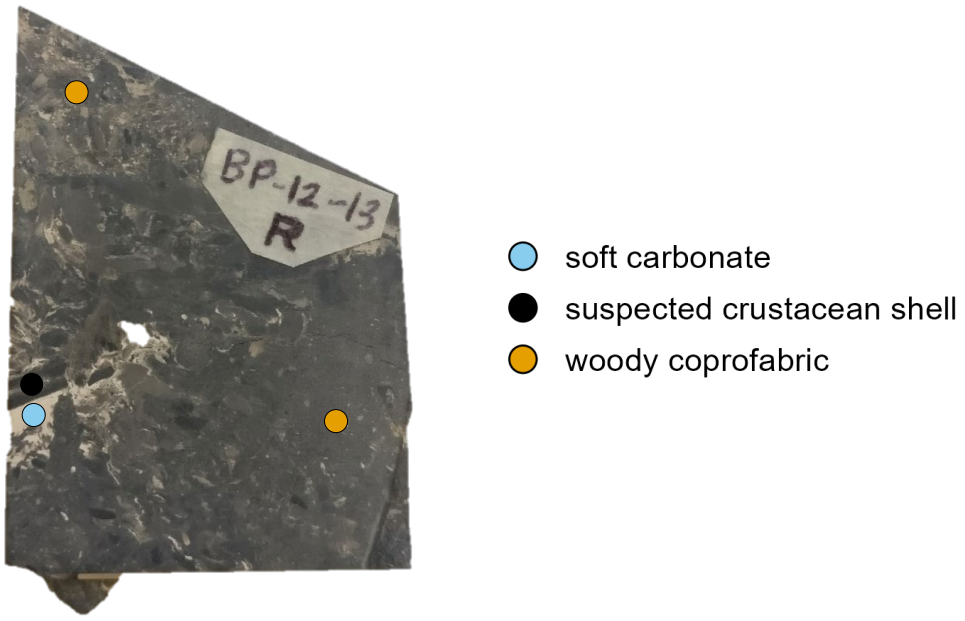

Figure 5. Carbonate carbon and oxygen stable isotopes results for targeted sampling of BU-89-2.

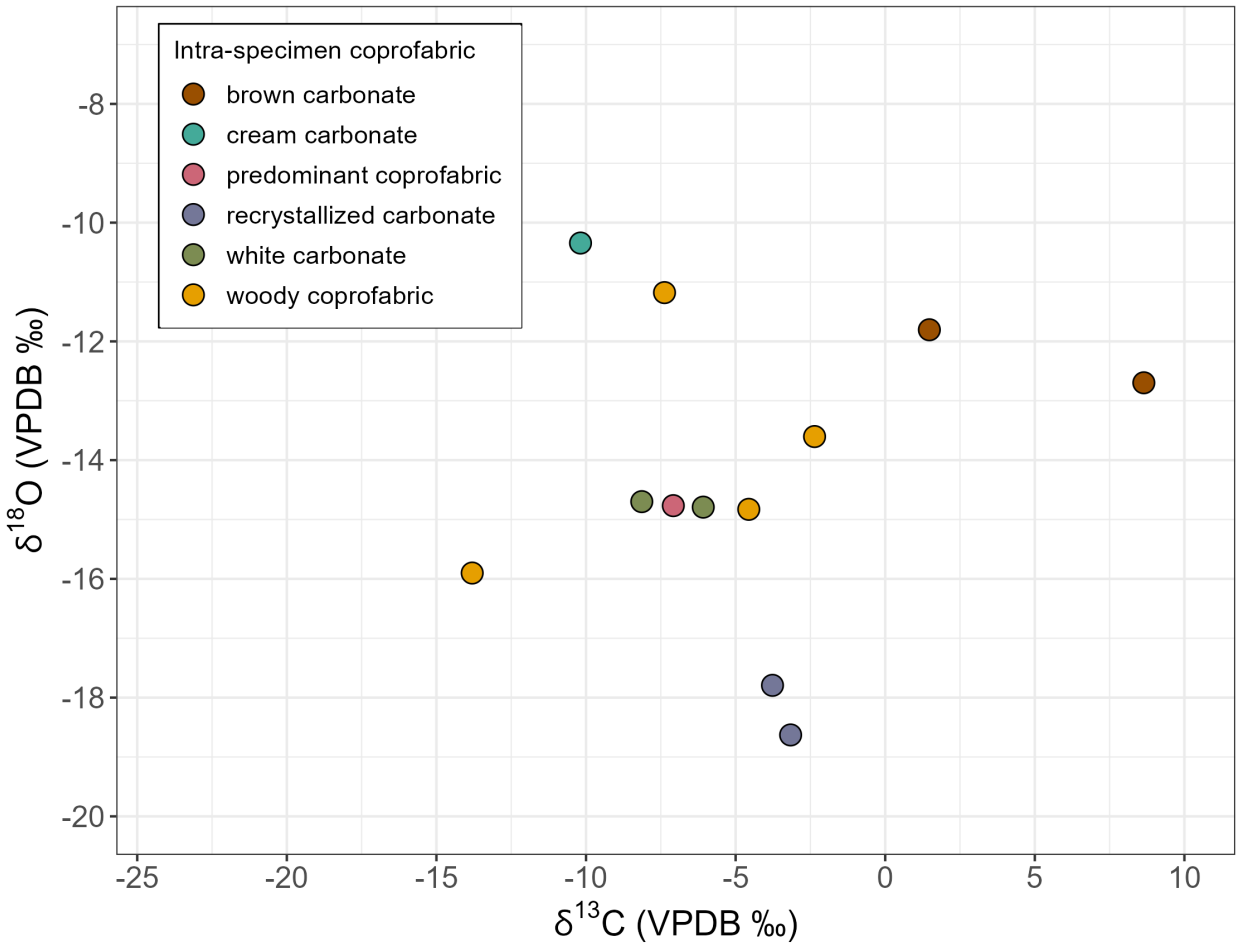

Figure 6. Carbonate carbon and oxygen stable isotopes results for targeted sampling of HN-94-6.

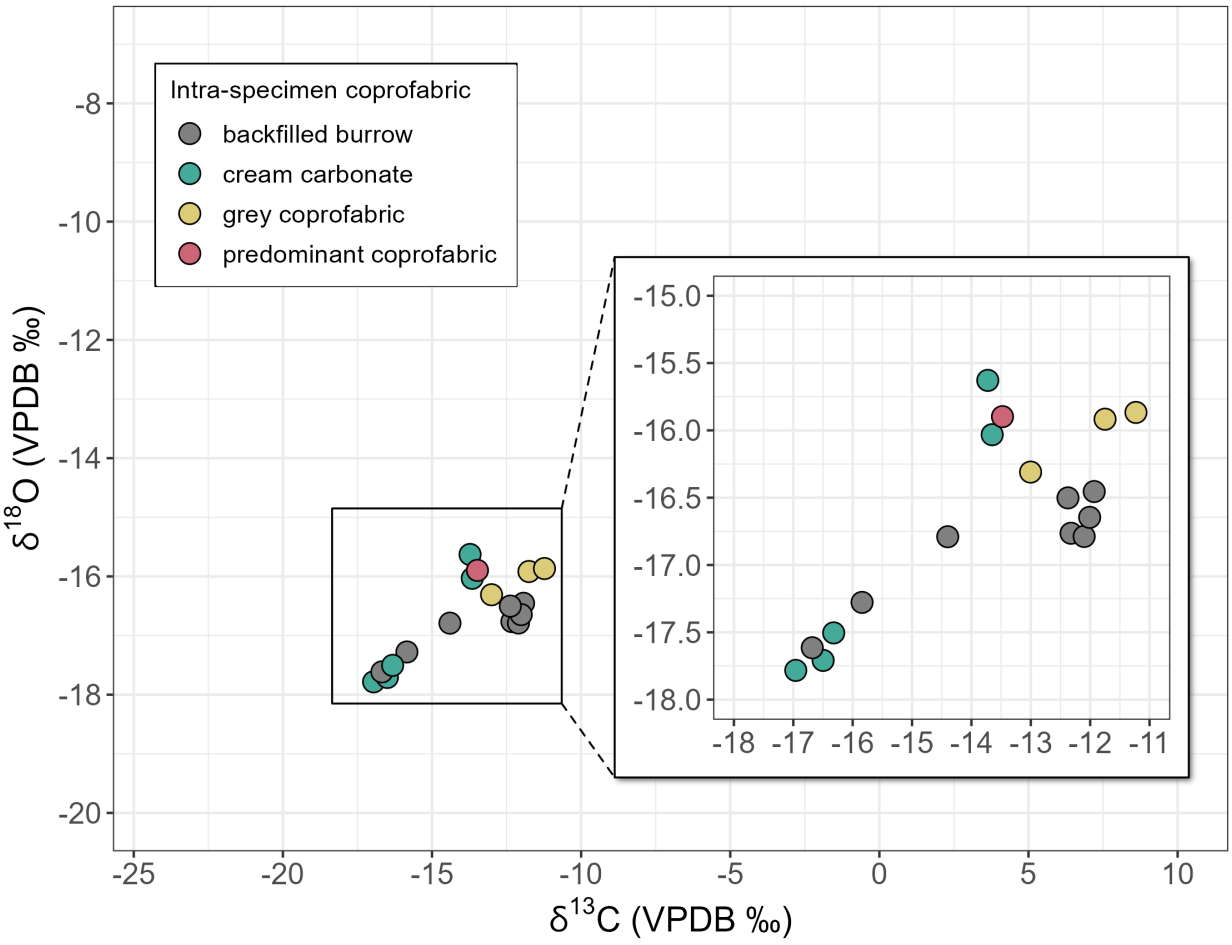

Figure 7. Carbonate carbon and oxygen stable isotopes results for targeted sampling of BP-12-13.

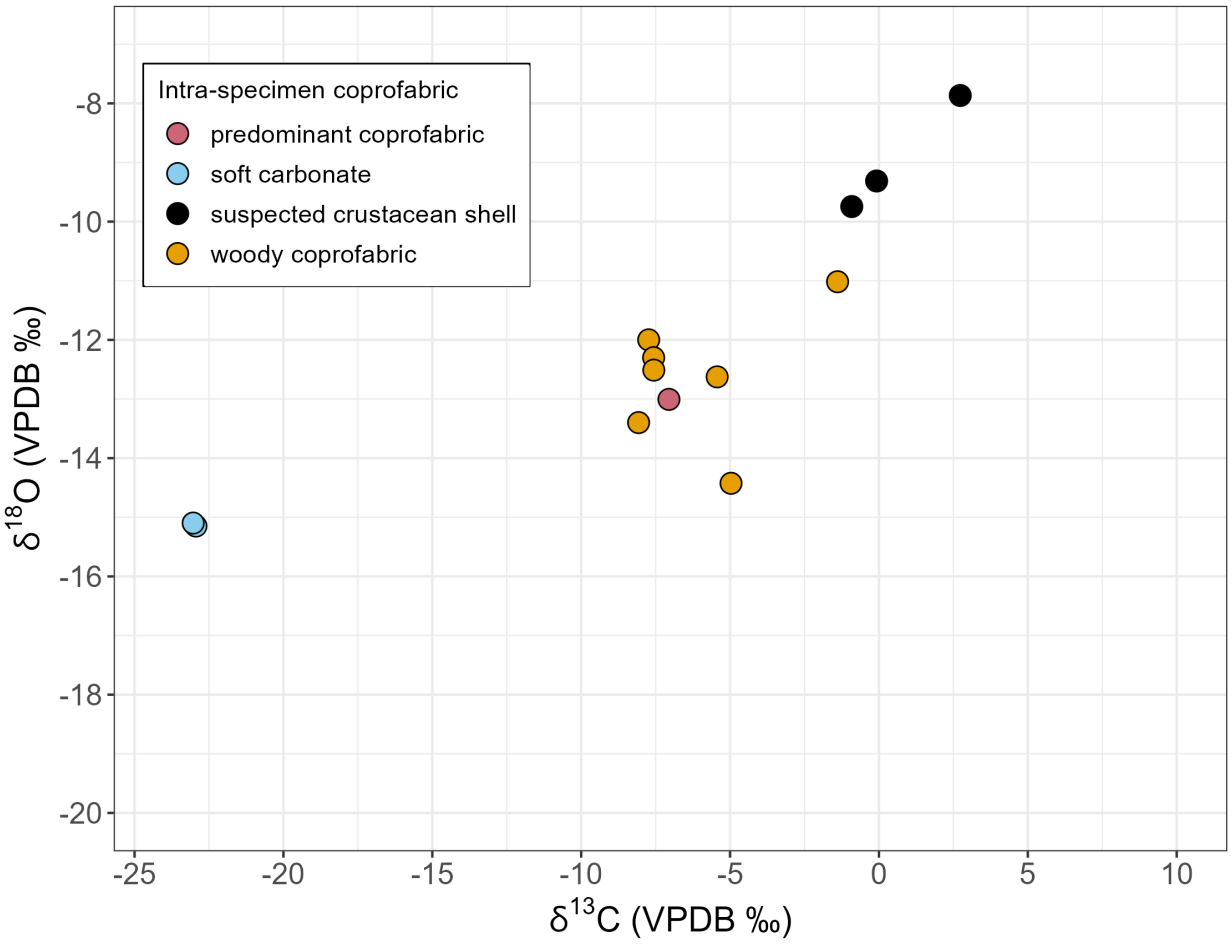

Overall, it was seen that there is variability when it comes to the $\delta^{13}C$ and $\delta^{18}O$ values of different intra-specimen coprofabrics. In both $\delta^{13}C$ and $\delta^{18}O$ space, there were variations of at least approximately 6‰ -7‰ within a single coprolite (of the ones with targeted sampling). The coprolite that showed the least range in values was HN-94-6, which has a general grey coprofabric. In comparison the other two coprolites with woody coprofabric showed a greater spread of carbon and oxygen isotope values. This could be consistent with the features of the respective coprofabrics, given that woody coprolites tend to have more heterogeneity within them than grey coprolites.

Discussion

To interpret the $\delta^{13}C$ results obtained for the carbonates in the coprolite specimens in this study, the Cerling (1984) soil respiration rates model was adapted (Equation 3) to calculate the respiration rates of the feces. The results for the respiration rates can be found in Figures 8, 9, 10, 11, and 12. Each figure shows density plots that represent the distribution of the respiration rates of each $\delta^{13}C$ value, and the bandwidth for the density plots was the default chosen by the ggridges R package. Each figure contains subsets of the coprolite data as follows: predominant coprofabrics of all the Two Medicine Fm. specimens in the study (Figure 8), predominant coprofabrics of all the Kaiparowits Fm. specimens in the study (Figure 9), coprofabrics sampled in BU-89-2 (Figure 10), coprofabrics sampled in HN-94-6 (Figure 11), and coprofabrics sampled in BP-12-13 (Figure 12). Every specimen-specific figure includes the corresponding rates for the predominant coprofabric showed in Figures 8 and 9. Additionally, each plot shows the results of the model applied to the $\delta^{13}C$ data for the paleosols in Burgener et al. (2019). The paleosol respiration rates shown in all figures correspond to the specific formation considered for the coprolite (either Two Medicine Fm. or Kaiparowits Fm.). Furthermore, each figure shows modern soil respiration rates (Jian et al., 2021) to compare to the coprolite rates. $\delta^{13}C$ values that did not yield a statistically significant number of rates were not included in these figures. As well, materials that were mineralized prior to ingestion (the crustacean shell) were not included.

Figure 8. Minimum and maximum modeled respiration rates for predominant coprofabrics of Two Medicine Fm. coprolites. Minimum rates were modeled with z sampled between the measured distance of the sampling location to the surface of the coprolite obtained for each sample and L =10 cm. Maximum rates modeled with z equal to the measured distance of the sampling location to the surface of the coprolite obtained for each sample and L = z. Dotted line represents median respiration rates for Two Medicine Fm. paleosols and dot and dash line represents the median soil respiration rates for modern soils. Labels show the specimen ID of rates.

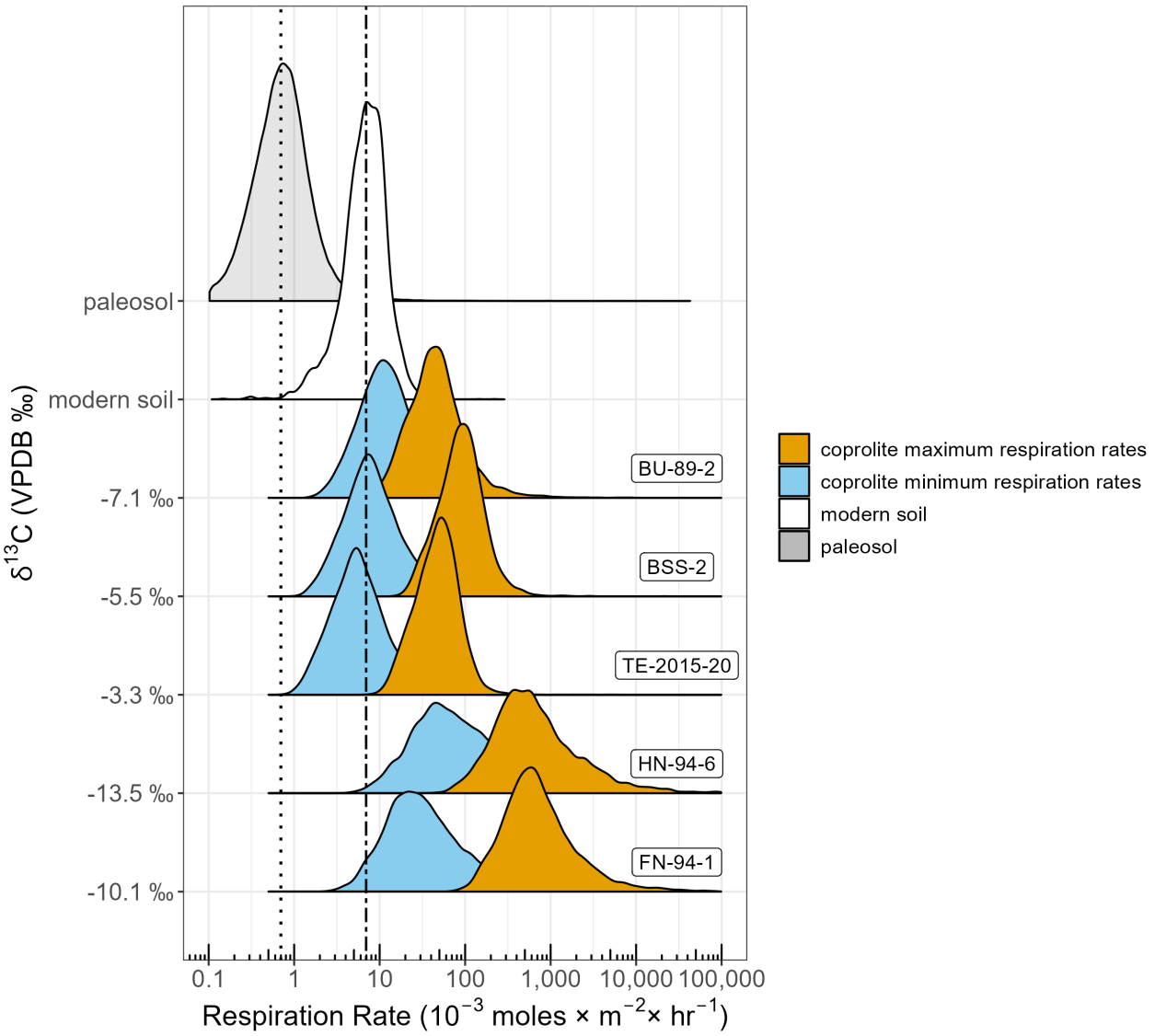

Figure 9. Minimum and maximum modeled respiration rates for predominant coprofabrics of Kaiparowits Fm. coprolites. Minimum rates were modeled with z sampled between the measured distance of the sampling location to the surface of the coprolite obtained for each sample and L =10 cm. Maximum rates modeled with z equal to the measured distance of the sampling location to the surface of the coprolite obtained for each sample and L = z. Dotted line represents median respiration rates for Kaiparowits Fm. paleosols and dot and dash line represents the median soil respiration rates for modern soils. Labels show the specimen ID of rates.

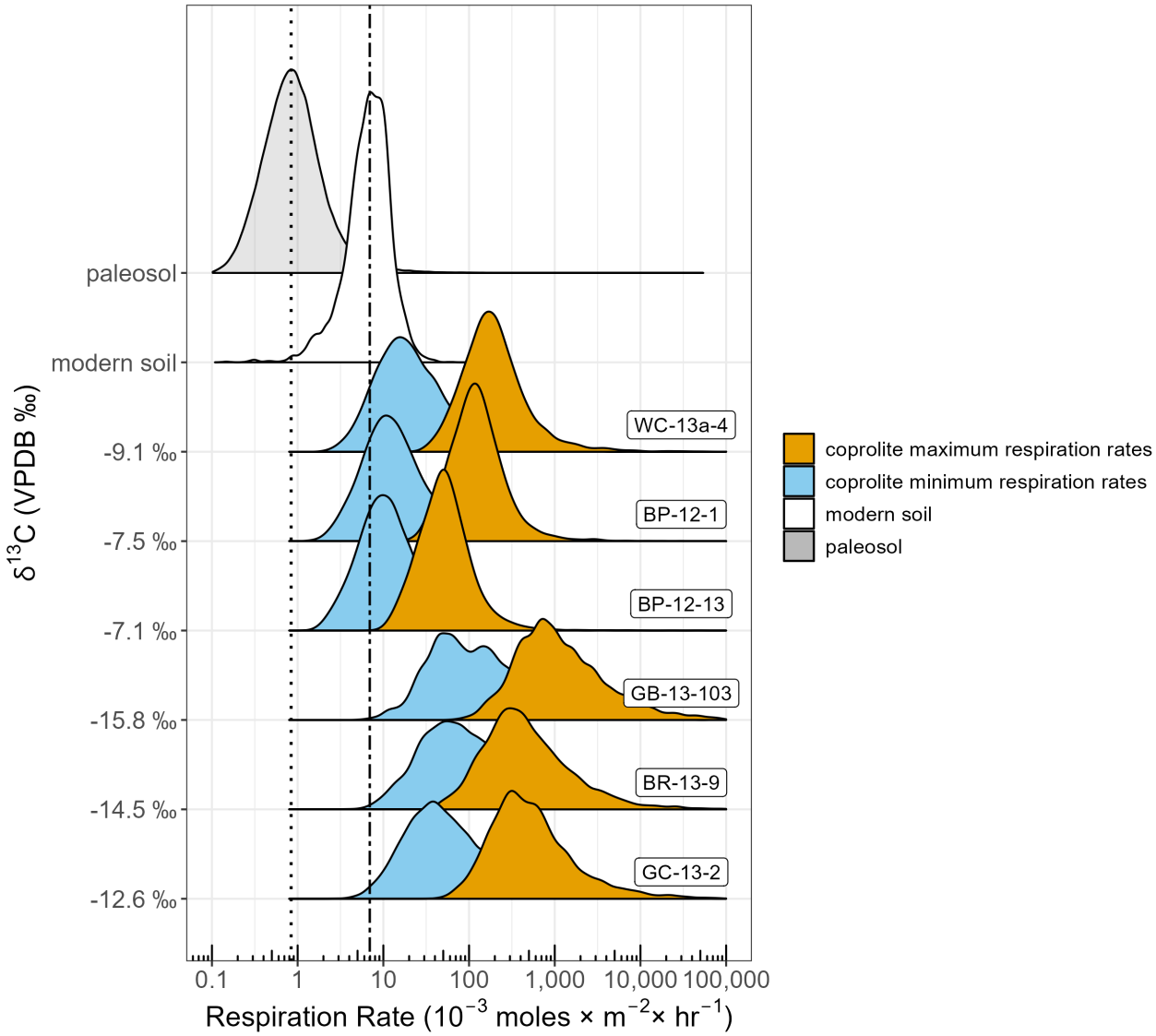

Figure 10. Respiration rates for targeted sampling done for coprolite BU-89-2, modeled per the parameters of Table 3. Dotted line represents median respiration rates for Two Medicine Fm. paleosols and dot and dash line represents the median soil respiration rates for modern soils.

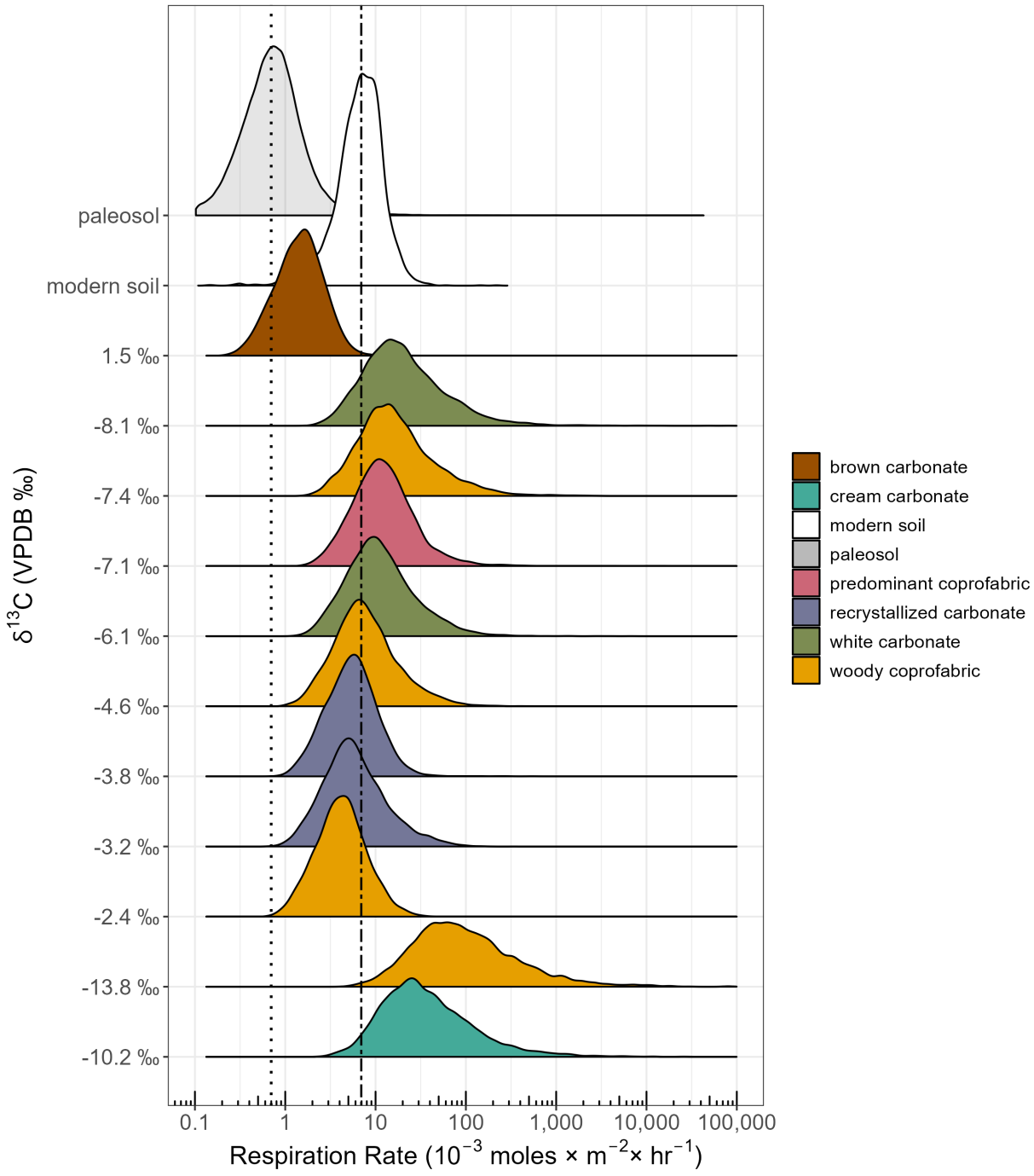

Figure 11. Respiration rates for targeted sampling done for coprolite HN-94-6, modeled per the parameters of Table 3. Dotted line represents median respiration rates for Two Medicine Fm. paleosols and dot and dash line represents the median soil respiration rates for modern soils.

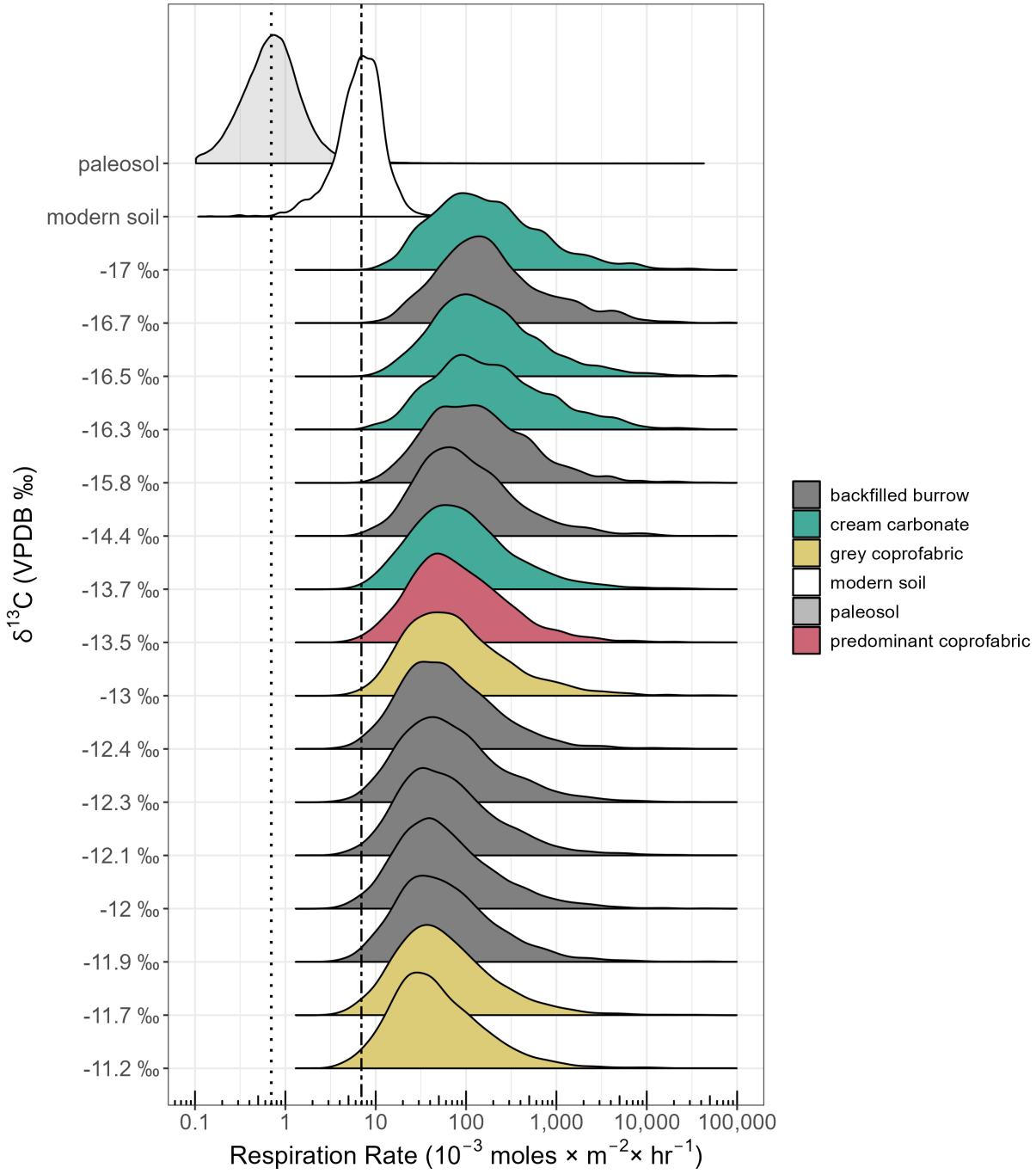

Figure 12. Respiration rates for targeted sampling done for coprolite BP-12-13, modeled per the parameters of Table 3. Dotted line represents median respiration rates for Kaiparowits Fm. paleosols and dot and dash line represents the median soil respiration rates for modern soils.

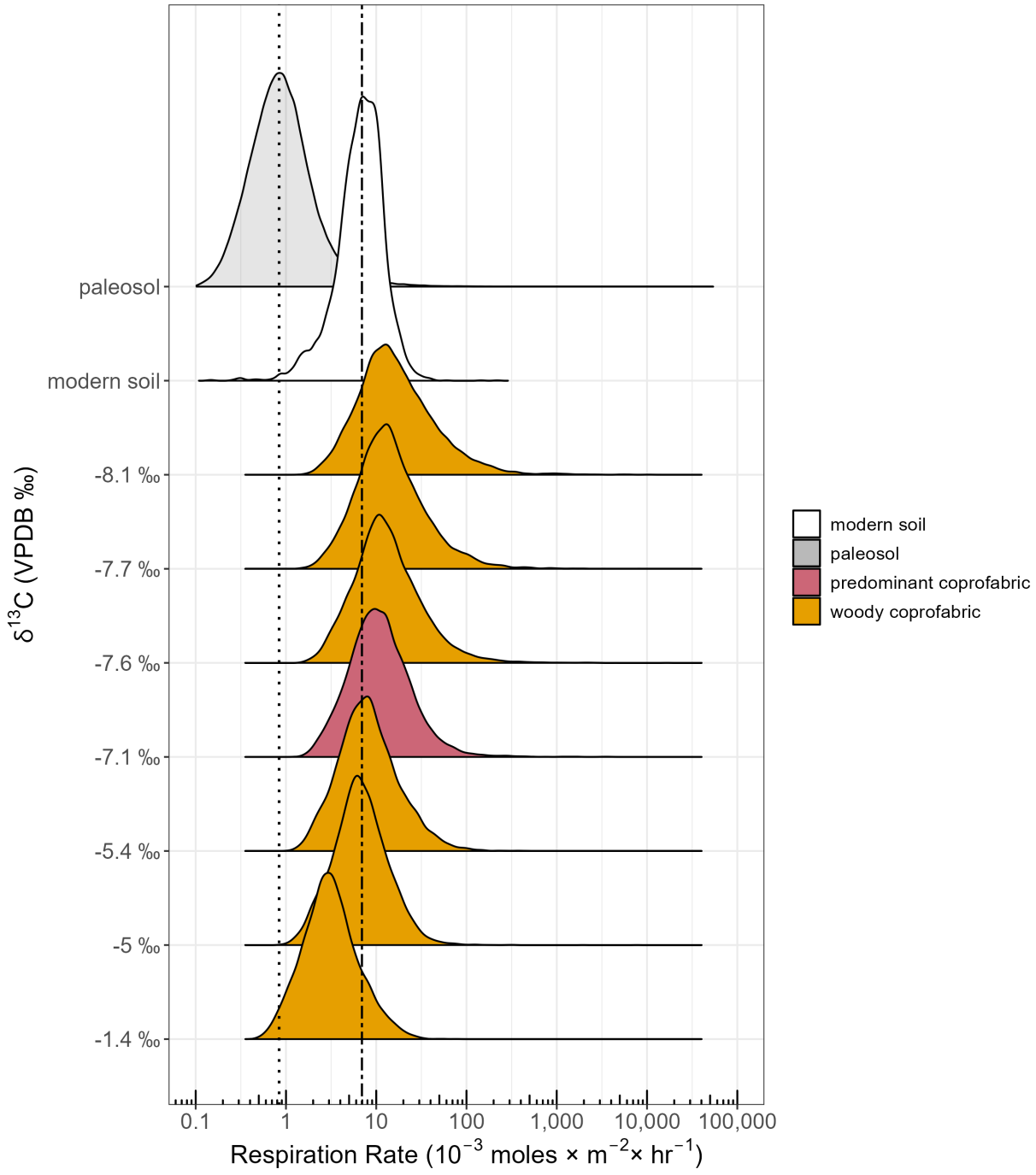

Predominant coprofabric respiration rates

Figure 8 lacks respiration rates for coprolite TE-2015-19 given that its $\delta^{13}C$ value was greater than that of the more enriched end-member of the model (atmospheric CO_2 at ~ -6‰). Overall Figures 8 and 9 show that most coprolites had modeled respiration rates (for both minimum and maximum rates *z* and *L* parameters) that were higher than the respiration rates modeled for the paleosols of their respective formations. On the other hand, the same cannot be said when comparing the minimum rates modeled versus the modern soil respiration rates, as some of the coprolite minimum rates were similar to the modern soil respiration rates. However, the maximum rates modeled were all significantly higher than the modern respiration rates obtained from Jian et al. (2021). This could indicate a higher rate of microbial activity preserved in the coprolites than in modern soil, but the *z* and *L* parameters for this case are less conservative (smaller in magnitude) considering that some of these coprolite deposits had estimated volumes of a minimum of 1.5 liters, with some estimated up to 8 liters (Chin, 2007). Nonetheless, it could be argued that the dung beetle activity preserved in some of these specimens (Chin, 2007; Chin et al., 2017) might be better reflected by the maximum rates *L* and *z* parameter setup, where *L* and *z* are smaller in size, it is assumed that most areas of the coprolite were more directly exposed to atmospheric CO_2 due to the burrows created by dung beetles.

When comparing coprolites of different generalized coprofabrics and their respective respiration rates, the three grey coprolites of this study (HN-94-6B, FN-94-1B, and GB-13-103) had overall higher rates than some of the woody coprolites. This may be related to the lability of the original organic carbon within the different coprofabrics, grey containing more labile carbon than woody, given that the woody coprofabrics can contain more lignin from wood fragments. Disaggregated plant cells and tracheids (which were delignified) are a more labile source of

organic matter for microbes to consume than lignin (Chin, 2007; Cotrufo et al., 2013), which could then explain why grey coprolites generally have higher modeled respiration rates. Additionally, it has been reported that wood is less affected by microbial decay than leaves or roots (Chin, 2007; Highley, 1999), which usually has a higher percentage of water-soluble constituents (Cotrufo et al., 2013). Additional to lability, another factor for consideration for the different rates obtained for the coprolites is the sampling location for the predominant coprofabric. As shown in Figures 5, 6, and 7, sampling location does have an effect in the resulting $\delta^{13}C$ values of the coprolite carbonate, which in turn affects the resulting respiration rates. This intra-coprolite heterogeneity could skew the respiration rate results for each specimen given that the predominant coprofabric represents the most common intra-specimen coprofabric in each specimen, but it is not a true bulk average that represents a mixture of all the carbonates present in a coprolite specimen.

The respiration rates of modern manure (feces that is used to fertilize land that is usually mixed with binders like straw) were obtained from the literature for cattle, hen, pig, and human feces (Castro-Herrera et al., 2023; Chowdhury et al., 2014; Cronjé et al., 2004) and were converted to the same units as the ones in this chapter (10^{-3}moles per m^{-2} per hr^{-1}). The experiments done in incubators were assumed to be conducted in a 1 m^3 cube to calculate the conversion to the desired units. The results for these conversions and the collected data can be found in the Supplemental Materials section. When considering the respiration rates from all the papers used, the median value for modern manure respiration rates was 661 10^{-3}moles per m^{-2} per hr^{-1}, with a standard deviation of 393, a minimum of 86, and a maximum of 1535. When compared to the coprolite rates, the median of manure respiration rates was usually higher than the minimum coprolite respiration rates, meanwhile the maximum

coprolite respiration rates were closer to the median of manure respiration rates. The range of all the manure rates usually overlapped with some minimum coprolite respiration rates (GB-13-103, BR-13-9, GC-13-2, HN-94-6, FN-94-1) and with all the maximum coprolite respiration rates. Even though the coprolite respiration rates and manure respiration rates were not exactly the same, the overlap of these rates with each other suggests that the sensitivity analysis developed to assess the rates of the ancient feces in this study is somewhat capturing realistic respiration rates seen for manure today. Also note that the diet represented by the modern manure microbial respiration rates compiled from the literature is somewhat different from the diet preserved in the coprolites in this study, which showed the consumption of refractory materials like wood (Chin 2007; Chin 2017).

It is important to consider that these manure experiments (Castro-Herrera et al., 2023; Chowdhury et al., 2014; Cronjé et al., 2004) were done in controlled settings where variables like moisture, aeration, and temperature were manipulated for their experiment setups. The manipulation of these (as well as the passage of time in the composting process of manure) caused changes in the CO_2 emissions recorded by their experiments. On the other hand, coprolites represent a fully natural system without human intervention, where the feces are exposed to the environment and subsequently changes in temperature, humidity, and temperature that might not be consistent over time. These differences between the coprolite and manure system could be a reason as to why the values for respiration rates amongst each other do not fully overlap.

Intra-specimen coprofabric respiration rates

Figures 10, 11, and 12 show the respiration rate results for the sensitivity analysis on the $\delta^{13}C$ values from the multiple sampled carbonates within specimens BU-89-2 (Figure 10), HN-94-6 (Figure 11), and BP-12-13 (Figure 12). A significant number of estimates of rates were not

able to be obtained for the soft carbonate in BP-12-13 because the calculated $\delta^{13}C$ values of coprolite air (δ_s) (calculated from the carbonate to CO_2 gas fractionation) were too ^{13}C-depleted (around -33‰) relative to the to the end-member $\delta^{13}C$ values of the respiration rates model. The significant ^{13}C-depletion preserved in the soft carbonate could indicate coupled methanogenic and methanotrophic microbial activity. Methanogens produce ^{13}C-depleted methane, which is oxidized by methanotrophs to ^{13}C-depleted CO_2 that could mineralize into carbonate (Pancost et al., 2000; St-Pierre and Wright, 2013; Templeton et al., 2006). As methanogens are strictly anaerobic microbes often present in the guts of herbivorous vertebrates, this interpretation would be consistent with the coprolites preserving an isotopic record of the *Maiasaura* gut microbiome. However, further C isotope analyses need to be made on this particular intra-specimen coprofabric to determine with certainty the cause of its significantly ^{13}C-depleted reconstructed $\delta^{13}C$ values.

The main observation to note is that although specimens HN-94-6 and BP-12-13 showed more consistency in the calculated rates for their various intra-specimen coprofabrics, BU-89-2 had some coprofabrics (brown carbonate, cream carbonate, woody coprofabric) with rates that deviated from the majority of the rates calculated for other coprofabrics in that particular specimen. The results for the brown carbonate intra-specimen coprofabric are hard to interpret, as they do not relate to coprofabrics seen in other specimens with calculated rates. In terms of the woody coprofabric and the cream carbonate samples in BU-89-2, these might represent a potential carbonate replaced wood fragment and sediment, respectively. This would explain the differences between these two samples and the rest of the targeted samples, since the other samples could be representing areas that have a mixture of preserved plant materials, rather than exclusively wood or sediment.

When comparing the intra-coprofabric respiration rates of the grey generalized coprofabric coprolite (HN-94-6) to the respiration rates of the woody generalized coprofabric coprolites (BU-89-2 and BP-12-13), the rates of the grey coprolite, around 100 10^{-3}moles per m^{-2} per hr^{-1}, were consistently higher than the rates for the woody coprolites (except for the woody and cream carbonate samples in BU-89-2 which had similar rates to HN-94-6), which were around 10. This is similar to the observed trend of higher rates seen with the predominant coprofabric samples. Nonetheless, the predominant coprofabrics had some woody coprolites with comparable rates to the grey coprolites, which indicates that woody coprolites do not necessarily always have lower rates in comparison to their grey counterparts. Like in the predominant coprofabrics analysis, most targeted samples (except for HN-94-6 and some BU-89-2 samples) had respiration rates higher than the modeled paleosol rates and similar to modern respiration rates. HN-94-6 samples and the brown and cream coprofabrics samples of BU-89-2 had rates closer to modern manure, but still not quite as high as the manure rates. Lability of the digested plant material preserved in the coprolite could be a reason for the differing rates amongst intra-specimen and generalized coprofabrics, but overall the result is not conclusive.

Effects of depth parameters z and L on coprolite respiration rates

The coprolite respiration rates were recalculated by changing the position within the coprolite volume (z) and the maximum distance of the feces material to the surface of the coprolite (L) (where it is in contact with the atmosphere) parameters. The aim of this analysis was to see the effects caused on the coprolite respiration rate estimates if respiration occurred when the feces was buried rather than resting on the surface. The results of this analysis can be found in Figure 13.

Figure 13. Boxplots of results for z and L parameter variation on all coprolite rates. Dotted line represents median respiration rates for all the paleosols analyzed in this study. Black dots outside the colored boxes show potential outliers.

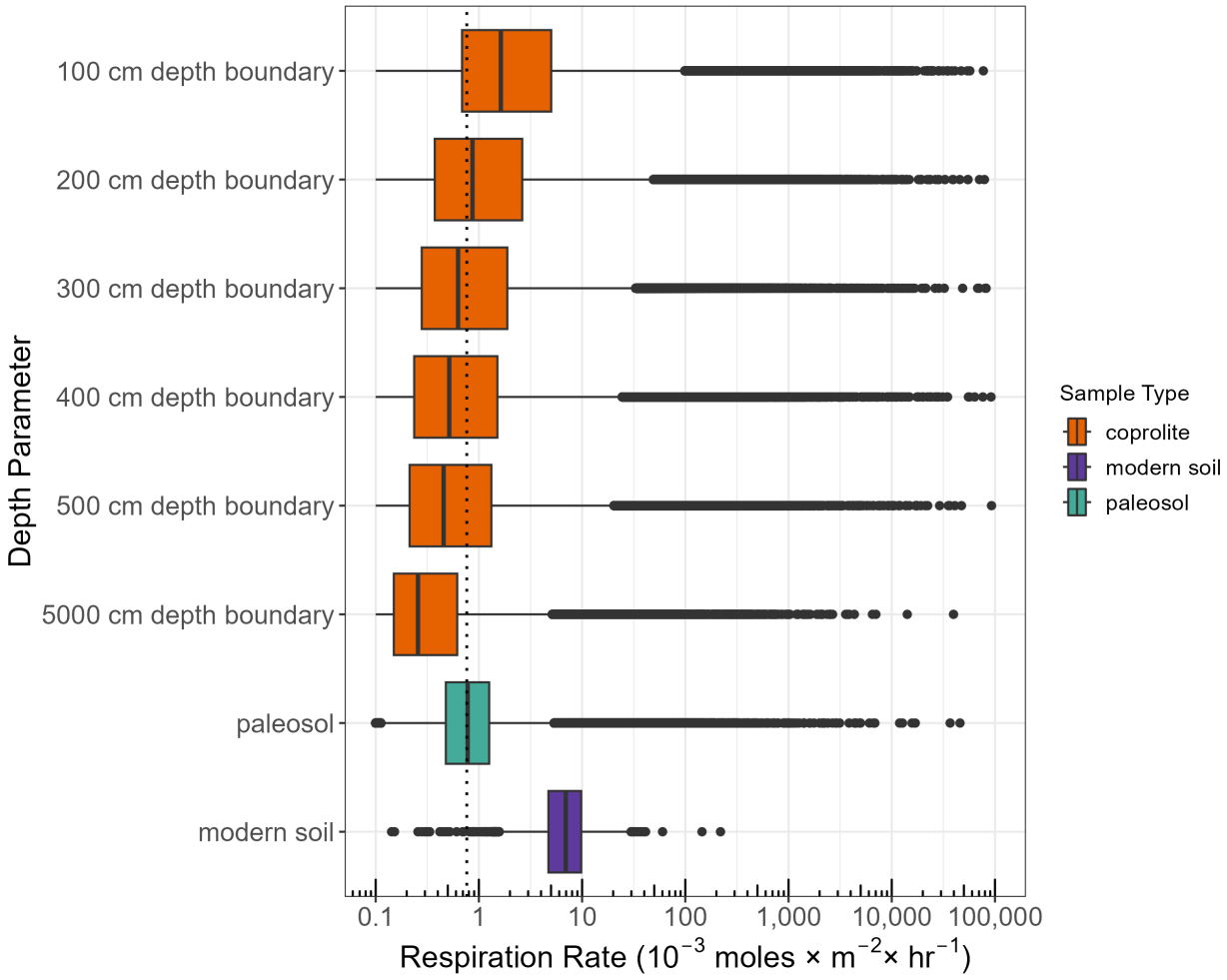

Cerling (1984) shows that paleosols forming in a case where the no-flux boundary is at L = 100 cm, the respiration rates calculated for one $\delta^{13}C$ of soil air (δ_s) can vary across the depth profile considered. The closer to the surface a soil carbonate with a more depleted $\delta^{13}C$ value forms, the more aggressive the respiration rates are, in order to compensate for the influence of atmospheric CO_2 in the system.

The coprolite respiration rates sensitivity analysis had values for parameter L (see Table 3) that were lower than the original Cerling (1984) model (L = 100 cm). It could be argued that

this parameter setup could result in artificially higher respiration rates for the coprolite samples than when considering a scenario where these samples were not in proximity to atmospheric CO_2. Proximity to the atmosphere allows for more atmospheric CO_2 to mix with the microbially respired CO_2, which can artificially elevate calculated rates given the greater $\delta^{13}C$ contribution of atmospheric CO_2 to the mineralized carbonate. Figure 13 shows that even when setting up the coprolite sensitivity analysis with parameters *z* and *L* similar to Cerling (1984), the overall rates for the coprolite samples were generally higher than what was modeled for the paleosols in this study. It takes *L* = 200 cm to make the median coprolite respiration rates overlap with the paleosol respiration rates. Usually soil carbonates are assumed to be formed at depths shallower than 100 cm (Caves et al., 2014; Cerling, 1984; Cerling and Quade, 1993; Licht et al., 2020), the scenarios shown in Figure 13 with *L* greater than 100 cm are more unlikely to represent a realistic soil carbonate formation scenario under this study's model. Given these results, the original respiration rates (see Figures 10-12) obtained for the coprolites are likely not higher than paleosol rates just due to the *z* and *L* parameter setup.

Diagenesis and the captured microbial respiration rates

Diagenesis could influence the microbial respiration rates estimated from the carbonate carbon stable isotopes of the coprolites. For this study diagenesis is defined as everything that occurs to the feces after it is deposited but before carbonate mineralization from the available CO_2 in the coprolite takes place. For example, if coprolite carbonates are mineralized in a similar way to soil carbonates, where the substrate has to somewhat dry out to and allow for carbonate supersaturation in the pore fluids that precipitates carbonates (Cerling, 1984; Licht et al., 2020), then feces would have to be somewhat dry prior to the mineralization process.

Given that in this proposed scenario feces would need to be somewhat dry to start the mineralization process, this could imply that some CO_2 might be lost to microbial respiration that

occurred before mineralization begins. Furthermore, if this is the case, CO_2 mineralization could be occurring when microbes are primarily respiring the recalcitrant organics available in the feces, as more labile organics tend to have faster microbial respiration rates, they are easier to decompose, and may have been respired quickly after fecal deposition (Davidson and Janssens, 2006; Ryan and Law, 2005). If recalcitrant carbon is dominant when feces is drier and commencing mineralization, then it could be expected that the captured microbial respiration rates in the coprolite carbonate carbon isotopes would be lower than respiration rates in modern feces, as the less labile organic carbon is harder to decompose (Davidson and Janssens, 2006; Ryan and Law, 2005).

The relationship between microbial respiration rates and mineralization rates over time could be hypothesized as shown in the plots in Figure 14. As time passes fecal microbial respiration rates may lower, given that the labile organic matter is consumed (Davidson and Janssens, 2006; Ryan and Law, 2005). These lowered microbial respiration rates over time are observed in Castro-Herrera et al. (2023), where the manure shows higher respiration rates at the start of the experiment. At the same time, the potential for mineralization might increase given that the feces are drying up, and the pore fluids are becoming more enriched with the aqueous species that will eventually precipitate as carbonate minerals (Cerling, 1984; Licht et al., 2020). As shown in Figure 14, if the rates of mineralization are fast, then the microbial respiration rates captured by the carbonate carbon isotopes in the coprolite will more closely record the full distribution of microbial respiration rates. However, if mineralization rates are slow, much of the early, fast respiration rates will not be captured by the carbonate carbon isotopes in the coprolite. Overall, this competition means that the distributions of respiration rates estimated from the carbonate carbon isotopes in the coprolite are likely to represent lower bounds when compared to

the full distribution of fecal microbial respiration rates. In this scenario, different microbial respiration rate distributions among the various specimens investigated here might reflect the age of the feces relative to the timing of mineralization, with higher rates capturing respiration in fresher feces and lower rates indicating respiration in more mature feces.

Figure 14. Proposed hypothesis for microbial respiration rate vs. rapid/slow carbonate mineralization rates. Rate and time increase towards the direction pointed by the arrow.

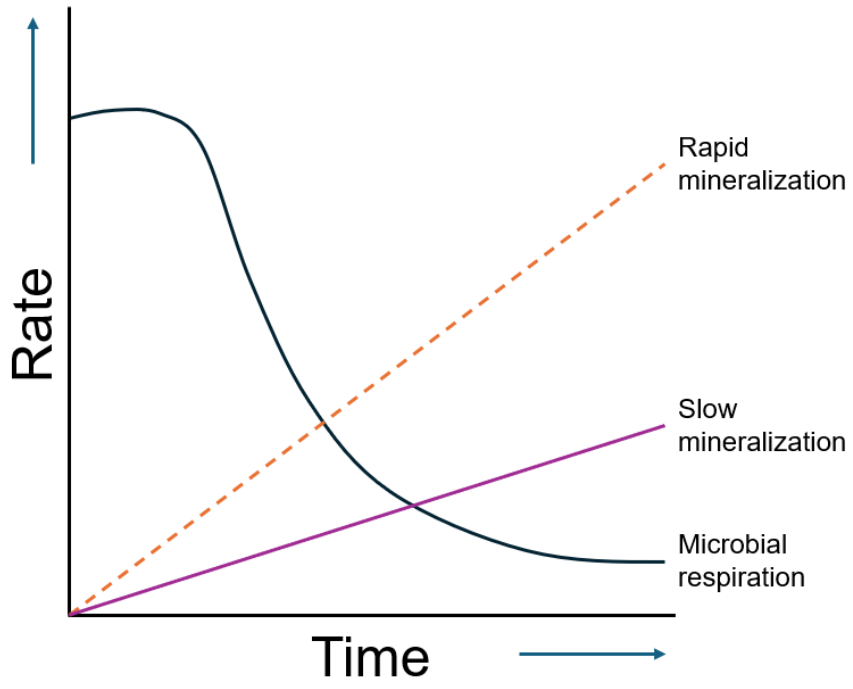

In addition to fecal age, the amount of labile organic material available for microbial respiration may also depend on the diet of the dinosaurs producing the coprolites. This is apparent in the specimens investigated here, given some have more preserved woody fragments, while others show more disaggregated plant cells (Chin, 2007; Chin et al., 2017). The lability of the consumed plant material in the feces could be another reason for why the estimated respiration rates vary amongst specimens, with herbivorous diets richer in polysaccharides producing higher respiration rates while those richer in lignin producing lower respiration rates.

In this scenario the microbial respiration rates captured by the carbonate carbon isotopes in coprolite might be a type of trophic indicator. This possibility should be considered alongside with diagenesis as factors that affect the production and preservation of fecal microbial respiration rates in the carbonate carbon isotopes of calcareous coprolites.

Effects of different parameters on paleosol respiration rates

Even though modern soil respiration rates and manure were used as a comparison point for the coprolite respiration rates, it is important to note that soil respiration rates have been recorded to change in space and time throughout geologic history (Caves et al., 2016, 2014; Gao et al., 2015; Licht et al., 2020), which would then establish a different baseline comparison with the coprolite rates. When considering this, a more suitable comparison point would be paleosol respiration rates, which record a more context-informed respiration rate distribution for the Campanian, when these feces were deposited.

The paleosol respiration rates modeled in this study for the Two Medicine Fm. and Kaiparowits Fm. are comparable to the rates modeled in Caves et al. (2016) for Neogene paleosols, but lower than the range of paleosol rates in Gao et al. (2015) for the Campanian (which range from ~ 5 to 10.5 millimoles per m^{-2} per hr^{-1}). This discrepancy could be a factor of the parameter setup in this study versus other studies. When modeling soil respiration rates, parameters like the concentration of CO_2 (C_0^*) can heavily influence the resulting rates of a sensitivity analysis, which is considered in Gao et al. (2015) as end-Cretaceous CO_2 concentration estimates have high uncertainties. In the model setup for the coprolites and paleosols in this study, the CO_2 concentration distribution had a large range of possible concentrations (~200 to 1,100 ppm), which could result in a conservative range of respiration rates that does not account for the increased CO_2 concentration reported in Gao et al. (2015) for

~76 Ma to ~74 Ma, where CO_2 was estimated no less than 300 ppm (within 1σ standard deviation). When assessing the effects of CO_2 concentration in our modeled paleosol rates, there was a slight positive correlation between the respiration rate and CO_2 concentration, given that the soil respiration rate would need to be more aggressive to maintain the $\delta^{13}C$ values recorded in the paleosols used in this study. Another parameter that could affect the results of the sensitivity analysis is the sampled temperature of carbonate formation used for the fractionation of calcite to CO_2 to obtain the $\delta^{13}C$ of soil air (δ_s) used in the model. The lower the temperature sampled, the larger the fractionation will be (Sharp, 2007). Other environmental parameters like the $\delta^{13}C$ of CO_2 or the $\delta^{13}C$ of respired organic matter did have an effect on the results of this study's model, but not to the extent that the concentration of CO_2 and the sampled temperature of carbonate formation had on the respiration rates.

Another factor that can affect the resulting respiration rates is the surrounding environment of carbonate mineralization. Increases in aridity can cause plant productivity to decline, which in turn can decrease soil respiration and cause the recorded $\delta^{13}C$ of paleosols to increase due to the greater ratio of atmospheric CO_2 to soil respired CO_2 (Caves et al., 2014). Soil moisture can also reduce free-air porosity, which in this study's model could decrease the CO_2 diffusion coefficient in air (D_s^*) and make the respiration rates calculated smaller (Cerling, 1984; Licht et al., 2020). As mentioned previously, temperature at the time of carbonate mineralization can affect its carbon isotopes and consequently the reconstructed rates for both paleosols and coprolites (Cerling, 1984; Sharp, 2007). As well, it is thought that respiration rates reconstructed from paleosols do not represent an annual trend in respiration rates, as most of these carbonates will form seasonally during moments of soil dewatering (dry soil) when the lack of moisture will allow for paleosols to be formed (Quade et al., 2013).

When it comes to how temperatures in an environment affect the soil respiration rates and the activity of the microbial communities there is no consensus on what the trend between these two variables is. One study observed that soil respiration rates are sensitive to temperature changes in the short term and that higher temperatures can lower respiration rates along longer periods of time (Dacal et al., 2019), while another study considered that soil respiration could increase if temperature increased (Azizi-Rad et al., 2022). Overall, it seems like the subject of temperature and soil respiration has not reached a community consensus (Davidson and Janssens, 2006) and that many other factors have to be considered in-context with temperature (moisture, general climate, microbial community response, day-today environmental variability) to understand the driving mechanisms that change soil respiration rates (Azizi-Rad et al., 2022; Dacal et al., 2019; Davidson and Janssens, 2006; Karhu et al., 2014; Sun et al., 2019). Given the lack of community consensus, no clear conclusions on the environmental temperature effects on the modeled paleosol respiration rates in this study can be made. The same can be concluded for the modeled coprolite respiration rates, although there might be variations in the rates that relate to the different environments (Chin et al., 2017) of the Two Medicine Fm. And Kaiparowits Fm. (temperate and subtropical respectively). However, such differences were not clearly observed in this study.

Conclusions

Stable carbon isotopes were successfully obtained from the organic and inorganic (carbonate) carbon present in Two Medicine Fm. and Kaiparowits Fm. coprolites. Although the $\delta^{13}C$ of the organic matter was −20‰ to −24‰ VPDB, which is consistent with the $\delta^{13}C$ range for C_3 plants (Tipple and Pagani, 2007), the $\delta^{13}C$ of the carbonates sampled showed significant heterogeneity among coprolite specimens and within singular coprolite specimens. To interpret the carbonate $\delta^{13}C$ values, the Cerling (1984) model was used to calculate respiration rates with a sensitivity analysis that integrated the carbonate $\delta^{13}C$ values of the coprolites alongside distributions for the other parameters in the model. The same sensitivity analysis was also done with data from Burgener et al. (2019) to obtain respiration rates for paleosol carbonates from the Two Medicine Fm. and Kaiparowits Fm. The results showed that the microbial respiration rates in most coprolites were higher than the respiration rates for the paleosol carbonates analyzed. This was also true when using the z and L parameters similar to the ones used in paleosol respiration rate analysis. When compared to modern soils, the respiration rates for coprolites were usually similar or somewhat higher than the rates obtained from the modern soil respiration database published by Jian et al. (2021). Finally, when compared to modern manure, the range of respiration rates from the coprolites sometimes overlapped with the range from modern manure rates, which could suggest that the model in this study captures ancient fecal respiration rates that are comparable to those in modern feces.

Differences in the modeled respiration rates amongst coprolites and within singular coprolites were also observed. It could be speculated that the lability of the fecal tissues preserved in the coprolites could explain why grey generalized coprofabric coprolites tended to have higher rates than woody generalized coprofabrics, as they could be more easily consumed by microbes after defecation. Nevertheless, this was not shown consistently with the coprolites in

this study, as some specimens with woody coprofabrics had rates as high as the rates shown by grey coprofabrics. Overall, these findings are relevant to future coprolite carbonate $\delta^{13}C$ analyses, as it was clear that the heterogeneity observed through the morphology of the coprolites can also be reflected in the geochemistry.

When considering the paleosol rates from this study in comparison with other studies (Caves et al., 2016, 2014; Gao et al., 2015; Licht et al., 2020), the rates obtained with this model were at times lower than those estimated for other Campanian paleosols. These rate differences could be due to differences in the climate and temperature of carbonate formation of this chapter's paleosol data versus other studies. As well, it could be related to the parameter setup for this model, where the temperature of carbonate formation and CO_2 concentration were seen to influence the results of the rates in the sensitivity analysis. Nonetheless, the variation in respiration rates through time, space and environment have to be considered, as rates have changed through geologic history and are even variable in modern environments, depending on the location and season of the respiration rate measurement (Azizi-Rad et al., 2022; Caves et al., 2016, 2014; Dacal et al., 2019; Davidson and Janssens, 2006; Gao et al., 2015; Jian et al., 2021; Karhu et al., 2014; Licht et al., 2020; Sun et al., 2019).

Overall, when considering coprolite respiration rate results versus paleosol rate results, the inferred microbial activity in the coprolites was generally higher than the usual microbial activity in the paleosols, which is consistent with the knowledge that feces are mostly composed of microbes (Sender et al., 2016). This significant microbial activity is consistent with Hollocher et al. (2001), who suggested that bacteria could have played a role in the mineralization of the Two Medicine Fm. coprolites. Given the high respiration rates, this study's analyses support the hypothesis that microbes were likely involved in the mineralization of these specimens, and that

they allowed for the unique calcareous preservation of these herbivorous dinosaur coprolites. As well, this study showed that $\delta^{13}C$ analysis of coprolite carbonates is a novel and useful tool to study coprolites that is currently underutilized in coprolite research (Bajdek et al., 2014; Barrios-de Pedro et al., 2020; Ghosh et al., 2003; Iacumin et al., 1998; Kocsis et al., 2014; Witt et al., 2021). $\delta^{13}C$ analysis can provide insights into coprolite diagenesis, microbial respiration rates and the connection of morphological evidence of heterogeneity in coprolite samples to geochemical heterogeneity. With novel geochemical analyses, coprolites can be exploited for their full potential in ancient environment reconstruction and become an even more useful tool in reconstructing details of ancient Earth.

Chapter 2: Minimally destructive sampling and preparation methodology for plant fossil stable isotope analysis

Introduction

Applications of carbon stable isotope analysis of fossil plants

Carbon stable isotope ($\delta^{13}C$) analysis of fossil plants (pollen, wood, leaves, coal, etc.) can be useful for getting a glimpse into past environments during geological history. The applications of carbon stable isotopes on plant material can help elucidate questions about atmospheric CO_2 (Arens et al., 2000; Franks et al., 2014), C_3 vs. C_4 photosynthesis abundance in an environment (Bocherens et al., 1993; Descolas-Gros and Schölzel, 2007; Sage et al., 1999), canopy effects (Bonafini et al., 2013), diagenesis/taphonomy (Gröcke, 1998), paleoecology (Bocherens et al., 1993; Forte et al., 2022), climate (Diefendorf et al., 2010; Kohn, 2010), and stratigraphy (Gröcke, 1998; Robinson and Hesselbo, 2004; Yans et al., 2010).

Out of all the applications for carbon stable isotopes on plants, distinguishing between C_3 vs. C_4 photosynthesis is one that has been of great use when it comes to understanding the emergence of C_4 photosynthesis in the geologic record. Photosynthesis is the autotrophic process that allows for plants to produce carbohydrates that store chemical energy that can later on be used by the plant (Lambers and Oliveira, 2019). There are three main types of photosynthesis, C_3 photosynthesis the C_4 photosynthesis, and Crassulacean acid metabolism (CAM) photosynthesis. C_3 and C_4 plants have distinct carbon stable isotope ($\delta^{13}C$) signatures due to physiological and biochemical differences in their photosynthetic pathways. Usually, the $\delta^{13}C$ of C_3 plants ranges from $-20‰$ to $-35‰$ VPDB, meanwhile for C_4 plants $\delta^{13}C$ ranges between $-10‰$ to $-14‰$ VPDB (Tipple and Pagani, 2007).

C_3 originated before C_4 in the geological record. Molecular phylogenies have dated the earliest C_4 photosynthetic pathway origins at around the Early Oligocene (~30-32 Ma) (Edwards

et al., 2010), meanwhile the geologic record shows evidence of C_4 plants at around the Early Miocene (~22 Ma) (Strömberg, 2011). The C_4 photosynthetic pathway appears to have convergently evolved through time over 60 times (Atkinson et al., 2016) across different plant families, but the means through which this pathway emerged from C_3 photosynthesis are still poorly known.

Current state of carbon isotope analysis of fossil plants

A challenge presented by carbon stable isotope ($\delta^{13}C$) analyses of fossil plants is the amount of material that needs to be collected from a fossil to obtain $\delta^{13}C$ data. Sampling fossil specimens sometimes results in much of the fossil specimen being destroyed or damaged in ways that can impede future morphological research of said specimen (N. Neu-Yagle, personal communication). Some studies reported using milligrams of material to prepare samples (usually though acidification, which removes unwanted carbonates from the sample) prior to their analysis with isotope ratio mass spectrometers (IRMS) (Bechtel et al., 2008; Bush et al., 2017; Gröcke, 1998; Gröcke et al., 2002; Larson et al., 2008; Yans et al., 2010), meanwhile traditional IRMS analysis can successfully analyze samples around with 2µmol of carbon, which would be approximately 24µg of carbon (Forte et al., 2022; Polissar et al., 2009). Rendering specimens unusable is not necessary for traditional bulk carbon IRMS analysis, as plant fossils can contain around 40% carbon (Bush et al., 2017), which would require approximately 60µg of sample to retrieve the 2µmol of carbon necessary for IRMS analysis. Even considering that preliminary work at the University of Colorado Boulder showed that some leaf fossils could have carbon percentages as low as 20%, that would still require less than 150µg of sample to obtain carbon stable isotope ($\delta^{13}C$) data (A. Grajales, personal communication).

Forte et al. (2022) showed that with about 35µg of fossil plant material they were able to acidify and analyze samples to obtain carbon stable isotope data. Their method used in-situ

acidification using the same silver capsules where samples were then wrapped and analyzed in a mass spectrometer. This procedure significantly reduces the loss of sample present in other methods where the plant material is added to a tube to react with an acid (usually HCl) to remove the sample's carbonate which can interfere with the $\delta^{13}C$ values obtained (Gröcke, 1998; Larson et al., 2008; Robinson and Hesselbo, 2004).

Project goals and plant specimens' background

Considering the matter of C_4 emergence, and all the knowledge that can be acquired through the carbon stable isotope ($\delta^{13}C$) analysis of fossil plants, this research aimed to develop a method that allows for minimal destructive sampling of fossil plant specimens without relocating specimens from their museum or repository. This method's goal was to allow for plant fossils to remain mostly unchanged after carbon stable isotope analysis so no future research on the specimen is impacted, putting museums and repositories needs at the forefront. With minimal disturbance, new (less rare or protected) samples would not need to be collected from the field to perform carbon stable isotope analysis, and alternatively, could be obtained from the vast collections at museums and repositories. To assess potential sample contamination, this method also included sampling of the rock matrix of plant fossils, which is an approach that is usually not included in other studies working on carbon stable isotope analysis of fossil plants. This contamination assessment was important in the method as small amounts of rock/matrix from the fossil could alter the $\delta^{13}C$ values obtained from the small mass of plant fossil material collected for each specimen.

To achieve this goal, the Larson et al. (2008) organic matter extraction and acidification protocol was adapted to analyze Denver Museum of Nature & Science (DMNS) fossil plant specimens from the Oligocene Creede Fm. and fossil plant specimens from the Eocene Green River Fm. collected during field work at Douglas Pass, Colorado during Summer 2021. The

Creede Fm. represents a caldera lake sedimentary sequence that was deposited in the Late Oligocene (~27 Ma), and it includes lacustrine and alluvial deposits (Lanphere, 2000; Larsen and Crossey, 1996; Wolfe and Schorn, 1989). Fossil plants are usually preserved within deposits associated with the structural moat of the Creede Caldera. It has been discussed that the Creede flora deposits can be mostly found in lacustrine sediments or in water-laid tuffs (Wolfe and Schorn, 1989). The climate of this formation has been described as a cool and montane climate, particularly due to the evidence of the carbonate mineral ikaite in the formation's lake beds, as well as the paleoflora preserved in the formation (Larsen and Crossey, 1996). Some of the common flora found in the Creede Fm. includes firs, spruces, pines, and shrubs (Wolfe and Schorn, 1989). The specimens for this study were found at the northernmost area of the ancient caldera, where most paleoflora has been described in the literature (Wolfe and Schorn, 1989).

The Green River Fm. is a mainly lacustrine sedimentary deposit, which existed in a warm, subtropical climate that preserved a rich fossil flora and fauna (Johnson et al., 1995). Green River Fm. is also referred to as the Eocene (~53.5 Ma to ~48.5 Ma) Green River lake system, as it constituted of three main lakes: Lake Uinta, Lake Gosiute and Fossil Lake (Grande, 1984; Smith et al., 2003). The samples in this study were obtained from private land at Douglas Pass, Colorado, near the Grand Junction Federal Aviation Administration (FAA) Radar Site, which is colloquially known as the Douglas Pass Radar Dome. This locality is close to Loma, Colorado, and it contained plant fossils within a tan to gray carbonate-rich siltstone (Johnson et al., 1995) that is most likely at the intertongue of the Lower Evacuation Creek Member and the Upper Parachute Creek Member (~ 49.6 Ma) of the paleo Lake Uinta Basin of the Green River Fm. (Roehler, 1972; Smith and Carroll, 2015).

Both the Creede Fm. and Green River Fm. plant fossils come from localities with carbonate minerals present in the preserved matrix of the fossil specimens and their ages correspond to time periods that most likely preceded plants with C_4 photosynthesis, given that evidence for pre-Miocene C_4 plants is rare. Although these formations differ in climate and some of their geological context (caldera vs. lakes), both sites still represent lacustrine deposits and can serve well to test the method proposed in this chapter.

Methods

Sample selection and imaging

Access to fossil plants specimens from the Creede Fm. was facilitated by the Denver Museum of Nature & Science (DMNS) for carbon stable isotope ($\delta^{13}C$) analysis. Each specimen was chosen based on the color of the preserved plant material and the amount of material available. Darker colored plant material was preferable, as it was more likely to have a higher carbon percentage composition (Gröcke et al., 2002), which would in turn require less sample to successfully analyze for $\delta^{13}C$. Specimens that were too small or had very little accessible fossil material were not used, since sampling would most likely damage the specimen extensively in order to obtain enough material. A total of 41 specimens from DMNS were chosen for the study from multiple Creede Fm. localities, which represented the northernmost area of the Creede Caldera. Each specimen was photographed with a high-resolution stack photography station at DMNS to preserve the details of the specimen prior to being sampled. For the Green River Fm., three samples from one locality were selected to run two replicates for the plant material and three replicates for the rock material. Samples were selected if they contained plentiful organic material that was easy to obtain from the specimen. In order to have a record of the original specimen, these specimens were photographed prior to having their leaf material sampled. All the specimens in the study can be found in Table 8.

Table 8. Specimen list for carbon stable isotope analysis of plant fossils. Taxon and anatomical element provided by DMNS for Creede Fm. samples.

Specimen ID	Formation	Taxon	Plant anatomical element	Sample treatment	Total Analy-ses	Sample analysis specifics
DMNH EPI.54082	Creede Fm.	Polypodiopsida; Plantae	leaf	Samples analyzed treated with HCl	n = 2	1 plant analysis, 1 rock analysis

DMNH EPI.54090	Creede Fm.	Polypodiopsida; Plantae	leaf	Samples analyzed treated with HCl	n = 2	1 plant analysis, 1 rock analysis
DMNH EPI.59436	Creede Fm.	Pinus; Pinoideae; Pinaceae; Pinales; Pinopsida; Tracheophyta; Plantae	leaf	Samples analyzed treated with HCl	n = 2	1 plant analysis, 1 rock analysis
DMNH EPI.59437	Creede Fm.	Plantae	leaf	Samples analyzed treated with HCl	n = 2	1 plant analysis, 1 rock analysis
DMNH EPI.59438	Creede Fm.	Pinus; Pinoideae; Pinaceae; Pinales; Pinopsida; Tracheophyta; Plantae	leaf	Samples analyzed treated with HCl	n = 2	1 plant analysis, 1 rock analysis
DMNH EPI.59439	Creede Fm.	Plantae	leaf	Samples analyzed treated with HCl	n = 2	1 plant analysis, 1 rock analysis
DMNH EPI.59441 b	Creede Fm.	Eleopoldia lipmanii; Eleopoldia; Rosaceae; Rosales; Magnoliopsida; Magnoliophyta; Plantae	leaf	Samples analyzed treated with HCl	n = 2	1 plant analysis, 1 rock analysis
DMNH EPI.59451	Creede Fm.	Plantae	leaf	Samples analyzed treated with HCl	n = 2	1 plant analysis, 1 rock analysis
DMNH EPI.59454 a	Creede Fm.	Eleopoldia lipmanii; Eleopoldia; Rosaceae; Rosales; Magnoliopsida; Magnoliophyta; Plantae	leaf	Samples analyzed treated with HCl	n = 2	1 plant analysis, 1 rock analysis

DMNH EPI.59456 b	Creede Fm.	Eleopoldia lipmanii; Eleopoldia; Rosaceae; Rosales; Magnoliopsida; Magnoliophyta; Plantae	leaf	Samples analyzed treated with HCl	n = 2	1 plant analysis, 1 rock analysis
DMNH EPI.59476	Creede Fm.	Plantae	leaf	Samples analyzed treated with HCl	n = 2	1 plant analysis, 1 rock analysis
DMNH EPI.59477	Creede Fm.	Plantae	leaf	Samples analyzed treated with HCl	n = 2	1 plant analysis, 1 rock analysis
DMNH EPI.59478	Creede Fm.	Plantae	leaf	Samples analyzed treated with HCl	n = 2	1 plant analysis, 1 rock analysis
DMNH EPI.59483	Creede Fm.	Plantae	leaf	Samples analyzed treated with HCl	n = 2	1 plant analysis, 1 rock analysis
DMNH EPI.59487	Creede Fm.	Ribes robinsonii; Ribes; Grossulariaceae; Saxifragineae; Saxifragales; Rosanae; Rosidae; Magnoliopsida; Magnoliophyta; Plantae	leaf	Samples analyzed treated with HCl	n = 2	1 plant analysis, 1 rock analysis
DMNH EPI.59498	Creede Fm.	Pinus; Pinoideae; Pinaceae; Pinales; Pinopsida; Tracheophyta; Plantae	branches, stems	Samples analyzed treated with HCl	n = 2	1 plant analysis, 1 rock analysis
DMNH EPI.59519	Creede Fm.	Plantae	leaf	Samples analyzed treated with HCl	n = 2	1 plant analysis, 1 rock analysis
DMNH EPI.59552	Creede Fm.	Plantae	leaf	Samples analyzed	n = 2	1 plant analysis,

				treated with HCl		1 rock analysis
DMNH EPI.59555 a	Creede Fm.	Plantae	leaf	Samples analyzed treated with HCl	n = 2	1 plant analysis, 1 rock analysis
DMNH EPI.59558	Creede Fm.	Plantae	leaf	Samples analyzed treated with HCl	n = 2	1 plant analysis, 1 rock analysis
DMNH EPI.59571	Creede Fm.	Plantae	leaf	Samples analyzed treated with HCl	n = 2	1 plant analysis, 1 rock analysis
DMNH EPI.59654	Creede Fm.	Pinus; Pinoideae; Pinaceae; Pinales; Pinopsida; Tracheophyta; Plantae	detached pine cone scale	Samples analyzed treated with HCl	n = 2	1 plant analysis, 1 rock analysis
DMNH EPI.59768 a	Creede Fm.	Plantae	leaf	Samples analyzed treated with HCl	n = 2	1 plant analysis, 1 rock analysis
DMNH EPI.59774	Creede Fm.	Pinus; Pinoideae; Pinaceae; Pinales; Pinopsida; Tracheophyta; Plantae	pine cone	Samples analyzed treated with HCl	n = 2	1 plant analysis, 1 rock analysis
DMNH EPI.59800	Creede Fm.	Plantae	leaf	Samples analyzed treated with HCl	n = 2	1 plant analysis, 1 rock analysis
DMNH EPI.59801	Creede Fm.	Plantae	leaf	Samples analyzed treated with HCl	n = 2	1 plant analysis, 1 rock analysis
DMNH EPI.59812 b	Creede Fm.	Pinus; Pinoideae; Pinaceae; Pinales; Pinopsida; Tracheophyta; Plantae	needles	Samples analyzed treated with HCl	n = 2	1 plant analysis, 1 rock analysis

DMNH EPI.59827 b	Creede Fm.	Ribes obovatum; Ribes; Grossulariaceae; Saxifragineae; Saxifragales; Rosanae; Rosidae; Magnoliopsida; Magnoliophyta; Plantae	leaf	Samples analyzed treated with HCl	n = 2	1 plant analysis, 1 rock analysis
DMNH EPI.59830	Creede Fm.	Abies rigida; Abies; Pinaceae; Coniferales; Gymnospermopsida; Tracheophyta; Plantae	branch with needles	Samples analyzed treated with HCl	n = 2	1 plant analysis, 1 rock analysis
DMNH EPI.59853 b	Creede Fm.	Plantae	leaf	Samples analyzed treated with HCl	n = 2	1 plant analysis, 1 rock analysis
DMNH EPI.59855 b	Creede Fm.	Plantae	leaf	Samples analyzed treated with HCl	n = 2	1 plant analysis, 1 rock analysis
DMNH EPI.59872	Creede Fm.	Chamaebatiaria creedensis; Chamaebatiaria; Rosaceae; Rosales; Rosanae; Magnoliopsida; Plantae	frond	Samples analyzed treated with HCl	n = 2	1 plant analysis, 1 rock analysis
DMNH EPI.59895	Creede Fm.	Plantae	leaf	Samples analyzed treated with HCl	n = 2	1 plant analysis, 1 rock analysis
DMNH EPI.59896	Creede Fm.	Plantae	leaf	Samples analyzed treated with HCl	n = 2	1 plant analysis, 1 rock analysis
DMNH EPI.59898	Creede Fm.	Plantae	leaf	Samples analyzed treated with HCl	n = 2	1 plant analysis, 1 rock analysis

DMNH EPI.59937	Creede Fm.	Eleopoldia lipmanii; Eleopoldia; Rosaceae; Rosales; Magnoliopsida; Magnoliophyta; Plantae	leaf	Samples analyzed treated with HCl	n = 2	1 plant analysis, 1 rock analysis
DMNH EPI.59981 a	Creede Fm.	Plantae	pine cone	Samples analyzed treated with HCl	n = 2	1 plant analysis, 1 rock analysis
DMNH EPI.59982 a	Creede Fm.	Plantae	leaf	Samples analyzed treated with HCl	n = 2	1 plant analysis, 1 rock analysis
DMNH EPI.59983 b	Creede Fm.	Plantae	leaf	Samples analyzed treated with HCl	n = 2	1 plant analysis, 1 rock analysis
DMNH EPI.59985 b	Creede Fm.	Eleopoldia lipmanii; Eleopoldia; Rosaceae; Rosales; Magnoliopsida; Magnoliophyta; Plantae	leaf	Samples analyzed treated with HCl	n = 2	1 plant analysis, 1 rock analysis
DMNH EPI.59990	Creede Fm.	Plantae	leaf	Samples analyzed treated with HCl	n = 2	1 plant analysis, 1 rock analysis
WR1.A.5	Green River Fm.	Plantae	leaf	Sample analyzed untreated with HCl	n = 5	2 plant analyses, 3 rock analyses
WR1.A.5 Acid	Green River Fm.	Plantae	leaf	Samples analyzed treated with HCl	n = 5	2 plant analyses, 3 rock analyses
WR1.C.1	Green River Fm.	Plantae	leaf	Sample analyzed untreated with HCl	n = 5	2 plant analyses, 3 rock analyses
WR1.C.1 Acid	Green River Fm.	Plantae	leaf	Samples analyzed	n = 5	2 plant analyses,

				treated with HCl		3 rock analyses
WR1.C.2	Green River Fm.	Plantae	leaf	Samples analyzed untreated with HCl	n = 5	2 plant analyses, 3 rock analyses
WR1.C.2 Acid	Green River Fm.	Plantae	leaf	Samples analyzed treated with HCl	n = 5	2 plant analyses, 3 rock analyses

Specimen rock and leaf sampling

Each DMNS specimen was sampled at the museum to obtain plant and matrix (rock) material to analyze once without replicates, due to the goal of preserving as much of the specimen as possible. The plant material mostly came from preserved leaves and branches, though a few samples came from pinecone-like and seed-like structures preserved in the specimens. Before sampling plant material, the sampling station was wiped and cleaned with 95% ethanol. Afterwards, the fossil was dusted with a rubber air blower to remove surface debris and then it was doused with 95% ethanol and dabbed with a KimWipe to remove any additional surface particles. After cleaning the fossil, it was then allowed to dry (to evaporate all the ethanol). Using a scalpel and a microscope, the plant material was gently scraped from the specimen, avoiding the matrix/rock material to reduce sample contamination. The plant material was collected in a previously combusted (at 450°C for 8 hours in a furnace, to remove contaminants) 2mL gas chromatography screw top glass vial with a 250µL glass conical vial insert and a PTFE (polytetrafluoroethylene, commonly known as Teflon®) screw cap (see Figure 15 for schematic of the vial). The purpose of this vial with an insert was to reduce the contact surface area of the sample material with the glass, so the sample would not be lost due to it being stuck to the glass of the vial or to the bottom edges of the vial. As well, this vessel allowed for

Figure 15. Schematic of sampling vial with insert used to collect the samples fossil plant material.

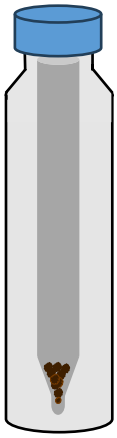

easy transport between the museum and the CUBES-SIL Facility at CU Boulder, where the samples would be prepared and analyzed for carbon stable isotopes.

The rock/matrix samples were cleaned in the same fashion as the plant material collection protocol (blown with a rubber air blower and doused with 95% ethanol) prior to preparing the specimens for sampling. As an additional step, the surface of the sampling location in the rock was drilled off with a Dremel with a round carbide burr (cleaned with 95% ethanol) to access fresh rock for sampling. Afterwards, it was cleaned with an air blower and ethanol before proceeding with the final rock sampling. To get the rock/matrix powder for analysis, each specimen's host rock was drilled again with a clean burr, and the powder was collected into combusted 1 dram and ½ dram glass vials with a combusted aluminum foil liner and a screw cap. Since there is usually less organic carbon in the host rock, more material was collected for the rock than the plant. Samples were drilled from the bottom or sides of the fossil specimen to not disturb the appearance of the front-facing part of the specimen with the preserved plant.

The same sample collection protocols were performed to obtain the plant and rock material from the Green River Fm. specimens. The only difference between the Green River Fm.

and Creede Fm. specimens was that for Green River Fm. more material was collected from the plant fossils to obtain replicates for each specimen and samples were analyzed for carbon stable isotopes treated with an acidification protocol and untreated. For the plant materials two replicates were done for each of the three fossil specimens and the two versions of the sample (treated/untreated), and for the rock material three replicates were done for each specimen and the two versions of the sample (treated/untreated).

Sample treatment with 6N HCl

A sample treatment protocol modified from Larson et al. (2008) was followed to acidify the samples and remove the carbonates present in the collected material. For both the plant material and rock material acidification was performed in the same vials in which the samples were collected to reduce material loss. The vials were heated to 50°C in a heat block with dry bath beads to hold them in place through the whole acidification procedure. For all samples, enough 6N HCl was added with a combusted glass Pasteur pipette to fully cover the sample in its respective vial. If necessary, samples were vortexed to make all the material be in contact with the acid. For the DMNS rock samples, about 3-5 drops of HCl were added to each sample and allowed to react overnight (each drop is about 50µL; Zidarič et al., 2023). This process was done three times in total, and after the last acid addition samples were left to dry in the heat block and then were put into storage. For the Green River Fm. rock samples, the same process was followed, but about 15 drops of HCl were added to each sample.

For all of the plant samples (DMNS and Green River Fm.) 1-2 drops of 6N HCl were added to each vial insert and allowed to mostly (or fully) evaporate before adding the next round of acid. Acid was added a total of three times, with about 3-4 hours of time between additions. After the last addition of acid, samples were allowed to dry overnight. Some samples had MilliQ

water added during the acidification to prevent them from fully drying out as this could potentially get the sample stuck to the glass insert.

Preparing samples for EA analysis

After plant samples had fully dried post acidification, a drop of MilliQ water was added to each sample to then pipette it into pre-weighed 5 x 3.5 mm tin capsules, using combusted glass Pasteur pipettes. The rehydrated organic matter usually had a low pH, but it was not acid enough to affect the integrity of the tin capsules. Afterwards, the samples were allowed to dry, then they were weighed and the tin capsules were folded for IRMS analysis. The rock samples were scooped out of their vials and weighed in tin capsules like traditional dry samples, instead of using the pipette method applied to the plant samples. A schematic summary of the acidification treatment for plants is shown in Figure 16. For the untreated samples, the acidification protocol was not performed. Untreated plant samples were pipetted out of their vials using the MilliQ method that was used for the treated samples, and the untreated rock sample material was weighed out from the tube in the same way as the other treated rock samples.

Figure 16. Schematic of the acidification treatment done for fossil plant samples.

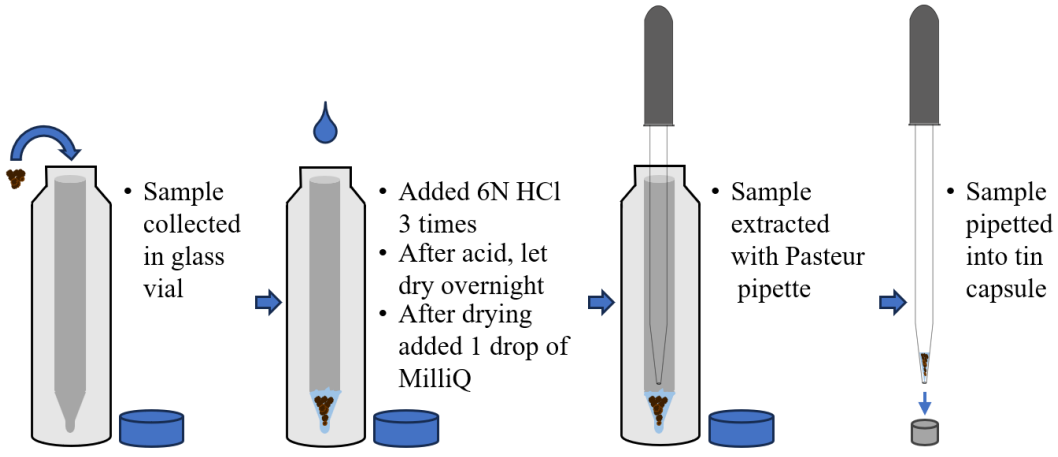

Isotope Ratio Mass Spectrometry

A ThermoScientific Delta V continuous flow isotope ratio mass spectrometer (CF-IRMS) was used to obtain the $\delta^{13}C$ values and total carbon percentage for all the samples in this study. Analyses were done with the equipment in the University at Colorado Boulder (CU Boulder) Earth Systems Stable Isotope Lab (CUBES-SIL) Core Facility (RRID:SCR_019300). All organic matter isotope analyses were done with a ThermoScientific Flash 2000 Organic Elemental Analyzer peripheral. All carbon isotope values were corrected using standards USGS41a (for blank correction), L-glutamic acid, EDTA2, and Pugel. For plant samples Pine and Peach leaves standards were used, and for rock samples Low organic content soil (LOS), High organic content soil (HOS), Acetanilide #1, and RODR were used. These corrections assist with potential size dependance effects on the carbon isotope values and the normalization of the values to the Vienna Pee Dee Belemnite (VPDB) scale.

Results

Yield of acidification protocol for Green River Fm. rock and plant samples

Three vials with rock material from the specimens of the Green River Fm. were acidified based on the preparation protocol described in the methods of this chapter. From each vial three replicate carbon isotope analysis were done using the material remaining in each vial prepared. The yield results for the acidification are in Table 9. It was observed that crystals slightly separated from the rest of the rock sample were formed during the drying process of the acidification. These precipitated crystals might explain the increase in mass seen in the sample pre to post treatment. This effect was noted by Larson et al. (2008), where they mention how acidification treatments without rinsing and decanting can result in the formation of hygroscopic salts like $CaCl \cdot H_2O$.

Table 9. Yield of acidified Green River Fm. rock samples.

Sample	Mass prior to acidification (mg)	Mass after acidification (mg)
WR1.C.1.Acid	148.8	210.6
WR1.C.2.Acid	139.9	203.3
WR1.A.5.Acid	187.9	235.9

The yield of plant material sampled from the Green River Fm. is shown in Table 10. The mass prior to acidification shows the amount of plant material collected from the fossil specimen into the glass vial shown in Figure 15. The mass after acidification shows the weight of the sample material once placed in the tin capsule. For the plant samples each replicate was treated separately, which is why Table 10 shows the sample names with A and B representing the replicates for each specimen. Overall, if not considering WR1.C.1.Acid.B and WR1.C.2.Acid.A which showed unusual yields in comparison to the other samples, the percentage of sample lost

was around ~ 40% after treating the samples with the protocol in Figure 16. Samples WR1.C.1.Acid.B and WR1.C.2.Acid.A likely showed the same effect seen in the rock acidification for Green River Fm. specimens, where hygroscopic salts formed due to the lack of rinsing and decanting in the preparation protocol (Larson et al., 2008).

Table 10. Yield of acidified Green River Fm. plant samples.

Sample	**Mass prior to acidification (µg)**	**Mass after acidification (mg)**	**Percent of sample lost or gained**
WR1.C.1.Acid.A	440	266	40% lost
WR1.C.1.Acid.B	379	413	9% gained
WR1.C.2.Acid.A	324	165	49% lost
WR1.C.2.Acid.B	302	280	7% lost
WR1.A.5.Acid.A	207	126	39% lost
WR1.A.5.Acid.B	193	134	31% lost

Success rate of minimally destructive sampling protocol

Out of the 41 DMNS specimens that were sampled for rock and plant material, 6 plant material samples (which were all treated using the protocol in Figure 16) were too small to have enough sample carbon detected in the IRMS analysis to be distinguishable from the blank (an empty tin capsule). Including these 6 samples, a total of 13 samples were smaller than the standards used in the IRMS analysis, which indicated that although that $\delta^{13}C$ data could be used, it has less precision and is prone to machinery analytical error in comparison to the data within the standards' range of masses. Of the rock samples only one sample (DMNH EPI.59437) was smaller than the standards used in the IRMS analysis. The mass of the smallest plant sample

analyzed within standard range was 20µg, which was obtained from specimen DMNH EPI.59478 (from an area sized about 2mm x 1mm).

All of the DMNS plant samples yielded some plant material after acidification (the smallest yielded 6µg). Figure 17 shows what was sampled from specimen DMNH EPI.59476, the sample with the smallest yield post-treatment, and Figure 18 shows what was sampled from specimen DMNH EPI.59937, which yielded a larger amount of material post treatment (216µg). It is important to note that due to the lack of microbalance equipment at DMNS, the amount of plant material obtained from each fossil specimen could not be recorded. Nonetheless, when

Figure 17. Sampled area in specimen DMNH EPI.59476 shown as a red dot.

developing the protocol at CU Boulder, the mass of plant material obtained from practice deaccessioned specimens (that were sampled in a similar fashion to the DMNS specimens) was around 100µg, which could be enough for traditional IRMS analysis (like what was done in this study). Sampling plant material that was dark and flaky was easier than sampling plants like the ones shown in Figures 17 and 18, given that the material was easier to access and remove

Figure 18. Sampled area in specimen DMNH EPI.59937 shown with red markings.

without contaminating with the rock matrix. Figure 19 shows two specimens, DMNH EPI.59487 and DMNH EPI.59981, with dark plant material which was easier to sample (than the specimens in Figure 17 and 18) and yielded 100µg and 712µg of plant material post-treatment, respectively.

Figure 19. Specimens DMNH EPI.59487 (left) and DMNH EPI.59981 (right).

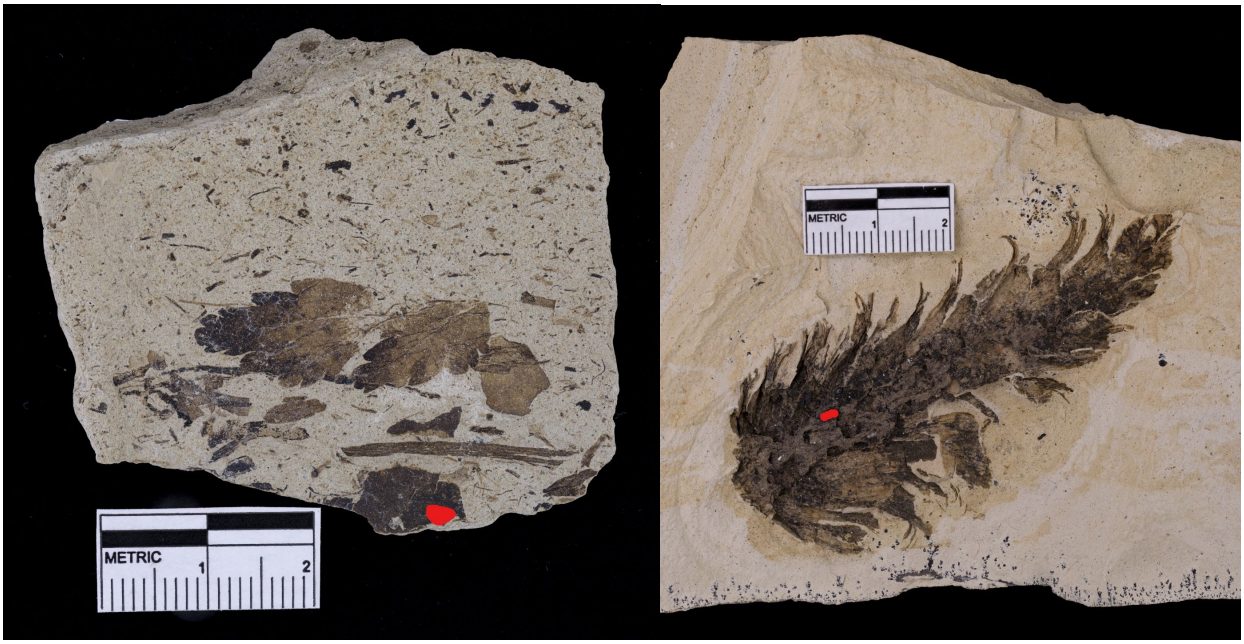

Carbon stable isotope results for Green River Fm. specimens

Figure 20 shows the results for the carbon stable isotope analysis of the Green River Fm. specimens. Each point shows the mean of all the replicates of each combination of specimen and treatment, and the lines show he standard deviation (1σ) of replicates.

Figure 20. Carbon stable isotope results for Green River Fm. specimens. Y-axis shows $\delta^{13}C$ results and x-axis shows the specimen name. Left shows treated (acid) and untreated (none) plant samples and right shows treated and untreated rock samples. The standard deviation (1σ) of replicates is shown with lines.

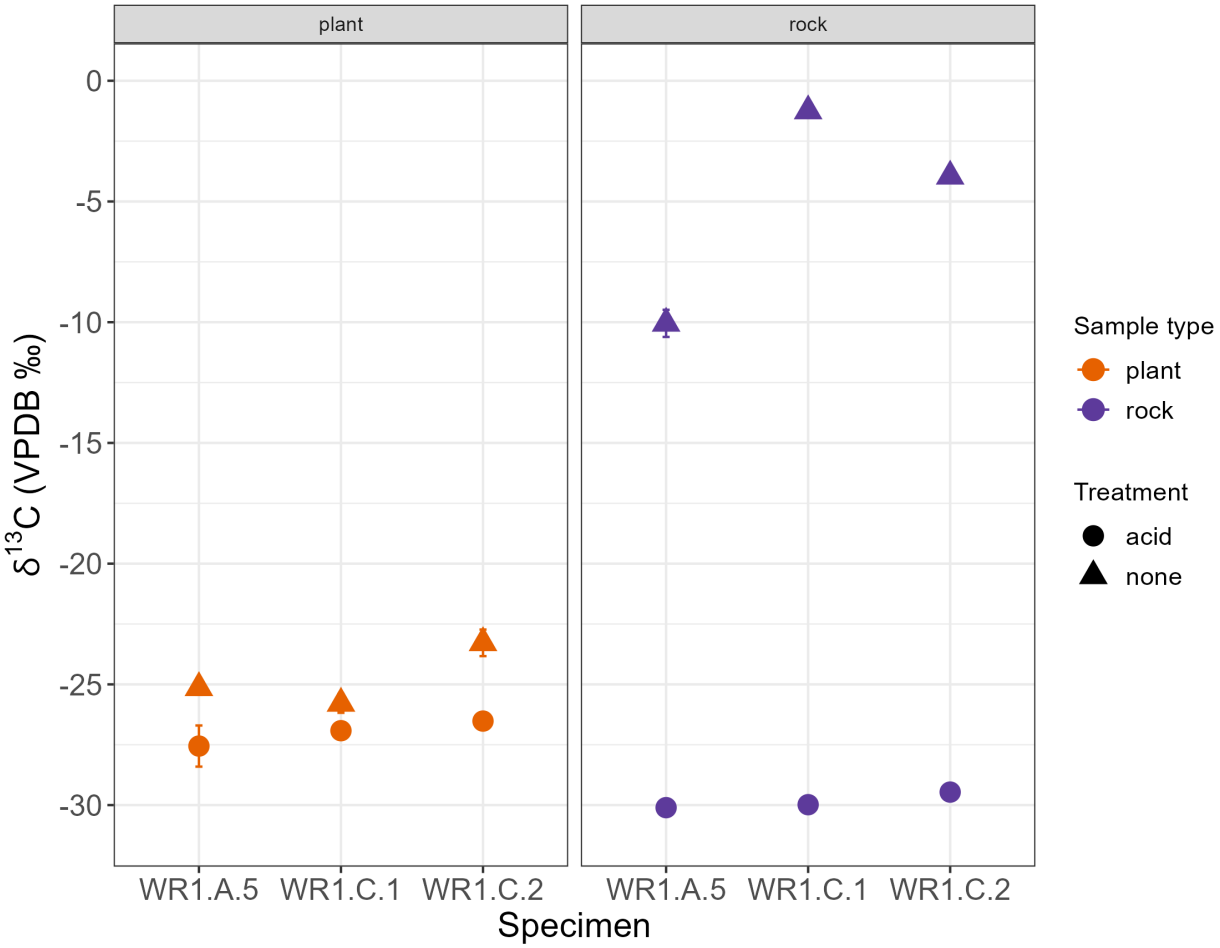

Treated plant samples usually have an about 2.3‰ difference when compared with the untreated samples. This difference is starker with treated and untreated rock samples, where the difference is generally about 24.8‰. These differences are usually due to the inorganic carbonate present (Larson et al., 2008) in the sample, which can alter the $\delta^{13}C$ values. The results showed

that the $\delta^{13}C$ treated rocks was more depleted than the carbon isotopes of treated plant samples. The $\delta^{13}C$ values of both the treated rock and plant samples are close to C_3 plant values, which is congruent with the origin of these specimens at the Green River Fm, which predates C_4 presence and is characterized by more organic rich rocks (Smith and Carroll, 2015).

Carbon stable isotope results for Creede Fm. specimens

Creede Fm. specimens were all treated with HCl acid to remove the carbonates present. The $\delta^{13}C$ results for these samples are found in Figure 21 (only specimens with suitable $\delta^{13}C$ data for both the rock and plant sample are included). The samples that were smaller than the blanks or smaller than the standards in the IRMS analysis were not included, as their $\delta^{13}C$ values are likely not very precise. Overall the rock samples showed a more consistent and low carbon percentage across samples (about 0.5%) in comparison to plant samples. The carbon isotope values of the rock samples ranged from about -10‰ to -18.3‰, and the values of the plant samples ranged from about -15.9‰ to -21.2‰.

Figure 21. Carbon stable isotope results for Creede Fm. specimens. Y-axis shows $\delta^{13}C$ results and x-axis shows the carbon percentage of each sample. Analytical error for $\delta^{13}C$ is smaller than the size of the points. Only complete rock/plant pairs of carbon stable isotope data are included.

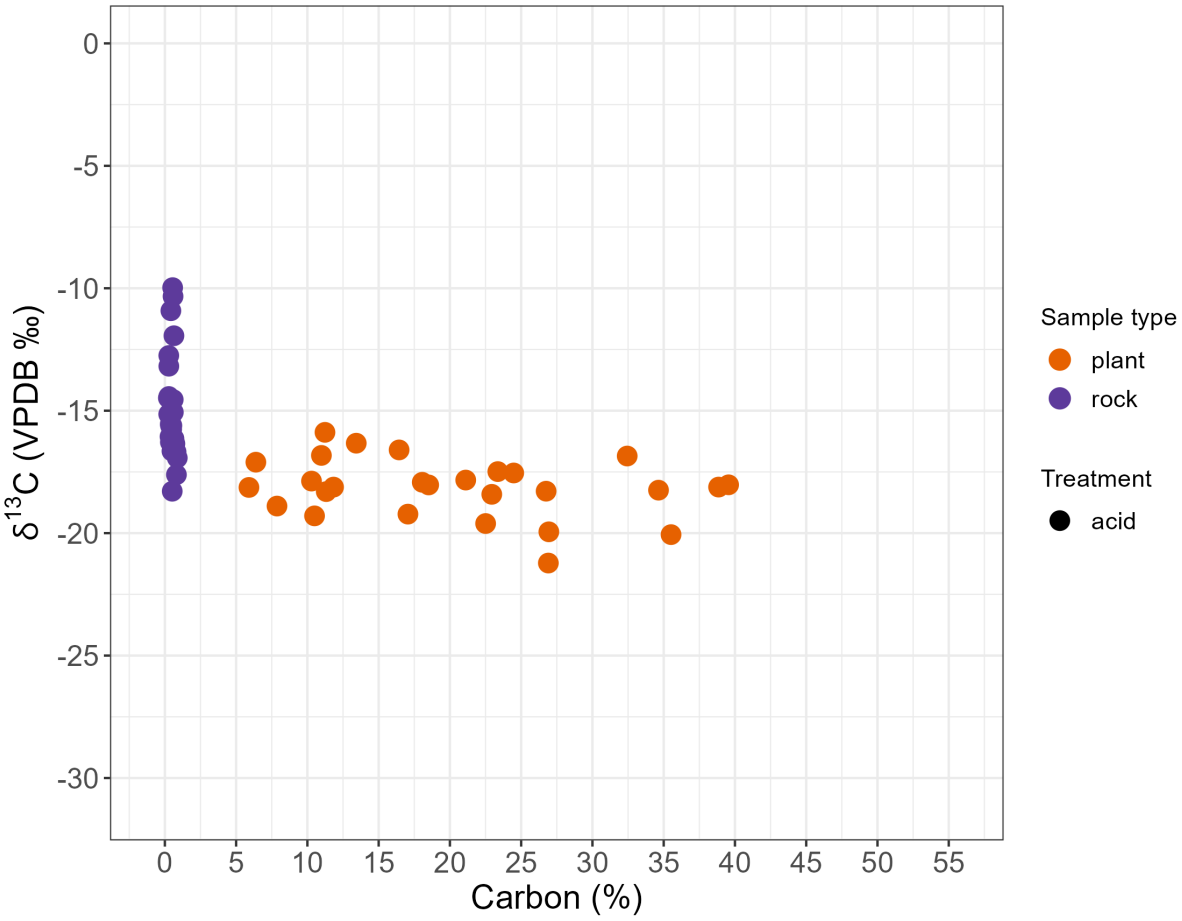

Discussion

Implications of minimally destructive sampling protocol

All Creede Fm. plant samples yielded some material post the acidification process. A sample that yielded just 20µg (with ~23% of that sample being carbon) was successfully analyzed for $\delta^{13}C$ under the developed protocol, and it only took sampling about 2 mm^2 of area of the specimen. The methodology developed for sampling and acidification greatly increased the convenience of sampling outside a laboratory environment, as samples were easily transported from museum to laboratory in a small box and there was no need to request an official museum loan that would require to transport specimens to the laboratory. Also, the sample could be processed in the same vial it was collected in and the use glassware with minimal surface area avoided sample being lost due to adherence to the sample vial. Recommendations for future iterations of this protocol would include weighing the vials prior to sample collection and post sample collection to get an accurate recording of the sample lost during the acidification process.

The ability to sample small parts of a plant fossil and transport said sample can be of great benefit to museums, as it ensures that a specimen can be used for future research and it also protects the specimens from transport that can end up damaging them. This would allow for many specimens that in some cases are off-limits for geochemical analysis to be analyzed, given that they would remain mostly intact. Collaboration with museums is essential so paleontologists and geochemists work together and take advantage of specimen collections that are accessible and do not require fieldwork to obtain. With newer IRMS systems that can measure $\delta^{13}C$ with less than 1µg of carbon (Polissar et al., 2009), minimally destructive sampling protocols can become the norm, and allow robust geochemical analyses of museum specimens.

Rock matrix contamination in plant samples

Green River Fm. rock samples contained carbon percentages as high as 2.8% when treated, and Creede Fm. rock samples had up to 0.9% carbon detected in the IRMS analysis. This organic carbon from the rocks, although a small fraction of the material, could contaminate the plant samples when analyzed for $\delta^{13}C$. Certainty that samples are not contaminated with matrix is necessary when working on projects where finer scale carbon isotopic differences (1-2‰) can influence the interpretation of $\delta^{13}C$ from plants (Bush et al., 2017).

To ascertain the potential contamination of rock matrix on the $\delta^{13}C$ of a plant sample, linear slopes were calculated from pairs of the $\delta^{13}C$ of a rock sample and the $\delta^{13}C$ of a plant sample from one specimen. These pairs were used to estimate a theoretical uncontaminated plant sample using the y-intercept. The assumption made for this model was that the uncontaminated plant sample would be 100% carbon. Equations 8 and 9 show how the slope and intercept were calculated for each rock/plant sample pair obtained from each specimen. With the slope and intercept calculated, the line that fits these two points could be found and expressed with the slope-intercept equation (see Equation 10).

Equation 8. Slope calculation using $\delta^{13}C$ and 1/carbon % obtained from each rock/plant sample pair.

$$Slope = \frac{\delta^{13}C_{plant} - \delta^{13}C_{rock}}{\frac{1}{\%C_{plant}} - \frac{1}{\%C_{rock}}}$$

Equation 9. Slope calculation using $\delta^{13}C$ and 1/carbon % obtained from each rock/plant sample pair.

$$Intercept = \delta^{13}C_{plant} - \left[slope * \frac{1}{\%C_{plant}}\right]$$

Equation 10. Slope-intercept linear equation for each rock/plant sample pair.

$$\delta^{13}C_{plant} = \left[slope * \frac{1}{\%C_{plant}}\right] + intercept$$

The y-intercept for this analysis would represent the $\delta^{13}C_{plant}$ of an 100% plant sample, given that plant samples usually have higher carbon percentages than rock samples, and the larger the carbon percentage is, the closer $\frac{1}{\%C}$ gets to 0. This relationship can be observed for example rock/plant sample pairs of specimens DMNH EPI.59456 (Creede Fm.) and WR1.A.5 (acid treated, Green River Fm.) shown in Figures 22 and 23.

Figure 22. $\delta^{13}C$ vs. $\frac{1}{\%C}$ of specimen DMNH EPI.59456 rock and plant samples. Slope-intercept equation is shown in the white box.

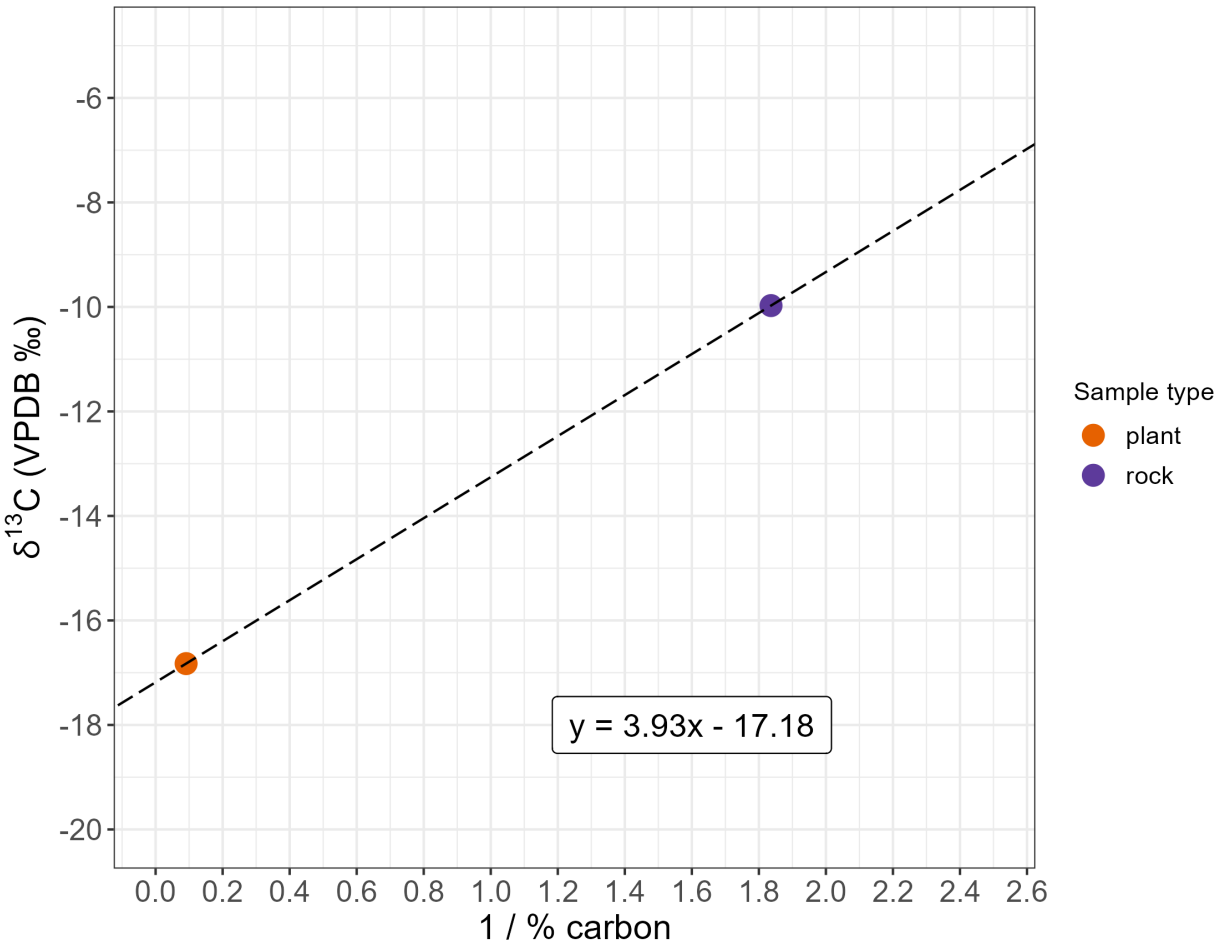

Figure 23. $\delta^{13}C$ vs. $\frac{1}{\%C}$ of specimen WR1.A.5 rock and plant samples. Slope-intercept equation is shown in the white box.

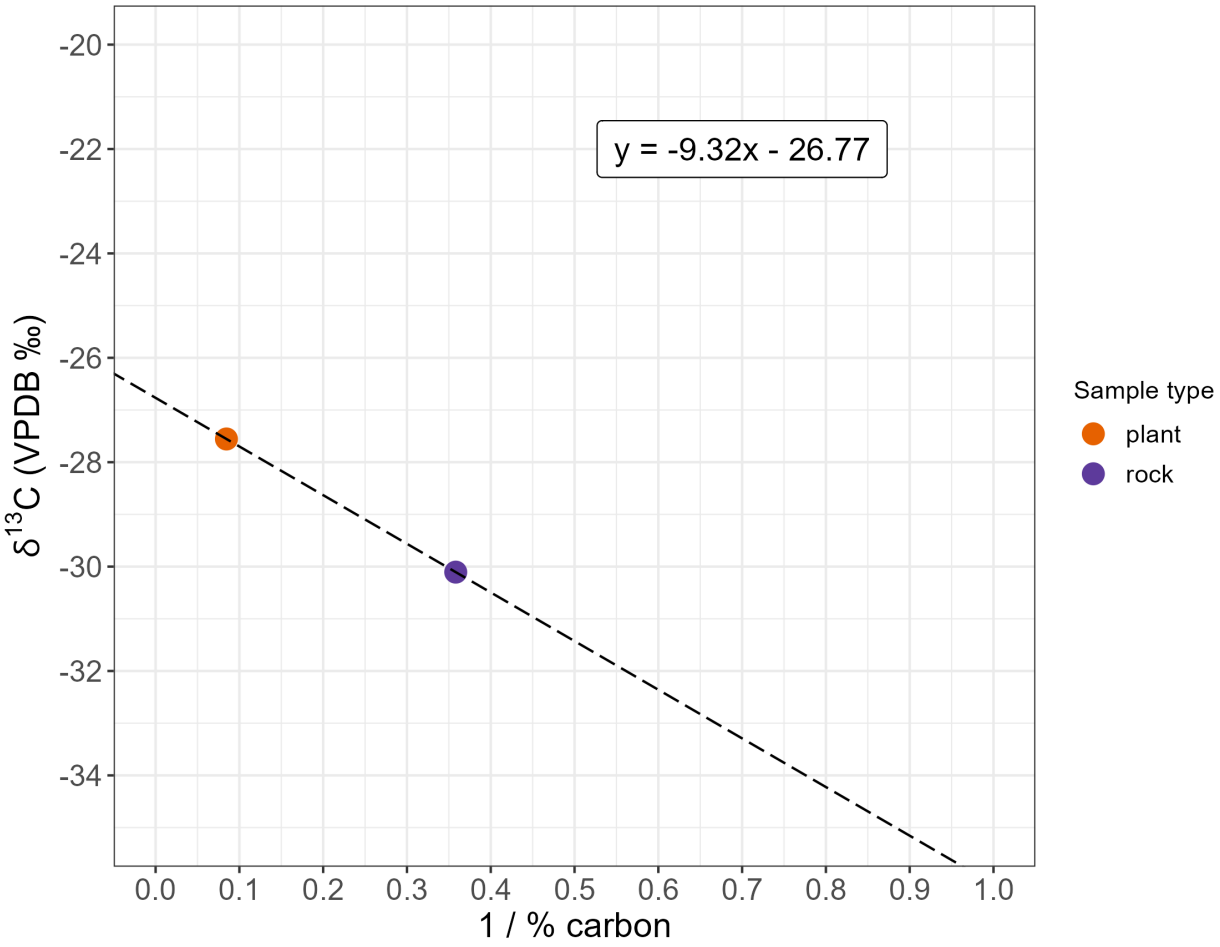

Overall, the slope-intercept model was able to provide a predicted theoretical $\delta^{13}C_{plant}$ of an 100% plant sample, but the changes from the original $\delta^{13}C_{plant}$ to the theoretical $\delta^{13}C_{plant}$ were minimal. For all Creede Fm. specimens, the mean difference between the original and theoretical $\delta^{13}C_{plant}$ values (Δ = original $\delta^{13}C_{plant}$ - theoretical $\delta^{13}C_{plant}$) was about 0.1‰. This change is not larger than the residual standard error that was obtained from the standard corrections done to the raw IRMS $\delta^{13}C$ data (0.2‰). All specimens, except for one, showed a positive slope when plotting $\delta^{13}C$ vs. $\frac{1}{\%C}$, which meant that almost all specimens had rock/plant sample pairs where plant $\delta^{13}C$ was more depleted and carbon percentage was higher

than for their respective rock sample. This positive slope meant that almost all theoretical $\delta^{13}C_{plant}$ values were more negative than the original $\delta^{13}C_{plant}$. The "correction" for $\delta^{13}C_{plant}$ values with the slope-intercept model were not significant enough for the Creede Fm. specimens, as it is not better than the error obtained for the IRMS standard correction, and it would not cause significant difference in the $\delta^{13}C_{plant}$ results when it comes to interpretation. The values of the treated plant $\delta^{13}C$ (original and theoretical) for Creede specimens fell along the more positive fringes of the $\delta^{13}C$ for C_3 plants, which is usually around −20‰ to −35‰ VPDB (Tipple and Pagani, 2007). The reason as to why the $\delta^{13}C_{plant}$ seems to be enriched (compared to typical C_3 plants) could be due to elevation and precipitation. Körner et al. (1988) reported a general increase in ^{13}C in plants located at higher altitudes, but their values are usually 2‰ lighter than the results in this study. Altitude could be a factor influencing the plants from Creede given that it represents a higher-altitude environment (Wolfe and Schorn, 1989). Lower precipitation has also been linked to more enriched plant $\delta^{13}C$ (Cernusak et al., 2013), and it has been considered that summers were dry at Creede and that most precipitation fell as snow (Wolfe and Schorn, 1989). For future research, more analyses could be done where the taxa of the Creede specimens in this study are considered and added as contextual evidence to understand the potential climate conditions represented by Creede Fm. flora.

For Green River Fm. specimens, the mean difference between the original and theoretical $\delta^{13}C_{plant}$ values were about 0.4‰. All specimens showed a negative slope when plotting $\delta^{13}C$ vs. $\frac{1}{\%C}$, which meant that almost all specimens had rock/plant sample pairs where rock $\delta^{13}C$ was more depleted than $\delta^{13}C_{plant}$. Still, the carbon percentages of plant samples were higher than for the rock samples. This negative slope meant that almost all theoretical $\delta^{13}C_{plant}$ values were more positive than the original $\delta^{13}C_{plant}$. For Green River Fm.

specimens, the slope-intercept model had a greater effect on the original $\delta^{13}C_{plant}$, but it was still less than 1‰ change from original $\delta^{13}C_{plant}$ to theoretical $\delta^{13}C_{plant}$. As to the values of the treated plant $\delta^{13}C$ (original and theoretical), these fell within the range seen for C_3 plants (Tipple and Pagani, 2007).

In general, the slope-intercept model showed that for the specimens in this chapter, the rock matrix contamination was minimal, and samples were collected successfully. Nonetheless, it is still important to consider the potential of matrix contamination in a plant sample depending on the research applications of the carbon stable isotope results and the amount of organic carbon in the matrix.

Sample acidification treatment

As shown by studies that have assessed the effects of acidification on $\delta^{13}C$ of organic carbon (Barral et al., 2015; Larson et al., 2008), pretreatment of samples is necessary for IRMS analysis as CO_2 from carbonates can influence the results of $\delta^{13}C$ values. This was observed in our Green River Fm. rock and plant samples, which had at least a 2.3‰ change from untreated to treated samples. This effect is even greater in rocks that have presence of carbonates like the specimens of Green River Fm. (Johnson et al., 1995). The treated Green River Fm. $\delta^{13}C$ rock results are consistent with kerogen analysis of Green River Fm. rocks (Katz, 1995). For the untreated Green River Fm. rocks, the $\delta^{13}C$ was likely enriched by the carbonates present in the sample, which can show significantly more enriched $\delta^{13}C$ in the Green River Fm. (Sarg et al., 2013). In Creede Fm. samples the effects of acidification could not be observed. It could be useful for future research to explore the effects of acidification on Creede Fm. rock and plant material, as it could maybe elucidate if the treatment is affecting the $\delta^{13}C$ values for the specimens in this study.

Conclusions

The sampling and acidification protocol developed to obtain rock and plant samples from the DMNS can be considered successful, as carbon stable isotope data was obtained for 66% of the museum plant samples with less than 1‰ error. The proposed method alleviates the need to transport specimens from a repository to a laboratory, allows for 50% of the sample to be recovered post-acidification, and minimally disturbs the fossil plant specimen, as sampling areas are in the millimeter to sub-centimeter scale range. Although in this study rock matrix contamination was not a significant contamination factor in the fossil plant samples, it was still important to consider it as organic carbon was detected in all the rock samples in the study (from Green River Fm. and Creede Fm.). When comparing acid-treated versus untreated samples, acidification was shown to heavily impact $\delta^{13}C$ values, as inorganic carbonates could release CO_2 during IRMS analysis (Larson et al., 2008). Developing methods like the one studied in this chapter can considerably benefit collaborations between museums, paleontologists, and geochemists, and allow for negotiation with repositories as to which samples can be used for geochemical analysis and increase the information we learn from already collected specimens. With the advent of nano-IRMS (Polissar et al., 2009), sub-centimeter sampling is feasible and should be explored for future paleontological research involving fossil plants and paleobotany.

References

Arens, N.C., Jahren, A.H., Amundson, R., 2000. Can C3 Plants Faithfully Record the Carbon Isotopic Composition of Atmospheric Carbon Dioxide? Paleobiology 26, 137–164.

Atkinson, R.R.L., Mockford, E.J., Bennett, C., Christin, P.-A., Spriggs, E.L., Freckleton, R.P., Thompson, K., Rees, M., Osborne, C.P., 2016. C4 photosynthesis boosts growth by altering physiology, allocation and size. Nat. Plants 2, 1–5. https://doi.org/10.1038/nplants.2016.38

Azizi-Rad, M., Guggenberger, G., Ma, Y., Sierra, C.A., 2022. Sensitivity of soil respiration rate with respect to temperature, moisture and oxygen under freezing and thawing. Soil Biol. Biochem. 165, 108488. https://doi.org/10.1016/j.soilbio.2021.108488

Bajdek, P., Owocki, K., Niedźwiedzki, G., 2014. Putative dicynodont coprolites from the Upper Triassic of Poland. Palaeogeogr. Palaeoclimatol. Palaeoecol. 411, 1–17. https://doi.org/10.1016/j.palaeo.2014.06.013

Barral, A., Gomez, B., Legendre, S., Lécuyer, C., 2017. Evolution of the carbon isotope composition of atmospheric CO2 throughout the Cretaceous. Palaeogeogr. Palaeoclimatol. Palaeoecol. 471, 40–47. https://doi.org/10.1016/j.palaeo.2017.01.034

Barral, A., Lécuyer, C., Gomez, B., Fourel, F., Daviero-Gomez, V., 2015. Effects of chemical preparation protocols on δ13C values of plant fossil samples. Palaeogeogr. Palaeoclimatol. Palaeoecol. 438, 267–276. https://doi.org/10.1016/j.palaeo.2015.08.016

Barrios-de Pedro, S., Rogers, K.M., Alcorlo, P., Buscalioni, Á.D., 2020. Food web reconstruction through isotopic compositions of fossil faeces: Insights into the ecology of a late Barremian freshwater ecosystem (Las Hoyas, Cuenca, Spain). Cretac. Res. 108, 104343. https://doi.org/10.1016/j.cretres.2019.104343

Battin, T.J., Luyssaert, S., Kaplan, L.A., Aufdenkampe, A.K., Richter, A., Tranvik, L.J., 2009. The boundless carbon cycle. Nat. Geosci. 2, 598–600. https://doi.org/10.1038/ngeo618

Bechtel, A., Gratzer, R., Sachsenhofer, R.F., Gusterhuber, J., Lücke, A., Püttmann, W., 2008. Biomarker and carbon isotope variation in coal and fossil wood of Central Europe through the Cenozoic. Palaeogeogr. Palaeoclimatol. Palaeoecol. 262, 166–175. https://doi.org/10.1016/j.palaeo.2008.03.005

Blair, N., Leu, A., Muñoz, E., Olsen, J., Kwong, E., Des Marais, D., 1985. Carbon isotopic fractionation in heterotrophic microbial metabolism. Appl. Environ. Microbiol. 50, 996–1001.

Bocherens, H., Friis, E.M., Mariotti, A., Pedersen, K.R., 1993. Carbon isotopic abundances in Mesozoic and Cenozoic fossil plants: Palaeoecological implications. Lethaia 26, 347–358. https://doi.org/10.1111/j.1502-3931.1993.tb01541.x

Bonafini, M., Pellegrini, M., Ditchfield, P., Pollard, A.M., 2013. Investigation of the 'canopy effect' in the isotope ecology of temperate woodlands. J. Archaeol. Sci. 40, 3926–3935. https://doi.org/10.1016/j.jas.2013.03.028

Burgener, L., Hyland, E., Huntington, K.W., Kelson, J.R., Sewall, J.O., 2019. Revisiting the equable climate problem during the Late Cretaceous greenhouse using paleosol carbonate clumped isotope temperatures from the Campanian of the Western Interior Basin, USA. Palaeogeogr. Palaeoclimatol. Palaeoecol. 516, 244–267. https://doi.org/10.1016/j.palaeo.2018.12.004

Bush, R.T., Wallace, J., Currano, E.D., Jacobs, B.F., McInerney, F.A., Dunn, R.E., Tabor, N.J., 2017. Cell anatomy and leaf δ13C as proxies for shading and canopy structure in a Miocene forest from Ethiopia. Palaeogeogr. Palaeoclimatol. Palaeoecol. 485, 593–604. https://doi.org/10.1016/j.palaeo.2017.07.015

Castro-Herrera, D., Prost, K., Kim, D.-G., Yimer, F., Tadesse, M., Gebrehiwot, M., Brüggemann, N., 2023. Biochar addition reduces non-CO2 greenhouse gas emissions during composting of human excreta and cattle manure. J. Environ. Qual. n/a. https://doi.org/10.1002/jeq2.20482

Caves, J.K., Moragne, D.Y., Ibarra, D.E., Bayshashov, B.U., Gao, Y., Jones, M.M., Zhamangara, A., Arzhannikova, A.V., Arzhannikov, S.G., Chamberlain, C.P., 2016. The Neogene de-greening of Central Asia. Geology 44, 887–890. https://doi.org/10.1130/G38267.1

Caves, J.K., Sjostrom, D.J., Mix, H.T., Winnick, M.J., Chamberlain, C.P., 2014. Aridification of Central Asia and uplift of the Altai and Hangay Mountains, Mongolia: Stable isotope evidence. Am. J. Sci. 314, 1171–1201. https://doi.org/10.2475/08.2014.01

Cerling, T.E., 1984. The stable isotopic composition of modern soil carbonate and its relationship to climate. Earth Planet. Sci. Lett. 71, 229–240. https://doi.org/10.1016/0012-821X(84)90089-X

Cerling, T.E., Quade, J., 1993. Stable Carbon and Oxygen Isotopes in Soil Carbonates, in: Climate Change in Continental Isotopic Records, Geophysical Monograph Series. pp. 217–231. https://doi.org/10.1029/GM078p0217

Cernusak, L.A., Ubierna, N., Winter, K., Holtum, J.A.M., Marshall, J.D., Farquhar, G.D., 2013. Environmental and physiological determinants of carbon isotope discrimination in terrestrial plants. New Phytol. 200, 950–965. https://doi.org/10.1111/nph.12423

Chin, K., 2007. The Paleobiological Implications Of Herbivorous Dinosaur Coprolites From The Upper Cretaceous Two Medicine Formation Of Montana: Why Eat Wood? Palaios 22, 554–566. https://doi.org/10.2110/palo.2006.p06-087r

Chin, K., Eberth, D.A., Schweitzer, M.H., Rando, T.A., Sloboda, W.J., Horner, J.R., 2003. Remarkable Preservation of Undigested Muscle Tissue Within a Late Cretaceous Tyrannosaurid Coprolite from Alberta, Canada. Palaios 18, 286–294. https://doi.org/10.1669/0883-1351(2003)018<0286:RPOUMT>2.0.CO;2

Chin, K., Feldmann, R.M., Tashman, J.N., 2017. Consumption of crustaceans by megaherbivorous dinosaurs: dietary flexibility and dinosaur life history strategies. Sci. Rep. 7, 11163. https://doi.org/10.1038/s41598-017-11538-w

Chin, K., Gill, B.D., 1996. Dinosaurs, Dung Beetles, and Conifers: Participants in a Cretaceous Food Web. Palaios 11, 280. https://doi.org/10.2307/3515235

Chowdhury, M.A., de Neergaard, A., Jensen, L.S., 2014. Potential of aeration flow rate and bio-char addition to reduce greenhouse gas and ammonia emissions during manure composting. Chemosphere 97, 16–25. https://doi.org/10.1016/j.chemosphere.2013.10.030

Cornwell, W., 2017. A versioned database for leaf 13C values from across the world : wcornwell/leaf13C v0.1.0. https://doi.org/10.5281/zenodo.569501

Cotrufo, M.F., Wallenstein, M.D., Boot, C.M., Denef, K., Paul, E., 2013. The Microbial Efficiency-Matrix Stabilization (MEMS) framework integrates plant litter decomposition with soil organic matter stabilization: do labile plant inputs form stable soil organic matter? Glob. Change Biol. 19, 988–995. https://doi.org/10.1111/gcb.12113

Cronjé, A.L., Turner, C., Williams, A.G., Barker, A.J., Guy, S., 2004. The Respiration Rate of Composting Pig Manure. Compost Sci. Util. 12, 119–129. https://doi.org/10.1080/1065657X.2004.10702170

Dacal, M., Bradford, M.A., Plaza, C., Maestre, F.T., García-Palacios, P., 2019. Soil microbial respiration adapts to ambient temperature in global drylands. Nat. Ecol. Evol. 3, 232–238. https://doi.org/10.1038/s41559-018-0770-5

Davidson, E.A., Janssens, I.A., 2006. Temperature sensitivity of soil carbon decomposition and feedbacks to climate change. Nature 440, 165–173. https://doi.org/10.1038/nature04514

Descolas-Gros, C., Schölzel, C., 2007. Stable isotope ratios of carbon and nitrogen in pollen grains in order to characterize plant functional groups and photosynthetic pathway types. New Phytol. 176, 390–401. https://doi.org/10.1111/j.1469-8137.2007.02176.x

Diefendorf, A.F., Mueller, K.E., Wing, Scott.L., Koch, P.L., Freeman, K.H., 2010. Global patterns in leaf 13C discrimination and implications for studies of past and future climate. Proc. Natl. Acad. Sci. 107, 5738–5743. https://doi.org/10.1073/pnas.0910513107

Edwards, E.J., 2014. The inevitability of C4 photosynthesis. eLife 3, e03702. https://doi.org/10.7554/eLife.03702

Edwards, E.J., Osborne, C.P., Stromberg, C.A.E., Smith, S.A., Bond, W.J., Christin, P.A., Cousins, A.B., Duvall, M.R., Fox, D.L., Freckleton, R.P., Ghannoum, O., Hartwell, J., Huang, Y., Janis, C.M., Keeley, J.E., Kellogg, E.A., Knapp, A.K., Leakey, A.D.B., Nelson, D.M., Saarela, J.M., Sage, R.F., Sala, O.E., Salamin, N., Still, C.J., Tipple, B., 2010. The Origins of C4 Grasslands: Integrating Evolutionary and Ecosystem Science. Science 328, 587–591. https://doi.org/10.1126/science.1177216

Falkowski, P., Scholes, R.J., Boyle, E., Canadell, J., Canfield, D., Elser, J., Gruber, N., Hibbard, K., Högberg, P., Linder, S., Mackenzie, F.T., Moore III, B., Pedersen, T., Rosenthal, Y., Seitzinger, S., Smetacek, V., Steffen, W., 2000. The Global Carbon Cycle: A Test of Our Knowledge of Earth as a System. Science 290, 291–296. https://doi.org/10.1126/science.290.5490.291

Forte, G., Kustatscher, E., Preto, N., 2022. Carbon (δ13C) isotope variations indicate climate shifts and reflect plant habitats in the Middle Triassic (Anisian, Pelsonian) succession at Kühwiesenkopf/Monte Prà della Vacca (Dolomites, Northeast Italy). Palaeogeogr. Palaeoclimatol. Palaeoecol. 601, 111098. https://doi.org/10.1016/j.palaeo.2022.111098

Foster, G.L., Royer, D.L., Lunt, D.J., 2017. Future climate forcing potentially without precedent in the last 420 million years. Nat. Commun. 8, 14845. https://doi.org/10.1038/ncomms14845

Franks, P.J., Royer, D.L., Beerling, D.J., Van de Water, P.K., Cantrill, D.J., Barbour, M.M., Berry, J.A., 2014. New constraints on atmospheric CO2 concentration for the Phanerozoic. Geophys. Res. Lett. 41, 4685–4694. https://doi.org/10.1002/2014GL060457

Gao, Y., Ibarra, D.E., Wang, C., Caves, J.K., Chamberlain, C.P., Graham, S.A., Wu, H., 2015. Mid-latitude terrestrial climate of East Asia linked to global climate in the Late Cretaceous. Geology 43, 287–290. https://doi.org/10.1130/G36427.1

Ghosh, P., Bhattacharya, S.K., Sahni, A., Kar, R.K., Mohabey, D.M., Ambwani, K., 2003. Dinosaur coprolites from the Late Cretaceous (Maastrichtian) Lameta Formation of India: isotopic and other markers suggesting a C3plant diet. Cretac. Res. 24, 743–750. https://doi.org/10.1016/j.cretres.2003.08.002

Grande, L., 1984. Paleontology of the Green River Formation, with a review of the fish fauna. Geological Survey of Wyoming Laramie, Wyoming.

Gröcke, D.R., 1998. Carbon-isotope analyses of fossil plants as a chemostratigraphic and palaeoenvironmental tool. Lethaia 31, 1–13. https://doi.org/10.1111/j.1502-3931.1998.tb00482.x

Gröcke, D.R., Kucera, M., Grocke, D.R., 2002. The carbon isotope composition of ancient CO2 based on higher-plant organic matter. Philos. Trans. R. Soc. Lond. Ser. Math. Phys. Eng. Sci. 360, 633–658. https://doi.org/10.1098/rsta.2001.0965

Highley, T.L., 1999. Biodeterioration of wood. Wood Handb. Wood Eng. Mater. Madison WI USDA For. Serv. For. Prod. Lab. 1999 Gen. Tech. Rep. FPL GTR-113 Pages 131-1316 113.

Hollocher, T.C., Chin, K., Hollocher, K.T., Kruge, M.A., 2001. Bacterial Residues in Coprolite of Herbivorous Dinosaurs: Role of Bacteria in Mineralization of Feces. PALAIOS 16, 547. https://doi.org/10.2307/3515628

Iacumin, P., Bocherens, H., Chaix, L., Marioth, A., 1998. Stable Carbon and Nitrogen Isotopes as Dietary Indicators of Ancient Nubian Populations (Northern Sudan). J. Archaeol. Sci. 25, 293–301. https://doi.org/10.1006/jasc.1997.0206

Jian, J., Vargas, R., Anderson-Teixeira, K.J., Stell, E., Herrmann, V., Horn, M., Kholod, N., Manzon, J., Marchesi, R., Paredes, D., Bond-Lamberty, B.P., 2021. A Global Database of Soil Respiration Data, Version 5.0. https://doi.org/10.3334/ORNLDAAC/1827

Johnson, K.R., Plumb, C., Averett, W.R., 1995. Common plant fossils from the Green River Formation at Douglas Pass, Colorado, and Bonanza, Utah. Green River Form. Piceance Creek East. Uinta Basins 1995 121–130.

Karhu, K., Auffret, M.D., Dungait, J.A.J., Hopkins, D.W., Prosser, J.I., Singh, B.K., Subke, J.-A., Wookey, P.A., Ågren, G.I., Sebastià, M.-T., Gouriveau, F., Bergkvist, G., Meir, P., Nottingham, A.T., Salinas, N., Hartley, I.P., 2014. Temperature sensitivity of soil respiration rates enhanced by microbial community response. Nature 513, 81–84. https://doi.org/10.1038/nature13604

Katz, B.J., 1995. The Green River Shale: an Eocene Carbonate Lacustrine Source Rock, in: Katz, Barry J. (Ed.), Petroleum Source Rocks, Casebooks in Earth Sciences. Springer, Berlin, Heidelberg, pp. 309–324. https://doi.org/10.1007/978-3-642-78911-3_16

Kocsis, L., Gheerbrant, E., Mouflih, M., Cappetta, H., Yans, J., Amaghzaz, M., 2014. Comprehensive stable isotope investigation of marine biogenic apatite from the late Cretaceous–early Eocene phosphate series of Morocco. Palaeogeogr. Palaeoclimatol. Palaeoecol. 394, 74–88. https://doi.org/10.1016/j.palaeo.2013.11.002

Kohn, M.J., 2010. Carbon isotope compositions of terrestrial C3 plants as indicators of (paleo)ecology and (paleo)climate. Proc. Natl. Acad. Sci. 107, 19691–19695. https://doi.org/10.1073/pnas.1004933107

Körner, Ch., Farquhar, G.D., Roksandic, Z., 1988. A global survey of carbon isotope discrimination in plants from high altitude. Oecologia 74, 623–632. https://doi.org/10.1007/BF00380063

Lambers, H., Oliveira, R.S., 2019. Photosynthesis, Respiration, and Long-Distance Transport: Photosynthesis, in: Lambers, H., Oliveira, R.S. (Eds.), Plant Physiological Ecology. Springer International Publishing, Cham, pp. 11–114. https://doi.org/10.1007/978-3-030-29639-1_2

Lanphere, M.A., 2000. Duration of sedimentation of Creede Formation from 40Ar/39Ar ages, in: Bethke, P.M., Hay, R.L. (Eds.), Ancient Lake Creede: Its Volcano-Tectonic Setting, History of Sedimentation, and Relation to Mineralization in the Creede Mining District. Geological Society of America, p. 0. https://doi.org/10.1130/0-8137-2346-9.71

Larsen, D., Crossey, L.J., 1996. Depositional environments and paleolimnology of an ancient caldera lake: Oligocene Creede Formation, Colorado. GSA Bull. 108, 526–544. https://doi.org/10.1130/0016-7606(1996)108<0526:DEAPOA>2.3.CO;2

Larson, T.E., Heikoop, J.M., Perkins, G., Chipera, S.J., Hess, M.A., 2008. Pretreatment technique for siderite removal for organic carbon isotope and C:N ratio analysis in geological samples. Rapid Commun. Mass Spectrom. 22, 865–872. https://doi.org/10.1002/rcm.3432

Licht, A., Dupont-Nivet, G., Meijer, N., Caves Rugenstein, J., Schauer, A., Fiebig, J., Mulch, A., Hoorn, C., Barbolini, N., Guo, Z., 2020. Decline of soil respiration in northeastern Tibet through the transition into the Oligocene icehouse. Palaeogeogr. Palaeoclimatol. Palaeoecol. 560, 110016. https://doi.org/10.1016/j.palaeo.2020.110016

Pancost, R.D., Sinninghe Damsté, J.S., de Lint, S., van der Maarel, M.J.E.C., Gottschal, J.C., The Medinaut Shipboard Scientific Party, 2000. Biomarker Evidence for Widespread Anaerobic Methane Oxidation in Mediterranean Sediments by a Consortium of Methanogenic Archaea and Bacteria. Appl. Environ. Microbiol. 66, 1126–1132. https://doi.org/10.1128/AEM.66.3.1126-1132.2000

Polissar, P.J., Fulton, J.M., Junium, C.K., Turich, C.C., Freeman, K.H., 2009. Measurement of 13C and 15N Isotopic Composition on Nanomolar Quantities of C and N. Anal. Chem. 81, 755–763. https://doi.org/10.1021/ac801370c

Quade, J., Eiler, J., Daëron, M., Achyuthan, H., 2013. The clumped isotope geothermometer in soil and paleosol carbonate. Geochim. Cosmochim. Acta 105, 92–107. https://doi.org/10.1016/j.gca.2012.11.031

Roberts, E.M., 2007. Facies architecture and depositional environments of the Upper Cretaceous Kaiparowits Formation, southern Utah. Sediment. Geol. 197, 207–233. https://doi.org/10.1016/j.sedgeo.2006.10.001

Roberts, E.M., Deino, A.L., Chan, M.A., 2005. 40Ar/39Ar age of the Kaiparowits Formation, southern Utah, and correlation of contemporaneous Campanian strata and vertebrate faunas along the margin of the Western Interior Basin. Cretac. Res. 26, 307–318. https://doi.org/10.1016/j.cretres.2005.01.002

Robinson, S.A., Hesselbo, S.P., 2004. Fossil-wood carbon-isotope stratigraphy of the non-marine Wealden Group (Lower Cretaceous, southern England). J. Geol. Soc. 161, 133–145. https://doi.org/10.1144/0016-764903-004

Roehler, H.W., 1972. Geologic map of the Brushy Point quadrangle, Rio Blanco and Garfield Counties, Colorado. Geol. Quadrang. https://doi.org/10.3133/gq1018

Rogers, R., Swisher, C., Horner, J., 1993. 40ArI39Ar age and correlation of the nonmarine Two Medicine Formation (Upper Cretaceous), northwestern Montana, U.S.A. Can. J. Earth Sci. 30, 1066–1075.

Ryan, M.G., Law, B.E., 2005. Interpreting, measuring, and modeling soil respiration. Biogeochemistry 73, 3–27. https://doi.org/10.1007/s10533-004-5167-7

Sade, Z., Hegyi, S., Hansen, M., Scholz, D., Halevy, I., 2022. The effects of drip rate and geometry on the isotopic composition of speleothems: Evaluation with an advection-diffusion-reaction model. Geochim. Cosmochim. Acta 317, 409–432. https://doi.org/10.1016/j.gca.2021.10.008

Sage, R.F., Wedin, D.A., Li, M., 1999. 10 - The Biogeography of C4 Photosynthesis: Patterns and Controlling Factors, in: Sage, R.F., Monson, R.K. (Eds.), C4 Plant Biology, Physiological Ecology. Academic Press, San Diego, pp. 313–I. https://doi.org/10.1016/B978-012614440-6/50011-2

Sarg, J.F., Suriamin, Tänavsuu-Milkeviciene, K., Humphrey, J.D., 2013. Lithofacies, stable isotopic composition, and stratigraphic evolution of microbial and associated carbonates, Green River Formation (Eocene), Piceance Basin, Colorado. AAPG Bull. 97, 1937–1966. https://doi.org/10.1306/07031312188

Selley, R.C., 2005. SEDIMENTARY ROCKS | Mineralogy and Classification, in: Selley, Richard C., Cocks, L.R.M., Plimer, I.R. (Eds.), Encyclopedia of Geology. Elsevier, Oxford, pp. 25–37. https://doi.org/10.1016/B0-12-369396-9/00304-X

Sender, R., Fuchs, S., Milo, R., 2016. Revised Estimates for the Number of Human and Bacteria Cells in the Body. PLOS Biol. 14, e1002533. https://doi.org/10.1371/journal.pbio.1002533

Sharp, Z., 2007. Principles of Stable Isotope Geochemistry. Pearson/Prentice Hall.

Smith, M.E., Carroll, A.R., 2015. Introduction to the Green River Formation, in: Smith, M.E., Carroll, A.R. (Eds.), Stratigraphy and Paleolimnology of the Green River Formation, Western USA, Syntheses in Limnogeology. Springer Netherlands, Dordrecht, pp. 1–12. https://doi.org/10.1007/978-94-017-9906-5_1

Smith, M.E., Singer, B., Carroll, A., 2003. 40Ar/39Ar geochronology of the Eocene Green River Formation, Wyoming. GSA Bull. 115, 549–565. https://doi.org/10.1130/0016-7606(2003)115<0549:AGOTEG>2.0.CO;2

Stephen, A.M., Cummings, J.H., 1980. The microbial contribution to human faecal mass. J. Med. Microbiol. 13, 45–56. https://doi.org/10.1099/00222615-13-1-45

St-Pierre, B., Wright, A.-D.G., 2013. Diversity of gut methanogens in herbivorous animals. animal 7, 49–56. https://doi.org/10.1017/S1751731112000912

Strömberg, C.A.E., 2011. Evolution of Grasses and Grassland Ecosystems. Annu. Rev. Earth Planet. Sci. 39, 517–544. https://doi.org/10.1146/annurev-earth-040809-152402

Sun, S., Lei, H., Chang, S.X., 2019. Drought differentially affects autotrophic and heterotrophic soil respiration rates and their temperature sensitivity. Biol. Fertil. Soils 55, 275–283. https://doi.org/10.1007/s00374-019-01347-w

Templeton, A.S., Chu, K.-H., Alvarez-Cohen, L., Conrad, M.E., 2006. Variable carbon isotope fractionation expressed by aerobic CH4-oxidizing bacteria. Geochim. Cosmochim. Acta 70, 1739–1752. https://doi.org/10.1016/j.gca.2005.12.002

Tipple, B.J., Pagani, M., 2007. The Early Origins of Terrestrial C4 Photosynthesis. Annu. Rev. Earth Planet. Sci. 35, 435–461. https://doi.org/10.1146/annurev.earth.35.031306.140150

Wang, H., Aguirre-Villegas, H.A., Larson, R.A., Alkan-Ozkaynak, A., 2019. Physical Properties of Dairy Manure Pre- and Post-Anaerobic Digestion. Appl. Sci. 9, 2703. https://doi.org/10.3390/app9132703

Witt, K.E., Yarlagadda, K., Allen, J.M., Bader, A.C., Simon, M.L., Kuehn, S.R., Swanson, K.S., Cross, T.-W.L., Hedman, K.M., Ambrose, S.H., Malhi, R.S., 2021. Integrative analysis of DNA, macroscopic remains and stable isotopes of dog coprolites to reconstruct community diet. Sci. Rep. 11, 3113. https://doi.org/10.1038/s41598-021-82362-6

Wolfe, J.A., Schorn, H.E., 1989. Paleocologic, Paleoclimatic, and Evolutionary Significance of the Oligocene Creede Flora, Colorado. Paleobiology 15, 180–198.

Yans, J., Gerards, T., Gerrienne, P., Spagna, P., Dejax, J., Schnyder, J., Storme, J.-Y., Keppens, E., 2010. Carbon-isotope analysis of fossil wood and dispersed organic matter from the terrestrial Wealden facies of Hautrage (Mons Basin, Belgium). Palaeogeogr. Palaeoclimatol. Palaeoecol., Charcoal and its use in palaeoenvironmental analysis 291, 85–105. https://doi.org/10.1016/j.palaeo.2010.01.014

Zidarič, T., Majer, D., Maver, T., Finšgar, M., Maver, U., 2023. The development of an electropolymerized, molecularly imprinted polymer (MIP) sensor for insulin determination using single-drop analysis. Analyst 148, 1102–1115. https://doi.org/10.1039/D2AN02025D

Supplemental Materials

All supplemental materials can be found in this Zenodo Repository:
https://doi.org/10.5281/zenodo.8239847

Supplemental materials include:

- Photographs of sampling locations for coprolite targeted sampling of specimens BU-89-2, HN-94-6, and BP-12-13
- Photographs of sampling locations for predominant coprofabric coprolite samples
- Photographs of sampling locations for DMNS Creede Fm. samples (sampling locations indicated with a circle or red markings)
- Carbon stable isotope data for coprolite carbonates
- Carbon stable isotope data for Creede Fm. and Green River Fm. rock and plant samples
- R Code for coprolite and paleosol respiration rate sensitivity analysis
- Conversion calculations for modern manure respiration rates